

Zero waste Heat vessel towards relevant Energy savings also thanks to IT technologies



D 1.1 | WHR for Maritime applications catalogue

WP1 – Vessel audit and requirement definition towards zero waste heat

Version 1.3 | February 2023

HORIZON-CL5-2021-D5-01-10

Clean and competitive solutions for all transport modes -
Innovative on-board energy saving solutions



This project has received funding from the European Union's Horizon Europe research and innovation programme under grant agreement No 101056801.



Funded by the
European Union

Disclaimer

Funded by the European Union. The content of this deliverable reflect the authors' views. Views and opinions expressed are however those of the author(s) only and do not necessarily reflect those of the European Union or the European Climate, Infrastructure and Environment Executive Agency (CINEA). Neither the European Union nor the granting authority can be held responsible for them.

Copyright Message

This report, if not confidential, is licensed under a Creative Commons Attribution 4.0 International License (CC BY 4.0). A copy is available here:

<https://creativecommons.org/licenses/by/4.0/>.

You are free to share (copy and redistribute the material in any medium or format) and adapt (remix, transform, and build upon the material for any purpose, even commercially) under the following terms:

(i) attribution (you must give appropriate credit, provide a link to the license, and indicate if changes were made; you may do so in any reasonable manner, but not in any way that suggests the licensor endorses you or your use); (ii) no additional restrictions (you may not apply legal terms or technological measures that legally restrict others from doing anything the license permits).

Document History

| | |
|----------------------|--|
| Project Acronym | ZHENIT |
| Project Title | ZHENIT - Zero waste Heat vessel towards relevant Energy savings also thanks to IT technologies |
| Project coordination | RINA-C |
| Project duration | 42 month – from 1/06/2022 to 30/11/2025 |
| Title | WHR for Maritime applications catalogue |
| Dissemination Level | PU - Public |
| Status | Final |
| Version | 1.3 |
| Work Package | WP1 |
| Lead Beneficiary | UoB |
| Other Beneficiaries | RINA-C, CNR, TECNALIA, NTUA |
| Author(s) | Robin Fisher (UoB) |
| Reviewers | RINA-C, NTUA |

| Date | Ver. | Contributors | Comment |
|------------|------|--|------------------------------------|
| 04/08/2022 | 0.1 | Robin Fisher (UoB) | Initial Structure |
| 25/01/2023 | 0.2 | Robin Fisher (UoB) | First Draft |
| 10/02/2023 | 1.0 | Samuele Da Ronch, Giorgio Bonvicini (RINA-C) | Review |
| 10/02/2023 | 1.0 | Konstantinos Braimakis (NTUA) | Review |
| 17/02/2023 | 1.2 | Robin Fisher (UoB) | Corrections from review applied |
| 28/02/2023 | 1.3 | Laura Bordo (RINA-C) | Final version ready for submission |

List of Organizations

| | Participant Name | Short Name | Country | Logo |
|-----|--|------------|----------------|---|
| 1 | RINA Consulting SpA | RINA-C | Italy |  |
| 1.1 | RINA Services SpA | RINA-S | Italy | |
| 2 | Ethnicon metsovion polytechnion | NTUA | Greece |  |
| 3 | Kyma as | KYMA | Norway |  |
| 4 | Fundacion tecnalía research & innovation | TECNALIA | Spain |  |
| 4.1 | Universidad del país vasco/ euskal herriko unibertsitatea | UPV/EHU | Spain |  |
| 5 | Anonimi naftiliaki eteria kritis (anek) s.a. | ANEK | Greece |  |
| 6 | Consiglio nazionale delle ricerche | CNR | Italy |  |
| 6.1 | Consorzio di ricerca per l'innovazione tecnologica, sicilia trasporti navali, commerciali e da diporto scarl | NAVTEC | Italy |  |
| 7 | Sorption technologies gmbh | SORTECH | Germany |  |
| 7.1 | Sorption technologies srl | SORTIT | Italy | |
| 8 | Bound 4 blue sl | B4B | Spain |  |
| 9 | Encontech bv | ECT | Netherlands |  |
| 10 | Gruppo sigla srl | SIGLA | Italy |  |
| 11 | The University of Birmingham | UoB | United Kingdom |  |

Table of Content

| | | |
|-------|---|----|
| 1 | Introduction | 17 |
| 2 | On-board WHR technologies in ZHENIT..... | 18 |
| 2.1 | Organic Rankine Cycles | 18 |
| 2.1.1 | Introduction..... | 18 |
| 2.1.2 | Technology overview..... | 18 |
| 2.1.3 | Architecture and implementation..... | 20 |
| 2.1.4 | Applications and uses | 25 |
| 2.1.5 | Techno-economics..... | 32 |
| 2.1.6 | Modelling organic Rankine cycles | 36 |
| 2.2 | Sorption Refrigeration & Desalination..... | 36 |
| 2.2.1 | Introduction..... | 36 |
| 2.2.2 | Technology overview..... | 37 |
| 2.2.3 | Architecture and implementation..... | 39 |
| 2.2.4 | Applications and uses | 42 |
| 2.2.5 | Techno-economics..... | 44 |
| 2.2.6 | Modelling adsorption refrigeration & desalination | 45 |
| 2.3 | Thermal Energy Storage..... | 46 |
| 2.3.1 | Introduction..... | 46 |
| 2.3.2 | Technology overview..... | 47 |
| 2.3.3 | Architecture and implementation..... | 51 |
| 2.3.4 | Applications and uses | 55 |
| 2.3.5 | Techno-economics..... | 60 |
| 2.3.6 | Modelling thermal energy storage..... | 61 |
| 2.4 | Isobaric Expansion Engines | 62 |
| 2.4.1 | Introduction..... | 62 |
| 2.4.2 | Technology overview..... | 63 |
| 2.4.3 | Architecture and implementation..... | 66 |
| 2.4.4 | Applications and uses | 68 |
| 2.4.5 | Techno-economics..... | 80 |
| 2.4.6 | Modelling the isobaric expansion engine..... | 82 |
| 3 | Consolidated and other developmental on-board WHR technologies..... | 85 |

| | | |
|-------|--|-----|
| 3.1 | Turbo-compounding | 85 |
| 3.1.1 | Introduction..... | 85 |
| 3.1.2 | Technology overview..... | 85 |
| 3.1.3 | Techno-economics..... | 89 |
| 3.1.4 | Modelling turbocompounding systems..... | 91 |
| 3.2 | Steam Rankine Cycles | 92 |
| 3.2.1 | Introduction..... | 92 |
| 3.2.2 | Technology Overview | 92 |
| 3.2.3 | Techno-Economics..... | 96 |
| 3.2.4 | Modelling the steam Rankine cycle..... | 99 |
| 3.3 | Thermoelectric Generation (using Seebeck effect) | 99 |
| 3.3.1 | Introduction..... | 99 |
| 3.3.2 | Technology overview..... | 99 |
| 3.3.3 | Applications | 102 |
| 3.3.4 | Techno-economics..... | 103 |
| 3.3.5 | Modelling thermoelectric generation | 105 |
| 3.4 | Absorption Refrigeration | 105 |
| 3.4.1 | Introduction..... | 105 |
| 3.4.2 | Technology overview..... | 106 |
| 3.4.3 | Applications | 109 |
| 3.4.4 | Techno-economics..... | 110 |
| 3.4.5 | Modelling absorption refrigeration systems..... | 111 |
| 3.5 | Organic Flash Cycles..... | 112 |
| 3.5.1 | Introduction..... | 112 |
| 3.5.2 | Technology Overview | 112 |
| 3.5.3 | Techno-economics..... | 115 |
| 3.5.4 | Modelling the organic flash cycle..... | 117 |
| 3.6 | Kalina Cycles..... | 118 |
| 3.6.1 | Introduction..... | 118 |
| 3.6.2 | Technology Overview | 118 |
| 3.6.3 | Techno-economics..... | 122 |
| 3.6.4 | Modelling the Kalina cycle..... | 125 |

| | | |
|---|-------------------|-----|
| 4 | Conclusions | 126 |
| | References..... | 128 |

List of Figures

| | |
|--|----|
| Figure 1 Rankine cycle (a) Basic system configuration [11] and (b) thermodynamic cycles in a T-s diagram with RE347mcc as working fluid [12] | 19 |
| Figure 2 (a) Typical layout and (b) T-s diagram of the regenerated/recuperated ORC process [13].... | 21 |
| Figure 3 (a) Typical layout and (b) T-s diagram of the bleeder regenerated ORC process [13]..... | 21 |
| Figure 4 Dual-loop ORC for using multiple waste heat streams [3]..... | 22 |
| Figure 5 (a) Two separate ORCs driven by exhaust gas and jacket cooling water, (b) ORC configuration with preheater and evaporator [12] | 22 |
| Figure 6 Parallel ORC architecture [15]..... | 23 |
| Figure 7 Recuperative ORC configuration [16]..... | 24 |
| Figure 8 Directly heated recuperative ORC [17] | 24 |
| Figure 9 ORC with multiple heat sources [18]..... | 25 |
| Figure 10 Experimental ORC prototype for naval applications [21] | 26 |
| Figure 11 Experimental ORC prototype [22] | 27 |
| Figure 12 ORC modules for naval applications, left: Alfa Laval ‘E-Power Pack’, [23], right: Orcan-Energy ePM 050.100 ‘Efficiency Pack’ [24] | 28 |
| Figure 13 Process layout for the Hydrocurrent™ Organic Rankine Cycle Module 125EJW | 29 |
| Figure 14 Enogia ENO-180LT [26]..... | 30 |
| Figure 15 Enerbasque HRU-25 [27]..... | 31 |
| Figure 16 Rank MT1 [28] | 31 |
| Figure 17 Thermal efficiency of on-board ORC cycles as a function of net power output | 34 |
| Figure 18 Specific cost of ORC modules and projects, and of ORC for naval applications. Economic data for ORC for heat recovery from [37], data for naval ORCs from [16,34,35] | 35 |
| Figure 19 Schematic representation of the hybrid refrigeration/desalination cycle, using a two-adsorber bed system for continuous operation [40] | 37 |
| Figure 20 Standard two-beds adsorption cooling and desalination architecture [42] | 39 |
| Figure 21 Four-beds adsorption cooling and desalination architecture [42]..... | 40 |

Figure 22 A sorption refrigeration system as a topping cycle using exhaust waste heat, with a compression vapour cycle operating as a bottoming cycle in a cascade layout. Numbers on the diagram refer to 1: engine and exhaust heat, 2: sorption chiller, 3: condenser heat exchanger using seawater, 4: vapour compression chiller, 5: cold storage [43] 41

Figure 23 Cooling hybrid configuration with series connection between sorption and compression system. 1—engine; 2—sorption chiller; 3—seawater condensing heat exchanger for sorption chiller; 4—vapour compression chiller; 5—seawater condensing heat exchanger for compression chiller; 6—brine heat exchanger for compression chiller; 7—brine heat exchanger for sorption chiller; 8–9—three way valves for series operation; 10—cold room [43] 42

Figure 24 Experimental prototype of a three-bed hybrid chilling (1.1 kW) and desalination adsorption device, front view (top picture) and back view (bottom picture) [44] 43

Figure 25 Overview of the four-beds AD cycle showing the heat recovery between the condenser and the evaporator [45] 44

Figure 26 (a) Schematic representation of TES concept (valid for both STES and LTES), (b) thermal energy storage material temperature as a function of stored heat, during sensible and latent heat storage [60] 48

Figure 27 Schematic representation of hot and cold two-tank TES layout, with (A) configuration where the HTF at the heat source is also the TES material, and (B) configuration where the HTF at the heat source is different from the TES material with an intermediate heat exchanger [80]..... 52

Figure 28 Schematic representation of thermocline TES with the temperature gradient shown at a function of its position along the thermocline, with A: a diffuse temperature gradient and B: a sharp temperature gradient [58] 53

Figure 29 Schematic representation of packed bed thermal energy storage, adapted from [83] 54

Figure 30 Schematic classification of LTES PCM-based storages in pipe layout based on container geometry and inner material distribution, proposed by Agyenim et al. [84] 55

Figure 31 (a) Conventional hot water system on a cruise ship (b) modified with TES [89] 56

Figure 32 (a) Thermal Battery by Energy Nest [85], (b) Eco Stock by EcoTech Ceram [90] 57

Figure 33 Lumenion steel-based thermal energy storage, left: conceptual design, right: actual 450 kWh implementation in University of Applied Sciences (HTW) laboratory [91] 58

Figure 34 Sunamp PCM-based LTES [92]..... 58

| | |
|--|----|
| Figure 35 Hybrid STES/LTES for on-board waste heat storage, targeted towards hot water production (a) detailed exploded tri-dimensional view and (b) schematic representation with sensors and flow direction [95]..... | 59 |
| Figure 36 Basic layout of isobaric expansion engines, (a) in the Worthington steam pump configuration. 1: steam cylinder, 2: pumping cylinder, 3: steam piston, 4; pumping piston, 5: connecting rod, 6: steam inlet valve, 7—steam outlet valve, 8—liquid inlet valve, 9—liquid outlet valve.and (b) in the Bush thermocompressor configuration. 10: linear actuator, 11: cold side cylinder, 12: sealed piston, 13: hot side cylinder [99] | 63 |
| Figure 37 Integration of the Worthington steam pump IEE into a power cycle. 1: feedwater pump, 2: internal heat recovery, 3: evaporator, 4: condenser, 5: low-pressure hydraulic accumulator, 6: high-pressure hydraulic accumulator, 7: hydraulic motor [99] | 66 |
| Figure 38 Various implementations and architectures of Worthington-type IEEs. (a) Simple non-regenerative with hydraulic motor and generator, (b) regenerative with hydraulic motor and generator, (c) regenerative with thermal barrier piston and diaphragm, (d) regenerative with crank-gear, (e) regenerative with rotary lobe-machine [105] | 67 |
| Figure 39 Integration of the Bush thermo-compressor-based IEE into a power cycle. 1: cylinder, 2: piston, 3: heater, 4: regenerator, 5: cooler, 6: connecting rod, 7: linear actuator, 8: diaphragm unit, 9: non-return valves, 10: high-pressure accumulator, 11: low-pressure accumulator, 12: hydraulic motor [99] | 68 |
| Figure 40 Schematic overview of the Up-THERM engine principle, assembly drawing and picture of the engine. For details, see [109]..... | 70 |
| Figure 41 Layout of the CHP system engine test setup | 71 |
| Figure 42 Scheme and picture of the experimental set up. 1: engine-pump (internal diameter 30 mm, stroke of the displacer 40 mm), 2: heating jacket, 3: cooling jacket, 4: diaphragm unit, 5: non-return valves, 6: high-pressure accumulator, 7: low-pressure accumulator, 8: throttle valve, FT: flow transmitter, PI: pressure indicators, PT: pressure transmitters, TT: temperature transmitter | 72 |
| Figure 43 Solar powered test setup for water desalination | 72 |
| Figure 44 Assembly drawing of the IE-compressor. 1: compressor cylinder cover, 2: compressor cylinder, 3a and 3b: compressor and driving pistons, 4: guiding cover, 5: connecting rod, 6: vapor driver cylinder, 7: inlet and outlet valves, 8: valve cover, 9: pillars, P1 and P2: ports for suction and discharge valves | 73 |

Figure 45 Experimental Worthington-type IEE-compressor schematic representation and picture of the experimental test rig. D: driving chamber, C-R: compression chambers, H-E: heater, P: feed pump, C-C: cooler, C: condenser, E: evaporator, EV: expansion valve/throttle. (Kronberg & Glushenkov 2022; Kronberg et al. 2022; Encontech IE-engine refrigerator)..... 74

Figure 46 Experimental Worthington-type IEE coupled with hydraulic motor, HM, its picture and picture of the test rig 75

Figure 47 Efficiency of IE cycle as a function of temperature and pressure difference generated by engine. Working fluids: R32 and CO₂ 76

Figure 48 Experimental Worthington-type IEE (a) schematic representation 1: driving cylinder, 2: pumping cylinder, 3: pistons, 4: connecting rods, 5: driving valve covers, 6: pumping valve covers, 7: valve actuators, 8: inlet suction valves, 9: discharge valves, 10: manifold. (b) picture of the experimental test rig [104]..... 78

Figure 49: Thermal efficiency of model IEE running on R134a (left) and a mixture of 80 mol% ammonia and water (right) 83

Figure 50 Power density of IE engine-pump 83

Figure 51 Example layout of power turbine and generator PTG WHR system (MAN [1]) 86

Figure 52 Example of a steam turbine, power turbine, gearboxes and generator interconnected on the same shaft [118] 87

Figure 53 Example of combined PT-ST system suggested by MAN [1] 88

Figure 54 Performance of combined PT-ST WHRS: fraction of engine load recovered as electrical power as a function of engine load. The total recovered energy is counted as the sum of electrical power outputs of the steam turbine and power turbine 89

Figure 55 Economic performance of various turbo compounding WHRS, cash flow normalised for engine power rating at 100% SMCR, 20 years system lifetime assumed, 6% interest rate 91

Figure 56 Basic layout of a Steam Rankine Cycle with energy and work flows [11]..... 92

Figure 57 Heat transfer diagrams for single and dual-pressure SRC systems [125] 93

Figure 58 Simplified steam Rankine cycle layout using exhaust gases to heat, evaporate and superheat a flow of water [124]. The steam turbine is commonly connected to a generator to convert the mechanical power output to electrical power. 94

Figure 59 Combined gas turbine cycle with steam Rankine cycle for marine energy systems [126]... 95

Figure 60 On-board steam Rankine cycle coupled with absorption refrigeration [127] 95

| | |
|--|-----|
| Figure 61 Typical layout of a thermoelectric generator [130]. Pairs of semiconductors are arranged electrically in series, and thermally in parallel..... | 100 |
| Figure 62 Thermoelectric efficiency values for various figures of merit ZT, compared to theoretical Carnot efficiency, with heat sink temperature $T_c = 50^\circ\text{C}$, adapted from [129] | 101 |
| Figure 63 TEG heat exchanger example [135]. TEM = thermoelectric module, L_{sec} = section length. | 102 |
| Figure 64 TEG designed for recovering waste heat from ship incinerator exhaust gas [134] | 103 |
| Figure 65 Absolute cost of commercial TEG modules as a function of maximum power output | 104 |
| Figure 66 Specific cost of commercial TEG modules as a function of surface power output..... | 104 |
| Figure 67 Basic Principle of Single-Effect Absorption Refrigeration Cycle [142] | 107 |
| Figure 68 Single-Effect Absorption Refrigeration Cycle with Intermediate Heat Exchanger and Rectifier [11]..... | 108 |
| Figure 69 (left) 2AA WHR absorption chiller by WorldEnergy which uses hot water at approx. 70°C as the heat source. Retrieved from [144]. (right) hot water driven absorption chiller designed by Kawasaki Thermal Engineering, retrieved from [145] | 108 |
| Figure 70 Integration of an absorption refrigeration cycle in a marine application, directly using exhaust gas waste targeted towards cabin air conditioning [142] | 109 |
| Figure 71 Schematic representation of a conventional Organic Flash Cycle layout [160]..... | 113 |
| Figure 72 Schematic representation of the double flash OFC layout [161]..... | 114 |
| Figure 73 Schematic representation of a Organic Flash Regenerative Cycle layout [160] | 115 |
| Figure 74 Effect of heat source temperature on the specific cost of regenerated OFCs, data from [162] and [164]..... | 117 |
| Figure 75 Bubble and dew point in phase diagram for the ammonia-water mixture as a function of ammonia mass content, for a constant pressure, adapted from [2]..... | 119 |
| Figure 76 Schematic representation of a Kalina cycle standard layout, adapted from [167] | 120 |
| Figure 77 Integration of a Kalina cycle as a bottoming cycle to a Diesel engine, generating useful work using the exhaust gases and engine coolant loop [169] | 121 |
| Figure 78 Schematic representation of a Kalina cycle in a Diesel engine WHR layout [170]..... | 122 |

List of Tables

| | |
|--|----|
| Table 1 Techno-economic parameters of on-board maritime ORC applications | 32 |
|--|----|

| | |
|--|-----|
| Table 2 CAPEX and power rating for different adsorption chillers | 44 |
| Table 3 PCMs, and their thermophysical properties, used for internal combustion engine waste heat recovery, list originally compiled in [65] | 49 |
| Table 4 TCM characteristics. List originally compiled in [78] | 50 |
| Table 5 Techno-economic properties of thermal energy storage. Storage costs are system-level i.e., cost of the entire process, material, and installation. Data originally synthesised in [97] | 60 |
| Table 6 Electricity generation in geothermal plants | 77 |
| Table 7 Performance and key properties of the dual-acting Worthington IEE.[104] | 78 |
| Table 8 Comparison of nonconventional heat engines [104] | 79 |
| Table 9 Performance of known CHP technologies | 80 |
| Table 10 Technical performance of proposed on-board integrated SRCs | 98 |
| Table 11 ICF's steam Rankine cycle cost estimates (capital investment and O&M) as a function of installed capacity, reported by Oak Ridge National Laboratory (ORNL) [123], costs converted to euros and annualised | 98 |
| Table 12 Performance and characteristics of sub-zero refrigerating absorption devices using ammonia as refrigerant, data originally synthesised in [143] | 110 |
| Table 13 Composite absorption chiller investment and O&M costs, costs converted and annualised, taken from US department of Energy document [156] | 111 |
| Table 14 Synthesis of technical performance data of Organic Flash Cycles in scientific literature | 115 |
| Table 15 Synthesis of technical performance data of Kalina cycles either commercially available or found in scientific literature. Data originally synthesised in and table adapted from European project SoWhat deliverable 1.6 [166] | 123 |
| Table 16 Costing elements for Kalina cycles taken from literature studies. Capacity refers to the power output of the Kalina heat recovery cycle. Costs annualised | 125 |
| Table 17 Summary of the investigated WHR technologies | 126 |

Abbreviation and Acronyms

| Acronym | Description |
|---------|-------------------------------------|
| CHP | Combined Heat and Power |
| COP | Coefficient of Performance |
| CSP | Concentrating Solar Power |
| EER | Energy Efficiency Ratio |
| EG | Exhaust Gas |
| EGR | Exhaust Gas Receiver |
| GHG | Green House Gas |
| HFO | Heavy Fuel Oil |
| HTF | Heat Transfer Fluid |
| ICE | Internal Combustion Engine |
| IEE | Isobaric Expansion Engine |
| IMO | International Maritime Organisation |
| KC | Kalina Cycle |
| LTES | Latent Thermal Energy Storage |
| NPV | Net Present Value |
| O&M | Operation and Maintenance |
| OFC | Organic Flash Cycle |
| OFRC | Organic Flash Regenerative Cycle |
| ORC | Organic Rankine Cycle |
| PGU | Power Generation Unit |
| PTG | Power Turbine and Generator |
| SCP | Specific Cooling Power |
| SDWP | Specific Daily Water Production |
| SFOC | Specific Fuel Oil Consumption |
| SMCR | Specified Maximum Continuous Rating |
| SRC | Steam Rankine Cycle |

| | |
|-------|---|
| STES | Sensible Thermal Energy Storage |
| STG | Steam Turbine and Generator |
| ST-PT | Steam Turbine – Power Turbine (combined system) |
| TCS | Thermochemical Energy Storage |
| TEG | Thermoelectric Generation |
| TES | Thermal Energy Storage |
| TRL | Technology Readiness Level |
| VLCC | Very Large Crude Carrier |
| WHR | Waste Heat Recovery |
| WHRS | Waste Heat Recovery System |

Executive Summary

The ZHENIT project aims to exploit waste heat recovery potential on-board vessels using energy management methods, clean energy solutions and low-emissions ship services. The targets of the project are new technologies development, on-board validation, a regulatory framework analysis and a replication roadmap at regulatory and economic level. Various waste heat recovery technologies will be paired synergistically, and the experience gained with this project in holistically integrating and managing different 'ready-to-go' WH-to-X systems, hybrid propulsion technologies, and energy management methods could be leveraged for future application in near zero waste-heat vessels.

Various technological options for the recovery of marine engine waste heat are currently or potentially available. However their temperature ranges of application, capacities, costs, efficiencies and overall levels of technological maturity vary greatly. The purpose of this report is (a) to give an overview of the state of the art of on-board waste heat recovery technologies for the shipping industry, (b) for each technology provide an overview of the basic operating principle, its techno-economic performance and review the potential for on-board integration, and (c) provide algorithmic models to support the techno-economic assessment of the energy system investigated in ZHENIT. The technologies are categorised into either developmental technologies investigated in ZHENIT, or other consolidated and developmental waste heat recovery technologies. Each technology is contained within its own subsection which is organised as follows: an overview of the technology basic working principle, the different architectures for the practical implementation of the technology, a discussion surrounding the specific application to marine energy systems, the techno-economic performance, and finally the algorithmic model for techno-economic assessment.

All of the waste heat recovery technologies either convert the excess heat from the engine into electrical power (waste heat-to-power), cooling power (waste heat-to-cold), mechanical power, or upgrade the excess thermal energy to generate added value for some on board demand such as steam or desalinated water.

The main technologies investigated in the context of the ZHENIT project are: organic Rankine cycles, thermal energy storage, sorption desalination and refrigeration and isobaric expansion engines. All of these technologies make use of thermal energy, which in on-board applications can be expected to be in the form of exhaust flue gas from ship diesel engines and the engine cooling fluids (jacket water, lubricants).

Organic Rankine cycles are waste heat-to-power thermodynamic cycles for power generation that can make use of thermal energy to evaporate a working fluid / refrigerant with a relatively low boiling point and run it through an expander to produce useful work.

Thermal energy storage enable the storage of waste heat from the afore-mentioned heat sources and is particularly suited to the intermittent nature of vessels' engine operation which is the main influencing factor on the availability of hot exhaust gas and cooling fluids.

Sorption technologies leverage carefully considered thermo-chemical adsorption reactions to generate both desalinated water from sea-water and a cooling/refrigeration effect, powered by on-board waste heat.

Isobaric engines are an uncommon type of heat-engine, which are aimed, on-board, at converting excess waste heat to mechanical work, which, as with the Organic Rankine Cycle, can be used to produce electrical power, drive a compressor, etc... In the context of the ZHENIT project, isobaric engines are aimed at fuel pumping in the on-board fuel-injection systems.

Six other technologies are investigated in the other consolidated and developmental waste heat recovery technologies section. It emerges from this section that the main currently implemented waste heat recovery is turbocompounding, which can recover between 3% and 10% of the fuel energy as electrical power depending on the level of complexity of the system. Other waste heat recovery methods with technological maturity levels varying from wide spread in the non-marine industry (such as steam Rankine cycles and absorption refrigeration) to very low maturity levels (thermo-electric generation and unconventional power cycles such as Kalina or organic flash cycles) are investigated in this section.

1 Introduction

Much of the energy input (fuel) used in industrial thermal processes, heating systems and transport does not result in useful work and is lost to the environment as converted as waste heat. Such energy inefficiencies are certainly an issue for marine applications. In a large-bore, two-stroke internal combustion diesel engine typically found in large modern-day vessels, as much as 50% of the input fuel is lost as thermal energy through various cooling fluid streams and through exhaust gases [1]. These types of engines constitute 96% of the propulsion methods for all civilian ships above 100 tons [2]. As a direct consequence of this high amount of released waste heat, the shipping industry is responsible for approximately 3% of total worldwide GHG emissions, with global trade through shipping expected to grow further [3]. These factors have pushed the International Maritime Organisation (IMO) to aim towards halving shipping-related emissions by 2050 through its Initial Strategy adopted in 2018 [4], in direct support of the United Nation's Sustainable Goal 13 ('Take urgent action to combat climate change and its impacts') [5].

Various strategies can improve the energy efficiency and lower GHG emission of ships [6]. Some of these approaches include using alternative fuels to the traditional sulfur-heavy fuel, such as LNG, hydrogen, ammonia and advanced bio-fuels, alternative means of propulsion such as modern sails, on-board carbon capture and storage to directly impact carbon emissions, inclusion of renewable energy generation technologies such as solar PV or solar hybrid systems, or even improving existing internal-combustion engine (ICE) technology.

Since roughly 50% of fuel input is lost as waste heat, waste heat recovery (WHR) could be an effective way to both improve vessel energy efficiency and lower GHG emissions. While some WHR methods are generally in place aboard vessels such as waste heat boilers, steam turbine cycles or turbocharging, there exist a number of potential technologies that could improve the energy efficiency of vessels beyond what is currently achieved. Current estimates show that total engine efficiency could be raised from 50% to 60%, and 4% to 16% fuel efficiency improvement is attainable [1,2].

2 On-board WHR technologies in ZHENIT

2.1 Organic Rankine Cycles

2.1.1 Introduction

The Rankine cycle is a thermodynamic cycle that converts thermal energy from a heat source into useful mechanical work through an expander/turbine train, generally to produce electricity. In its most basic configuration, a Rankine cycle is composed of an evaporator, an expander connected to a power generation unit, a condenser and a pump in a closed fluid loop. The traditional working fluid is water in so-called Steam Rankine Cycles (SRC). Steam turbine systems have been used for over a century in maritime applications [2]. However, the performance of on-board SRCs is limited by the temperature of the available waste heat combined with the high evaporation temperature of water [7], which for SRCs should ideally be above 350°C to produce high pressure steam; at lower temperatures, the equipment required is bulky, inefficient and expensive.

Organic Rankine cycles (ORC) leverage more effectively the lower temperature waste heat on-board ships by using organic fluids with low boiling points as the working fluid. ORCs are typically designed for biomass combined heat and power plants, waste heat recovery, low temperature geothermal sources, or solar applications [8]. Various different working fluids are available to best tailor the ORC to the available heat sources. Various ORC configurations exist to make best use of the available heat sources/sinks. Configuration and working fluid selection are two of the main factors which determine the performance of the ORC in the context of the application. Net power output of current commercial ORCs ranges from 10 kW_e to 10 MW_e [9]. Commercially available ORC systems, nowadays, range from a few kW_e up to 2.2 MW_e.

2.1.2 Technology overview

2.1.2.1 Thermodynamic cycle and basic operation

A fluid in an ideal organic Rankine cycle undergoes four thermodynamic processes. **Adiabatic pumping** - the pressure of a working fluid in the liquid phase is increased to the maximum cycle pressure in a pump. The required electrical power input should be negligible compared to the expander work output. **Isobaric heating** –the saturated liquid is heated by the heat source in the evaporator, brought to the boiling point and fully evaporated into vapour, and often superheated. In the ideal cycle, the pressure stays the same during this process. **Isentropic expansion**: the superheated vapour stream is expanded

isentropically in a turbine / expander train to produce useful mechanical work and low pressure vapour at the turbine outlet. Expanders are selected either from turbines or positive displacement engines. **Isoobaric cooling:** the low pressure vapour flow is cooled and condensed back to the liquid phase. Some thermal energy is extracted from the process at this stage, which can be useful depending on the integration of the Rankine cycle in the broader energy system [10]. Figure 1 shows the basic schematic layout of the ORC.

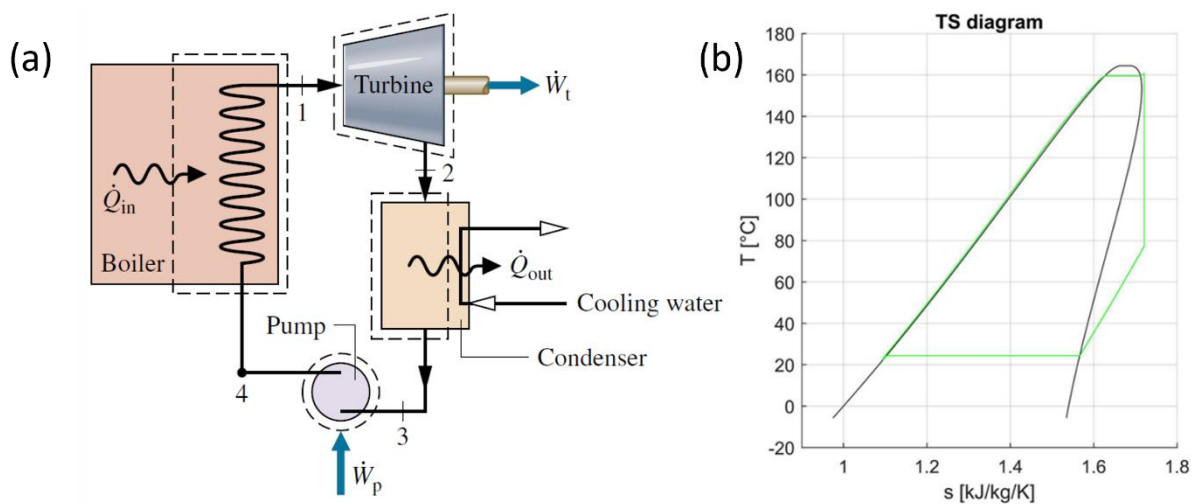


Figure 1 Rankine cycle (a) Basic system configuration [11] and (b) thermodynamic cycles in a T-s diagram with RE347mcc as working fluid [12]

2.1.2.2 Performance metrics

The performance of an ORC relates to the amount of useful work produced in relation to the thermal energy input to evaporate the working fluid and the electrical energy input to drive pumps and auxiliaries. The main technical performance indicators of ORCs are the net useful work output \dot{W}_{net} and the cycle thermal efficiency η_{th} . The net useful work produced by the cycle is the difference between the useful work produced at the expander \dot{W}_{exp} and the work absorbed by the pump \dot{W}_{pump} (equation (1)):

$$\dot{W}_{net} = \dot{W}_{exp} - \dot{W}_{pump} \quad (1)$$

The cycle thermal efficiency is the ratio between net useful work output \dot{W}_{net} produced by the cycle and the provided thermal energy \dot{Q}_{in} (equation (2)).

$$\eta_{th} = \frac{\dot{W}_{net}}{\dot{Q}_{in}} = \frac{\dot{W}_{exp} - \dot{W}_{pump}}{\dot{Q}_{in}} \quad (2)$$

Cycle thermal efficiency is generally proportional to the heat source temperature and the size of the system. Larger ORCs tend to be more efficient [9]. Another metric is the heat recovery effectiveness ϵ which quantifies the actual amount of energy extracted from the heat source \dot{Q}_{in} compared to the maximum extractable amount \dot{Q}_{max} , equivalent to the amount of energy removed from the heat source until it is cooled to ambient temperature T_{amb} (equation (3)):

$$\epsilon = \frac{\dot{Q}_{in}}{\dot{Q}_{max}} = \frac{T_{wh,in} - T_{wh,out}}{T_{wh,in} - T_{amb}} \quad (3)$$

With $T_{wh,in}$ the inlet waste heat stream temperature, and $T_{wh,out}$ the outlet waste heat stream temperature. The performance of the ORC depends mainly on the choice of the working fluid, in particular with respect to the heat source, and the cycle architecture. These two design choices are reviewed in the following section.

2.1.3 Architecture and implementation

2.1.3.1.1 General ORC configuration

The basic cycle configuration was presented in the overview of the technology, The following section discusses some more advanced cycle architectures developed to improve overall performance and which tend to be encountered in practice. The gaseous fluid at the turbine outlet needs to be cooled down to low-pressure saturated liquid temperature, and the liquid fluid at the pump outlet requires heating to the high pressure saturated vapour temperature. A common modification to the basic cycle is to recover the heat from the turbine outlet and transfer it to the fluid at the pump outlet via a heat exchanger called a recuperator (also regenerator) to form a so-called recuperated or regenerated cycle. Figure 2a schematically presents the layout of a typical regenerated cycle, and Figure 2b the associated T-s diagram.

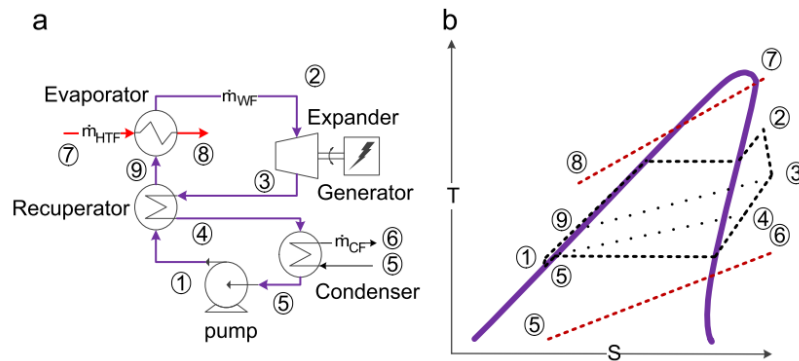


Figure 2 (a) Typical layout and (b) T-s diagram of the regenerated/recuperated ORC process [13]

Turbine bleeding uses part of the hot working fluid to preheat the stream ahead of the evaporator, resulting in an overall increase to efficiency. The working fluid is divided into different pressure levels and processed in two different expanders. Figure 3 shows the typical layout and T-s diagram of the regenerated cycle.

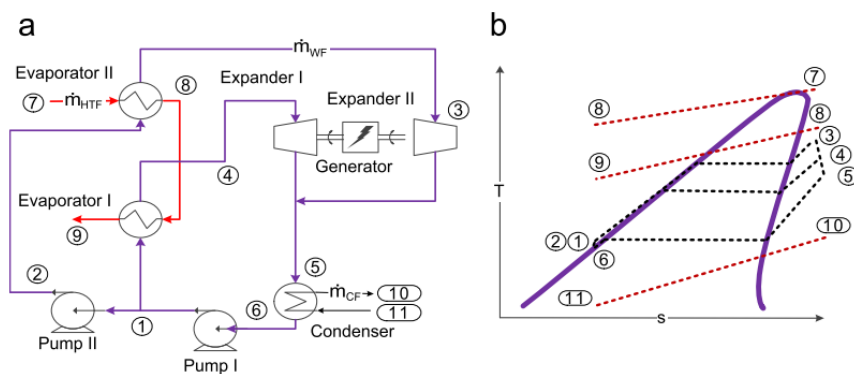


Figure 3 (a) Typical layout and (b) T-s diagram of the bleeder regenerated ORC process [13]

In dual loop or cascaded cycles, two ORCs operating with different working fluids leverage waste thermal energy from different temperature heat sources. This cycle is useful to combine multiple waste heat streams at different temperature levels, a likely scenario in marine energy systems. Figure 4 shows an example layout of a dual loop cycle.

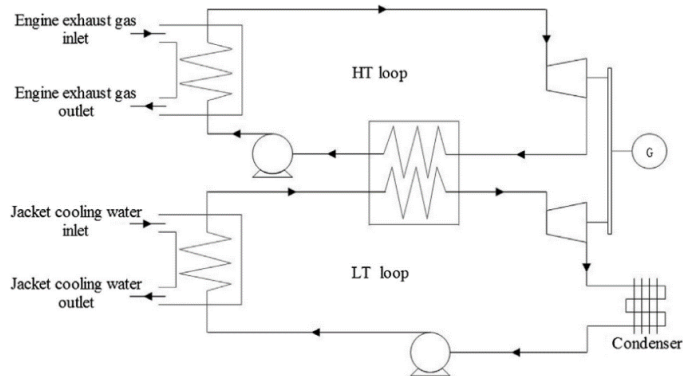


Figure 4 Dual-loop ORC for using multiple waste heat streams [3]

2.1.3.1.2 ORC configurations for marine applications

While the previous section discussed the more general configuration of ORCs, the following section explores the configurations specifically suited to on-board applications. Song et al [14] studied two different configurations that are directly connected to the main engine of a ship (Figure 5a). The first consists of two separate simple ORCs which recover heat from two sources: the exhaust gas and the jacket cooling water. The system was constructed by Tsinghua University and Hangzhou Chinen Steam Turbine Power Co., Ltd. This configuration is complicated, due to the existence of two separate ORC systems, and also requires a lot of space. Thus, in the above study, a modification to the configuration was investigated, consisting of a single ORC, in which the jacket cooling water was used for preheating the working fluid of the cycle and the exhaust gas for driving its evaporation (Figure 5b).

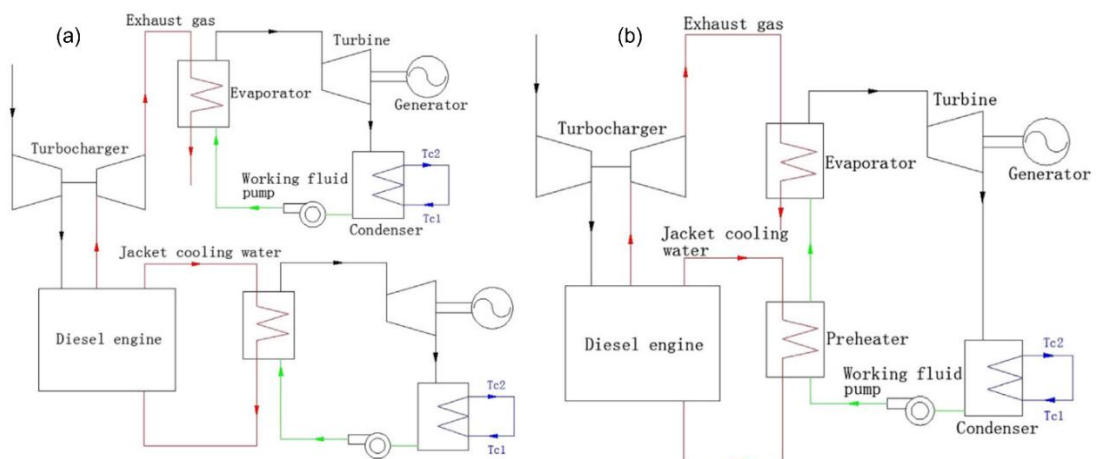


Figure 5 (a) Two separate ORCs driven by exhaust gas and jacket cooling water, (b) ORC configuration with preheater and evaporator [12]

Another configuration was analysed by Lion [15] and is depicted in Figure 6. The configuration is based on a parallel ORC architecture in which heat is received from the exhaust gas of the engine as well as the scavenge air cooler (SAC). The working fluid is pumped at cycle's high pressure and then split into two paths. One part of the working fluid is heated in the first stage of the scavenge air cooler while the other one is heated by the exhaust gas. The two streams are mixed before entering the ORC expander.

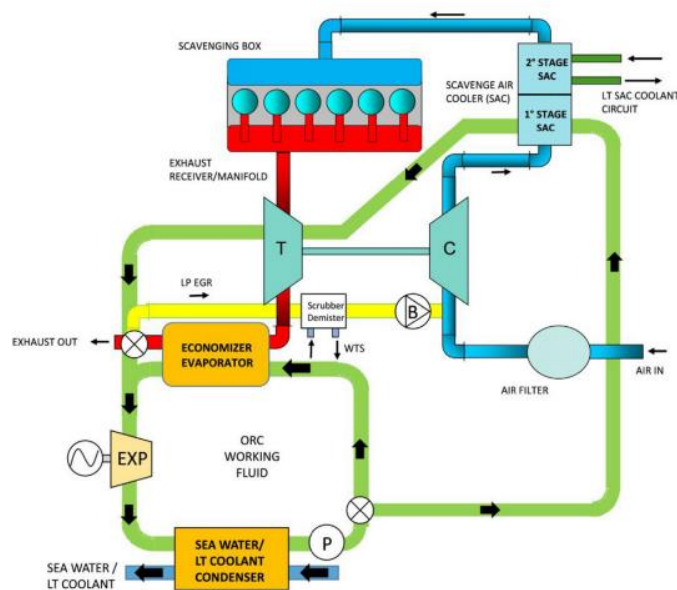


Figure 6 Parallel ORC architecture [15]

A recuperative ORC configuration to recover heat from exhaust gases including an intermediate heat transfer oil circuit was analysed by Casisi [16], shown in Figure 7. Four working fluids are examined: Benzene, Cyclohexane, MDM and Toluene. The net ORC power output, for engine loads varying from 25% to 100%, ranged from 288 to 684 kW_e.

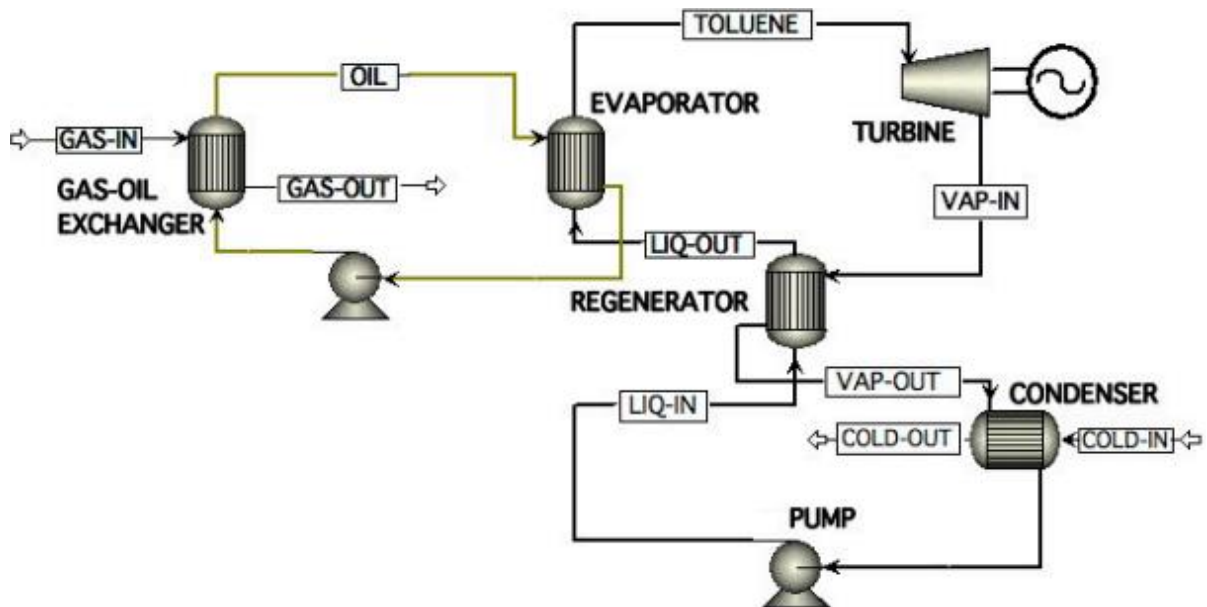


Figure 7 Recuperative ORC configuration [16]

A directly heated recuperative ORC (i.e. without an intermediate heat transfer oil circuit) in which preheating was carried out with the jacket cooling water and evaporation with the exhaust gases was studied by Liu [17], with the process shown schematically in Figure 8. The net power output is approximately 60.5 kW_e and natural hydrocarbons were selected as working fluids, due to their ability to work efficiently at high temperatures.

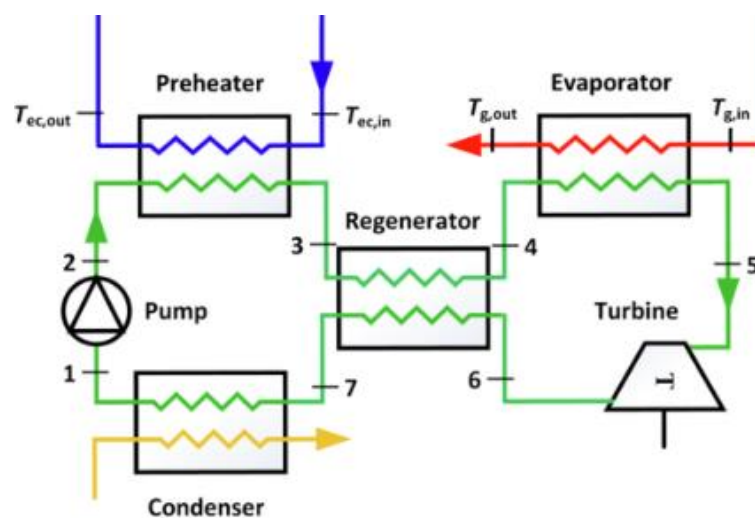


Figure 8 Directly heated recuperative ORC [17]

Mohammed et al [18] investigated an ORC to utilize multiple heat sources from a bulk carrier vessel, shown in Figure 9. The working fluid (R134a or R245fa) is heated in four stages: in the first one, the fluid passes through the lubrication oil heat exchanger and then goes into the jacket cooling water heat exchanger, with inlet temperatures of 65°C and 89°C. Subsequently, in the third stage the working fluid is heated by the scavenge air which exits the compressor of the turbocharger and has an approximate temperature of 140°C. Finally, the working fluid is heated by the exhaust gas before entering the expander. The evaporation pressure of the cycle was varied from 50 to 75 bar to maximise its thermal efficiency.

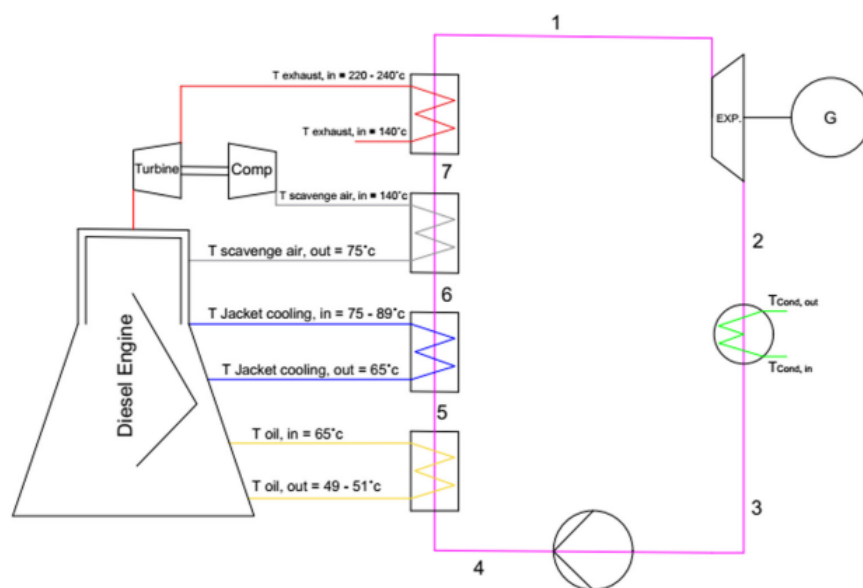


Figure 9 ORC with multiple heat sources [18]

2.1.4 Applications and uses

The principal manufacturers of ORCs as power generation systems are Ormat, Turboden and GE [19,20]. The main applications for ORCs are biomass combined heat and power plants, geothermal, solar and industrial waste heat recovery. Analysis of the waste heat source on ships point towards heat sources in the temperature range 90 – 300°C, in particular the waste heat from engine exhaust gases at 190-300 °C which constitutes 80% of the waste energy (generally after being cooled in a first stage inside the engine turbochargers), and a further 10% in jacket cooling fluids. ORCs with low boiling point working fluids have therefore good potential aboard large marine vessels and have been highlighted in a number of WHR technological reviews [1] .

Leontaritis et al. [21] designed a 5 kW_e experimental small-subscale ORC prototype running with R134a targeted towards maritime applications, specifically for exploiting waste heat from jacket cooling water of auxiliary diesel engines at 82°C and mass flow rate of approximately 1.5 kg/s. The ORC evaporation pressure of the working fluid reaches the 25 bar. The prototype was tested in a laboratory (Figure 10), with a boiler emulating the heat source characteristics. A compact version of this prototype was designed and experimentally tested for long operation, see Figure 11 [22].

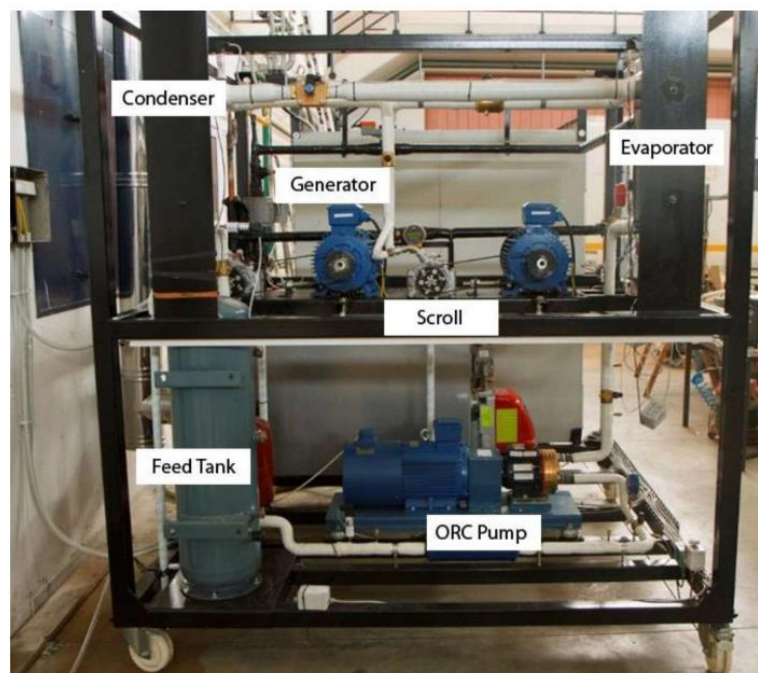


Figure 10 Experimental ORC prototype for naval applications [21]

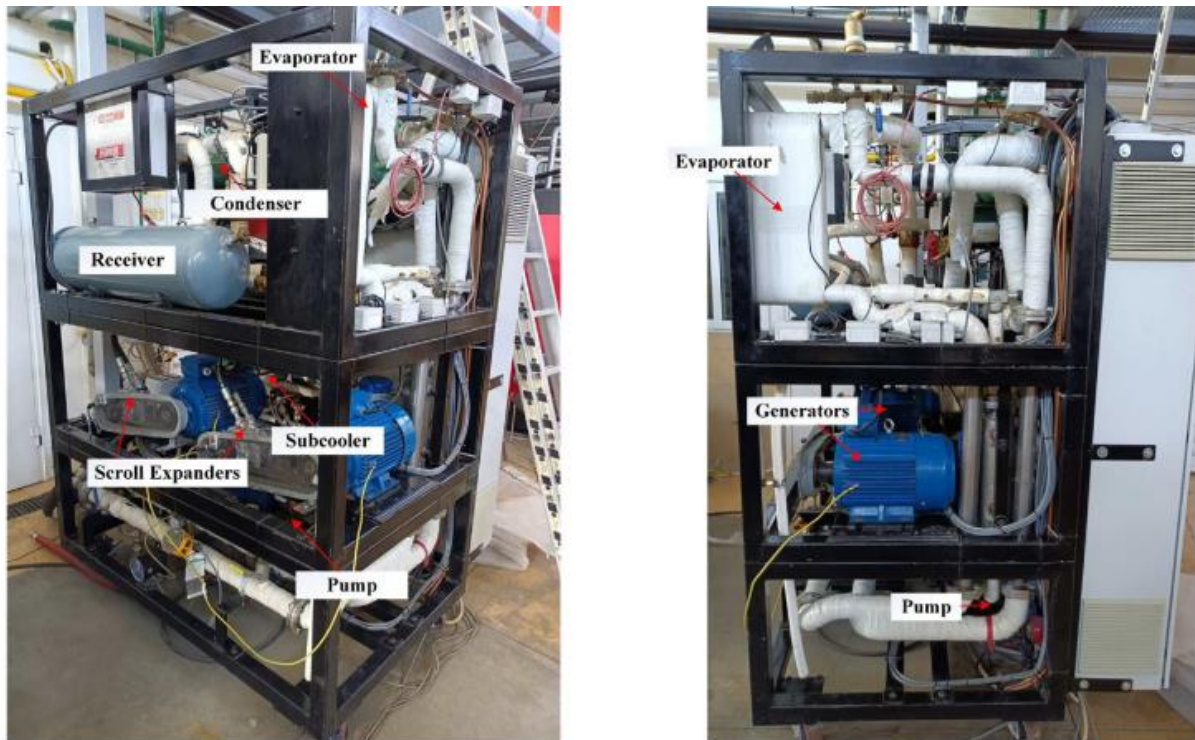


Figure 11 Experimental ORC prototype [22]

Some ORCs built for naval applications can currently be found on the market. Alfa Laval offer the ‘E-Power Pack’ (Figure 12) which are modular, stackable ORC units with rated electrical power output 100 kW_e to 200 kW_e. The product description claims that waste heat sources categorised into jacket water temperatures (75°C to 109°C), saturated steam temperatures (120°C to 180°C), thermal oil (120°C to 180°C) and the engine exhaust gas temperatures (up to 550°C) can power the cycle. The above unit’s weight is either 2300 kg or 4500 kg, depending on the electric output and the maximum module dimensions are 1130mm x 1394mm x 1982mm. Orca-Energy offer a similar product, called ‘Efficiency Pack’ (Figure 12), with electrical power generation ranging from 1 kW_e to 400 kW_e, which uses thermal power inputs of 25 kW to 4,000 kW, respectively. The fluid heat source range from 80 °C to 140°C and gaseous heat source temperatures are above 150°C.

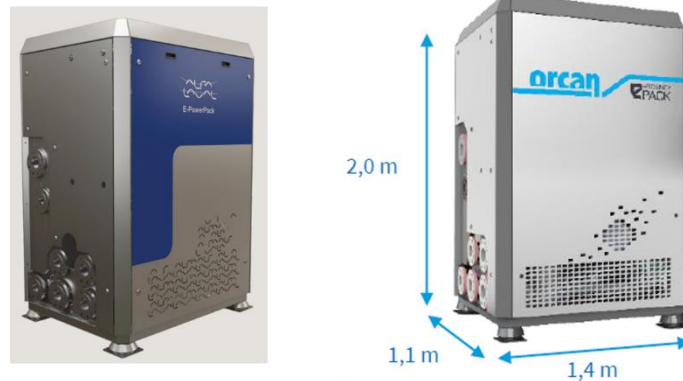


Figure 12 ORC modules for naval applications, left: Alfa Laval 'E-Power Pack', [23], right: Orcan-Energy ePM 050.100 'Efficiency Pack' [24]

In partnership with Mitsubishi Heavy Industries [25], Caltenix Technologies developed the Hydrocurrent™ Organic Rankine Cycle Module 125EJW (Engine Jacket Water), an ORC designed to use marine engine jacket water at 80-85°C as the heat source with R245fa as designed working fluid and deliver a gross power output of 125 kW_e [26]. The entire device measures 0.250m x 0.137m x 0.230m i.e. 7.9 m³ and weighs 3,738 kg. The process layout is shown in **Figure 13**. The condenser and evaporators are designed as brazed plate heat exchangers, with sea water being used as the heat sink for condensation. The expander/turbine train is an IPM Carefree Integrated Power Module (IPM), which consists in a radial turbine directly integrated with a generator in a single unit. The pump is 3-phase, 2-pole and is rated 7.5 kW_e, which with the 125 kW_e gross power output of the generator results in a net power generation of 119 kW_e at design conditions [27].

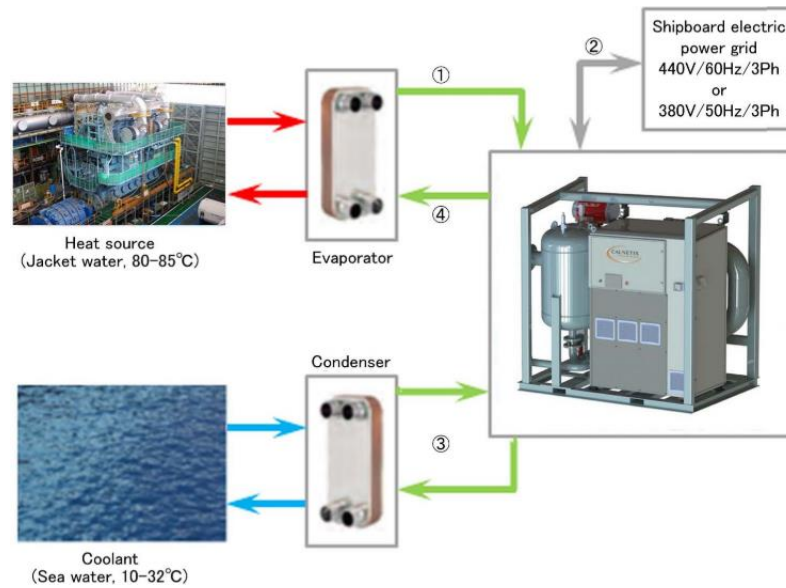


Figure 13 Process layout for the Hydrocurrent™ Organic Rankine Cycle Module 125EJW

Below, some commercial ORC products are discussed. These products are not designed for ships, but could be adjusted to exploit the waste heat from marine diesel engines. Enogia [28] offers a variety of products of ORC with nominal capacity from 10-180 kW_e. The products are: ENO-10LT, ENO-20LT, ENO-40LT, ENO-100LT and ENO-180LT. They are designed to use exhaust gas and water up to 120°C. Dimensions of the bigger ORC product ENO-180LT (shown in Figure 14) are 2.3m x 2m x 2.6m (11.96 m³ volume) and its weight is 7,500kg. The designed working fluid is R1233zd(E) and the expected lifetime is about 20 years. Heat exchangers are brazed plate type, the expander is a kinetic turbine, and the pump is of multi-stage magnetic coupling type, shown in [28].

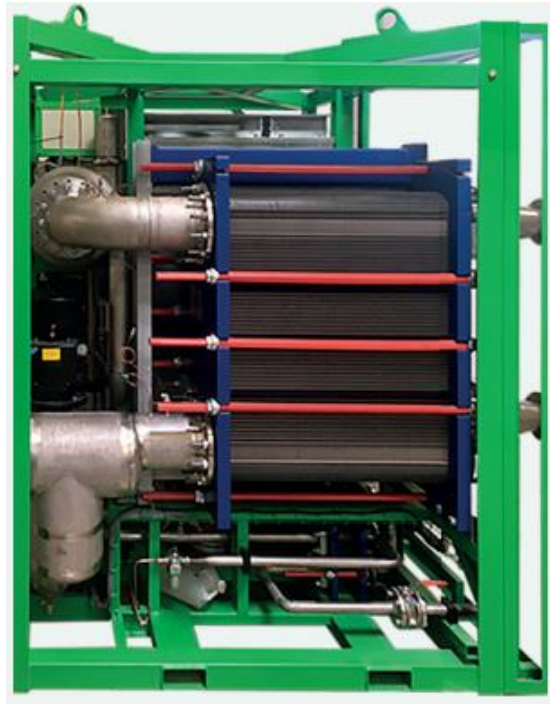


Figure 14 Enogia ENO-180LT [26]

Moreover, Enerbasque [29] has made a product called HRU-25, which is an ORC designed to convert waste heat at the range of 85-95 °C with a maximum electric power 25 kW_e that is suitable for waste heat recovery from jacket cooling water from a ship's main engine. The unit's maximum efficiency is 7.8% with 33 m³/h hot water flow whereas the total thermal power absorbed by the system is 275 kW_{th}. The heat exchangers are shell and tube type, but the configuration can also be fitted with plate types. The dimensions of the ORC are 3.15m x 2.38m x 1.75m (13.12 m³) and weighs about 2,100 kg. A general overview of the HRU-25 can be seen in Figure 15.



Figure 15 Enerbasque HRU-25 [27]

Lastly, the MT1 by Rank [30] is an ORC which is fitted to a container, generates electricity up to 20 kW_e and exploits heat sources at temperatures 150°C (see Figure 16). The heat exchangers are plate type, the dimensions are 3.35m x 1.55m x 2.2m (11.42 m³) and the weight is 5,500kg. Lastly, in this unit the heat produced in the condenser can be used at temperatures up to 50 °C and is available to several application up to 150 kW_{th}.



Figure 16 Rank MT1 [28]

2.1.5 Techno-economics

Table 1 shows the a summary of techno-economic parameters for on-board ORCs driven by engine waste heat. The basis for most of these results are simulations, as examples of practical applications of on-board ORCs are sparse. The technical performance parameters are those described earlier in **section 2.1.2.2**, while economic performance is measured by specific cost, relating to the ORC plant capacity.

Table 1 Techno-economic parameters of on-board maritime ORC applications

| Ship / Engine | Total Engine Power [kW] | Heat Source | Heat Source Temp [°C] | Layout | Working Fluid | Net Power Output [kW] | η_{th} | Specific Cost [€/kW] | Ref |
|----------------------|-------------------------|--------------|-----------------------|--------------------|--------------------|-----------------------|-------------|----------------------|------|
| LNG carrier | 23,375 | Cooling Fuid | 82.8 / 51.9 | Basic | R-245ca | 426.90 | 7.39% | | [31] |
| LNG carrier | 23,375 | Cooling Fuid | 82.8, / 51.9 | Basic | R-245fa | 424.60 | 7.33% | | [31] |
| LNG carrier | 23,375 | Cooling Fuid | 82.8 / 51.9 | Basic | R-227ea | 397.10 | 6.62% | | [31] |
| Diesel Engine (6cyl) | 1,000 | EG+JCW | 300 / 90 | 2 Heat Sources ORC | Cyclohexane | 95.70 | 20.75% | | [14] |
| Diesel Engine (6cyl) | 1,000 | EG+JCW | 300 / 90 | 2 Heat Sources ORC | Benzene | 93.35 | 20.22% | | [14] |
| Diesel Engine (6cyl) | 1,000 | EG+JCW | 300 / 90 | 2 Heat Sources ORC | Toluene | 92.15 | 19.95% | | [14] |
| Diesel Engine (6cyl) | 996 | EG+JCW | 300 | Two separated ORC | R245fa | 101.1 | 10.20% | 2000 | [14] |
| Passenger Cruise | 23,400 | EG | 190 | Regen. | Toluene | 481.99 | 20.90% | | [32] |
| Passenger Cruise | 23,400 | EG | 190 | Regen. | Methyl cyclohexane | 426.86 | 18.50% | | [32] |
| Passenger Cruise | 23,400 | EG | 190 | Regen. | Ethylbenzene | 425.65 | 18.40% | | [32] |
| Passenger Cruise | 23,400 | EG | 293.15 | Regen. | Benzene | 395.73 | 22.00% | | [33] |

| | | | | | | | | | |
|-----------------|-------------|-------------------|---------------------|--------------------|---------------------------|------------|-------------|---------|---------|
| Wartsila ME+AE | 5850 / 2760 | EG (ME+AE) | 315 | Basic | R123 | 625.28 | 16.38% | 4470.82 | [34] |
| - | - | EG | Up to 550 | - | - | 100 or 200 | ~10-20% | - | [23] |
| - | - | JCW | 75 - 109 | - | - | 100 or 200 | ~10-20% | - | [23] |
| - | 80,080 | EG | 160 | Basic | R236fa /R245fa | 994.48 | 8.43% | 2714.99 | [35] |
| - | 80,080 | EG | 160 | Basic | R236fa /R1234ze | 1013.37 | 8.28% | 2812.40 | [35] |
| - | 80,080 | EG | 160 | Basic | R600 /R1234ze | 971.49 | 8.44% | 2727.77 | [35] |
| - | 1,000 | EG(HT) +JCW(LT) | 300(HT) /90(LT) | Dual Loop | Water(HT) /R123(LT) | 100.50 | 10.13% | - | [36] |
| - | 1,000 | EG(HT) +JCW(LT) | 300(HT) /90(LT) | Dual Loop | Water(HT) /R236fa(LT) | 115.10 | 11.60% | - | [36] |
| - | 1,000 | EG(HT) +JCW(LT) | 300(HT) /90(LT) | Dual Loop | Water(HT) /R245fa(LT) | 103.90 | 10.47% | - | [36] |
| - | 16,600 | EG | | Simple | R1233zd(E) | 771.00 | | - | [15] |
| - | 16,600 | EG | | Simple | R1233zd(E) | 848.00 | | - | [15] |
| - | 16,600 | EG+SAC | | Dual Loop | R1233zd(E) | 584.00 | | - | [15] |
| - | 16,600 | EG+SAC | | Dual Loop | R1233zd(E) | 678.00 | | - | [15] |
| - | 1,950 | JCW | 80 | Basic | R245fa | 125.00 | 6.20% | - | [25–27] |
| - | 4700 | EG | 350 | Regen. | Toluene | 364 | 25.80% | 2919.23 | [16] |
| Wärtsilä 6L50DF | 5700 | Thermal oil (EG) | 145 | Regen. | Toluene | 684 | 26.70% | - | [16] |
| Wärtsilä 6L50DF | 5700 | Thermal oil (EG) | 174 | Basic | Toluene | 364 | 20.60% | - | [16] |
| ME 6S50 MC-C7 | 10,100 | EG, SAC, JCW, Oil | 240 / 140 / 89 / 65 | 4 Heat Sources ORC | R134a | 3398.7 | 41.10% | - | [18] |
| - | 996 | EG, JCW | 207 / 97 | Dual loop | Wet steam(HT) /R236fa(LT) | 115.1 | 13.1%/10.8% | - | [29] |

Based on literature articles, commercial product information, and reports, the main techno-economic parameters of some selected ORCs are presented in Table 1. A first observation that can be made is the wide range of temperatures of the available heat sources. Exhaust gases, cooling fluids (charge air or

jacket water) and lubricating oils are all waste heat carriers inside naval energy systems, and due to the range of potential working fluids could all be leveraged to power an ORC. Exhaust gases constitute the majority of the waste heat (roughly 80%), however their temperatures vary substantially depending on the existence of already in-place WHR methods (turbochargers etc.) and the variation in engine load from the different engine operation speeds. The variation in engine also affects the mass flow rate of the exhaust gases [16], which potentially complicates the design of the primary heat source heat exchanger at the evaporator stage. More advanced ORC cycles such as dual loop ORCs can harvest multiple waste heat streams at once, and these cycles exhibit high efficiency. Cycle efficiency of various ORC cycles designed for marine energy systems as a function of system net power output can be seen in Figure 17. Overall efficiencies can be expected in the range 5% to 25%.

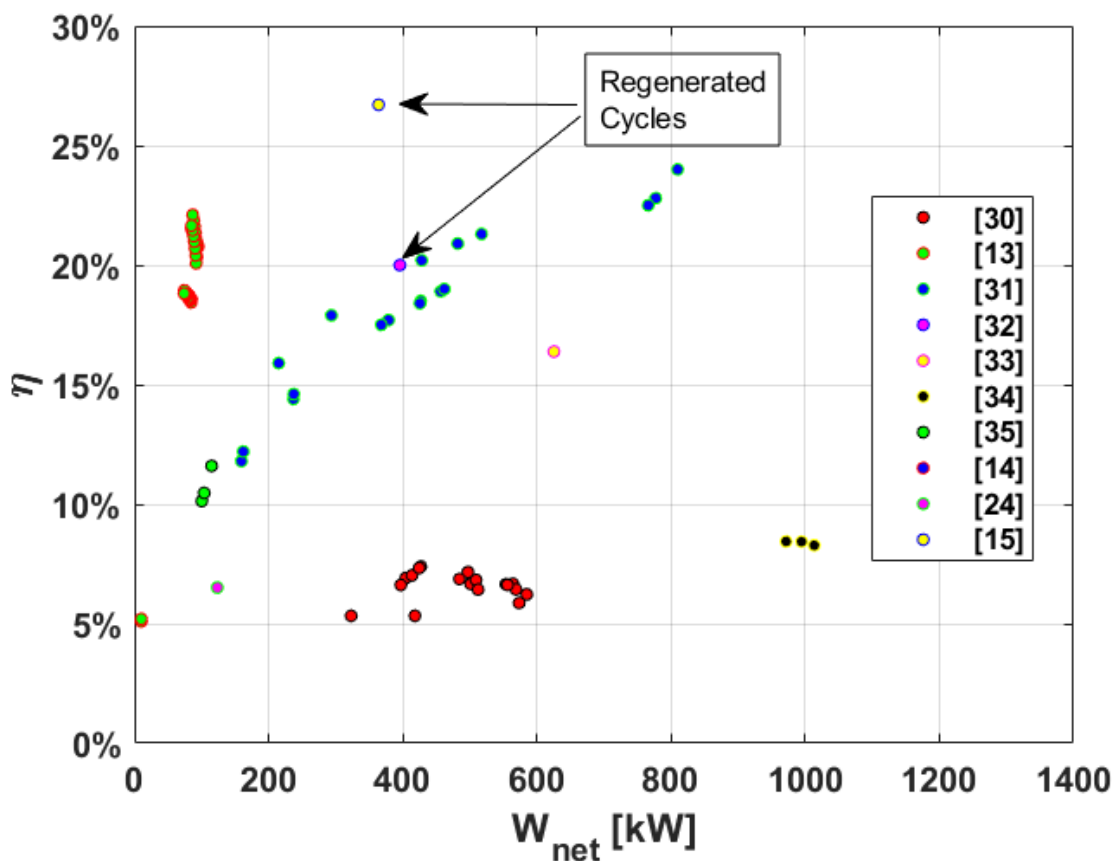


Figure 17 Thermal efficiency of on-board ORC cycles as a function of net power output

The economics of the generalised ORC are well studied in the literature through many studies and years of industrial and commercial implementation [19,37]. However, only in a small number of studies have the economics of ORCs for naval applications been analysed. The calculated specific cost of maritime ORCs at design conditions from three different studies [16,34,35] is shown in Figure 18 along with the calculated specific cost of ORCs for heat recovery in non-naval applications, taken from the review by Lemmens [37]. In two of these studies based on modelling work, cost functions from Turton et al. [38] are adjusted and used to calculate ORC economic performance. In the third, cost of components and balance of the system were taken from Aspen Tasc (r) and from manufacturer information.

In Shu et al.'s study [34], payback periods between 4 and 8 years were calculated depending on the working fluid. They estimated that the expander would represent the highest share in total cost (44% to 52% of total capital cost, depending on the fluid), followed by the evaporator (21% to 22%), the pump (13% to 19%) and the condenser (12% to 17%). In Yang's study [35], in the best cases, payback periods around 5.8 years were calculated, with specific cost of ORC around $\sim 4,500$ €/kW_e. In Casisi's study [16], the cost of individual components were obtained from manufacturer information, and summed along with a balance of system costs, and a 20% markup. The system cost was $\sim 10^6$ € for a 520 kW_e power output (design conditions at 100% engine load), which resulted in a specific cost of 2,214 €/kW_e and a payback period of 5-6 years depending on the underlying assumptions.

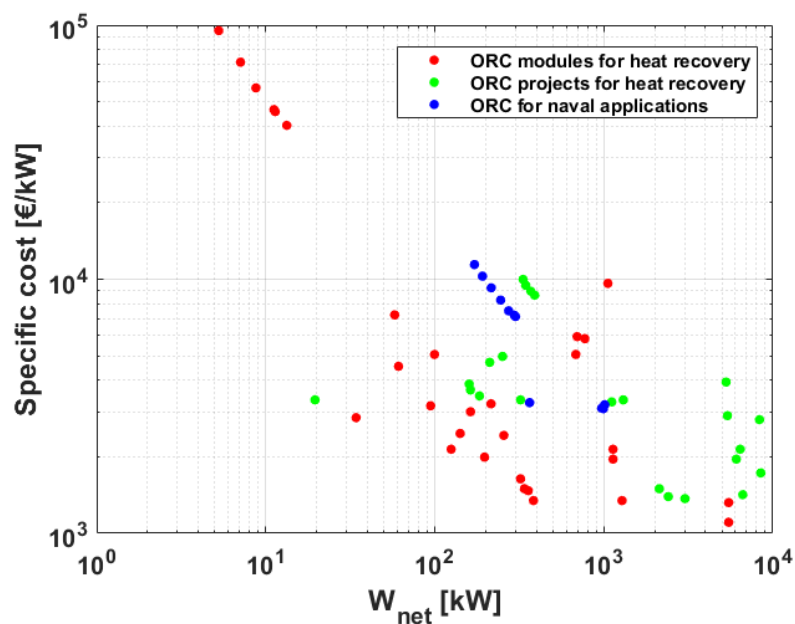


Figure 18 Specific cost of ORC modules and projects, and of ORC for naval applications. Economic data for ORC for heat recovery from [37], data for naval ORCs from [16,34,35]

2.1.6 Modelling organic Rankine cycles

The amount of energy absorbed by the ORC, $F_{ORC}(t)$, is expressed as a linear function (or piecewise linear function) of the net power drawn from the ORC, $P_{ORC}(t)$, using the performance indicator η_{ORC} (equation (4))

$$F_{ORC}(t) = \frac{1}{\eta_{ORC}} P_{ORC}(t) \delta_{ORC}(t) \quad (4)$$

Where η_{ORC} is the thermal efficiency of the ORC.

The power drawn from the ORC is constrained in Equation (5) using a rated design for ORC D_{ORC} , with upper and lower bounds indicated with variables $k_{3,ORC}$ and $k_{4,ORC}$. $x_{ORC}(t)$ is a binary decision variable which indicates whether the ORC is included or excluded in the energy system.

$$k_{3,ORC} D_{ORC} x_{ORC}(t) \leq P_{ORC}(t) \leq k_{4,ORC} D_{ORC} x_{ORC}(t) \quad (5)$$

2.2 Sorption Refrigeration & Desalination

2.2.1 Introduction

Sorption is a reversible thermochemical or thermophysical reaction used as the basis for certain technologies to produce cold power, clean water, or both simultaneously in hybrid systems, among other thermal effects. The working principle of sorption is the ability of a porous material to capture water vapour or some other gas and crystallise it onto its surface. **Sorption refrigeration** leverages the low evaporation temperature at low partial pressure of a refrigerant. Heat can be removed from a heat transfer fluid to evaporate this refrigerant and bring the heat transfer fluid down to low temperatures (-2°C to 5°C), which is the intended cooling effect of the cycle. The temperature of the generated cold stream therefore depends on the evaporation temperature at low partial pressure of the refrigerant. During **sorption desalination**, sea water is consecutively evaporated, adsorbed then desorbed into and from a sorbent material, and condensed back into clean desalinated water. In such sorption systems, sea water is used as the refrigerant. Thermal energy is required to regenerate the adsorbent material and desorb the water for condensation. **Sorption refrigeration and desalination** makes use of the two above technologies in a single hybrid system. The minimum temperature of the generated cold stream is limited by the evaporation temperature of sea water at low partial pressure, such that the cold stream

in these hybrid systems is intended for air conditioning and chilling rather than actual refrigeration as suggested by the name.

2.2.2 Technology overview

2.2.2.1 Basic cycle configuration

An adsorption refrigeration & desalination process contains three essential components (Figure 19). A low pressure and low temperature liquid sorbate (water) is turned to vapour in an **evaporator** by extracting heat from the surroundings, provided by a chilled water flow (which is cooled as a result). The refrigerant in the vapour state is flown into an **adsorber bed** where the sorption process takes place. In refrigeration systems, the choice of sorbate affects the temperature at which evaporation occurs and therefore the type of cooling effect obtained from the sorption cycle [39]. Water and ammonia are good candidates for refrigeration as evaporation can occur down to 0 °C and -60 °C respectively. In any adsorption system where desalination occurs, water is always the refrigerant. The water is later removed from the sorbent material (the device is referred to as a **desorber** during this mode of operation). In practice, adsorption and desorption cannot be carried out simultaneously; therefore in order to generate cooling continuously, two adsorbers need to be operated asynchronously in a so-called two-bed system such as shown in the schematic example. The desorbed water is transported in the vapour state into a **condenser** through natural convection where it is condensed using cooling water (CW) into a two-phase liquid/vapour state.

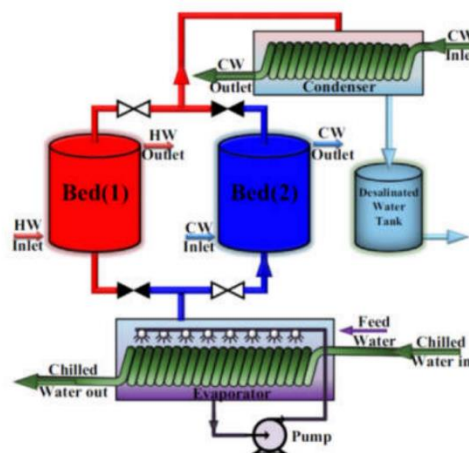


Figure 19 Schematic representation of the hybrid refrigeration/desalination cycle, using a two-adsorber bed system for continuous operation [40]

2.2.2.2 Performance metrics

The typical performance metric for refrigeration systems is the thermal coefficient of performance (COP). In traditional vapour compression systems, this metric would be the ratio of cooling effect to work provided to the compressor. In a sorption refrigeration system, the COP becomes the ratio of cooling effect to heat provided (equation (6)):

$$COP = \frac{Q_{cooling}}{Q_{heat\ source}} \quad (6)$$

Where $Q_{cooling}$ [kJ] is the cooling effect obtained at the evaporator, and $Q_{heat\ source}$ [kJ] the thermal energy provided to regenerate the sorbent. Two other frequently used metrics are Energy Efficiency Ratio (EER) and Specific Cooling Power (SCP). EER is the ratio of cooling energy over electricity required to operate the cycle (i.e. auxiliaries like such as pumps, valves etc..) (equation (7)):

$$EER = \frac{P_{cooling}}{E_{aux}} \quad (7)$$

SCP [kW/kg] is the specific cooling power i.e. the amount of cooling power per unit mass of sorbent (equation (8)):

$$SCP = \frac{Q_{cooling}}{m_{sorb} \tau_{cycle}} \quad (8)$$

Where m_{sorb} [kg] is the sorbent mass and τ_{cycle} [s] is the cycle time. SCP can be also weighted to the volume of the adsorption machine. In the case of the hybrid cooling/desalination adsorption system, the desalination performance of the system is measured with the Specific Daily Water Production (SDWP) [m³/(kg_{sorb} day)], expressed as (equation (9)) [41]:

$$SDWP = N_{cycle} \int_0^{\tau_{cycle}} \frac{\dot{Q}_{cond}}{\rho_w h_{fg}(T_{cond}) m_{sorb}} dt \quad (9)$$

Where N_{cycle} [1/day] is the number of cycles per day, calculated as $N_{cycle} = 86400 \text{ [s/day]} / \tau_{cycle}$, $h_{fg}(T)$ [kJ/kg] is the latent heat of vaporisation of water at temperature T , m_{sorb} [kg] is the mass of adsorbent, ρ_w [kg/m³] is the water density and \dot{Q}_{cond} [kW] is the heat transfer rate at the condenser..

2.2.3 Architecture and implementation

2.2.3.1 Standard systems

The adsorption and cooling desalination technology can be implemented employing different approaches and exploiting different architectures. The most common one is based on the two-beds architecture, as represented in Figure 20, where two adsorbent beds are operated in counter-phase, to continuously produce cooling and desalinated water. This architecture can be improved further, using heat recovery process between the beds, to increase the thermodynamic efficiency of the process.

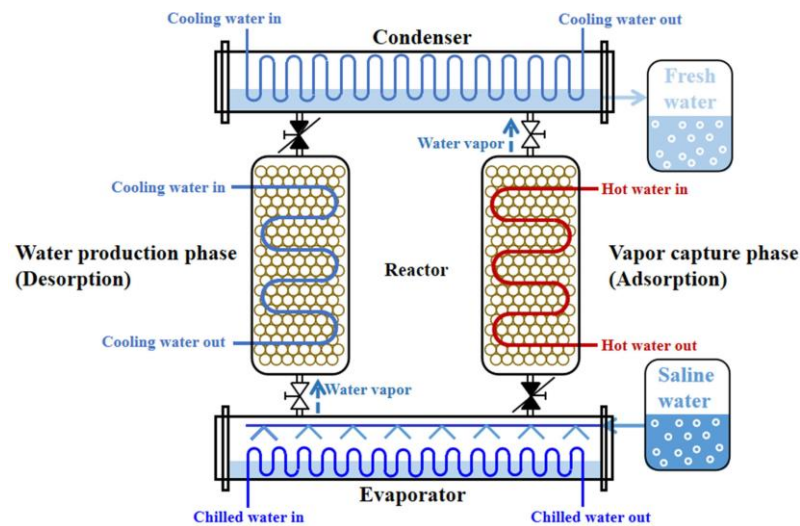


Figure 20 Standard two-beds adsorption cooling and desalination architecture [42]

Among the possible improvements of the technology architecture, one of the most commonly investigated is the four-beds one, as represented in Figure 21. This configuration allows to exploit most of the enthalpy of the driving heating source, by operating two adsorbers in series, even employing different adsorbent materials, thus exchanging a larger amount of water per cycle.

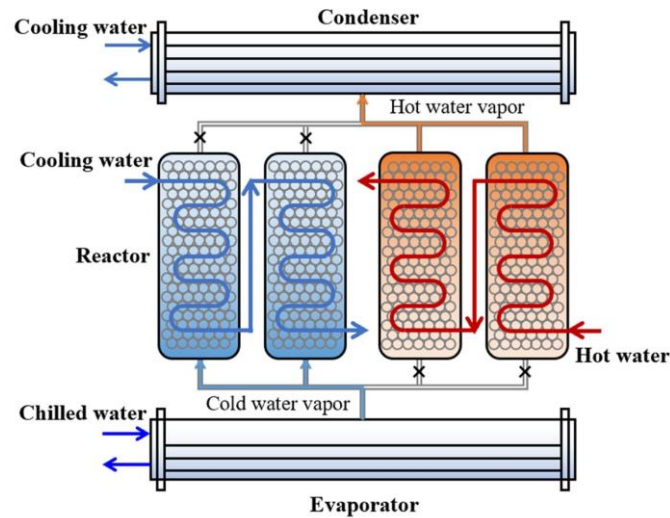


Figure 21 Four-beds adsorption cooling and desalination architecture [42]

The research and development surrounding hybrid sorption refrigeration and desalination systems is primarily driven by the need to displace the more traditional vapour compression system which tend to use environmentally damaging refrigerants (such as R22) and need to be phased out, and the on-board need for fresh water. However, compressor driven systems offer unique advantages such as their fast and precise response to varying loads, to which sorption systems tend to respond discontinuously. On the other hand, sorption systems require less moving parts, less electrical energy (only needed to drive auxiliaries), and use thermal energy as the main energy input which is abundant on diesel engine propelled ships [6]. Thus, several of the envisioned architectures on ships couple sorption cycles to existing compression vapour cycles to leverage the benefits of both technologies, at the cost of increased space and weight occupied by the system and the additional penalty on fuel consumption. The following section reviews some of the system architectures proposed to integrate sorption refrigeration to vessel energy systems.

2.2.3.2 Cascade systems

The layout of the cascade system, studied by Palomba et al. [43], is shown in Figure 22. An adsorption chiller in a basic configuration acts as a topping cycle by using hot engine exhaust gases as the heat source for desorption, and sea-water as the cooling/condensing fluid, to produce chilled water. This cold stream is then used to cool the condenser of a traditional vapour-compression refrigeration system

which operates as a bottoming cycle. The cooling effect produced in the vapour-compression cycle's evaporator is sent to the ship's cooling load (cold storage for fish in this case study).

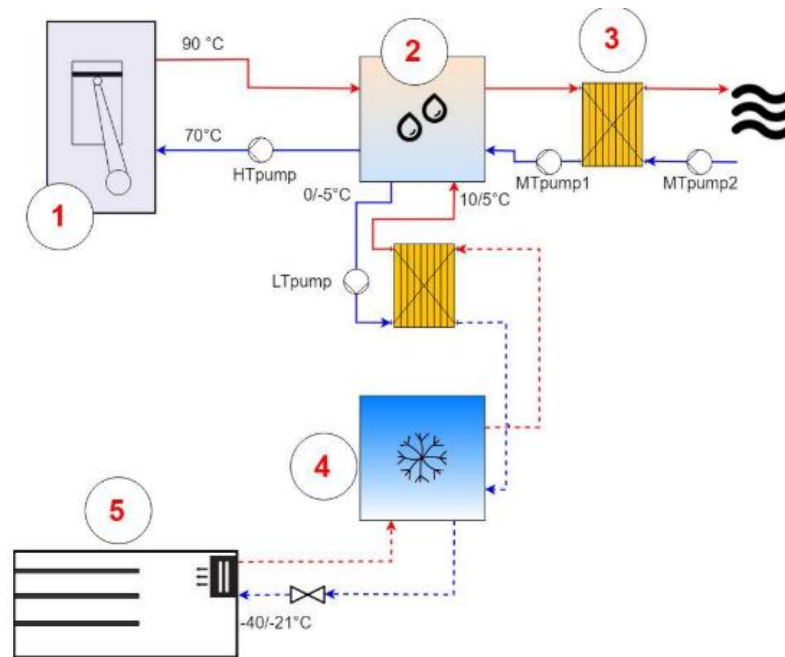


Figure 22 A sorption refrigeration system as a topping cycle using exhaust waste heat, with a compression vapour cycle operating as a bottoming cycle in a cascade layout. Numbers on the diagram refer to 1: engine and exhaust heat, 2: sorption chiller, 3: condenser heat exchanger using seawater, 4: vapour compression chiller, 5: cold storage [43]

2.2.3.3 Series hybrid system

The configuration employing a series connection between sorption and compression machine, Figure 23, is more relevant whenever both cooling and refrigeration loads are simultaneously present on-board. In those cases, the adsorption machine can be used either to cover the base load or to provide a cooling effect along with the compression machine. Usually it allows to achieve higher flexibility in operation thanks to the possibility of modulating the operation for the compression machine, thus reducing the electricity consumption as much as possible.

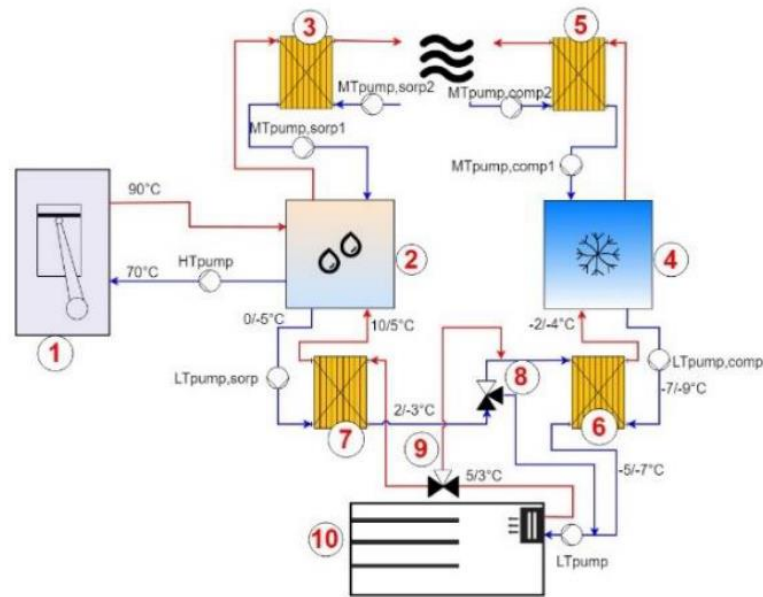


Figure 23 Cooling hybrid configuration with series connection between sorption and compression system. 1—engine; 2—sorption chiller; 3—seawater condensing heat exchanger for sorption chiller; 4—vapour compression chiller; 5—seawater condensing heat exchanger for compression chiller; 6—brine heat exchanger for compression chiller; 7—brine heat exchanger for sorption chiller; 8—9—three way valves for series operation; 10—cold room [43]

2.2.4 Applications and uses

Adsorption cooling and desalination technology is still in a developmental stage. In the literature there are some relevant studies reporting about the realization and testing of lab-scale installation for the validation of the technology. For instance, Sztekler et al. [44] developed an experimental laboratory-scale prototype of a combined chilling-desalination adsorption device, with roughly 1.1 kW cooling capacity, using a three-bed configuration, employing silica gel as adsorbent material, which is the most commonly employed due to the low cost and achievable good performance. Through a series of studies they presented the performance of the device, which can be seen in Figure 24, with various operating conditions, demonstrating the possibility of achieving COP up to 0.6 and SCP higher than 150 W/kg.



Figure 24 Experimental prototype of a three-bed hybrid chilling (1.1 kW) and desalination adsorption device, front view (top picture) and back view (bottom picture) [44]

One of the first large-scale prototypes was presented by Thu et al. [45], employing four-beds configuration with silica gel as adsorbent and implementing an internal heat recovery strategy to maximize the overall efficiency. Figure 25 represents the installation of the system at lab-scale. The prototype was operated under different conditions, varying the driving temperature in order to demonstrate the feasibility of operation at temperatures as low as 70 °C. The results confirmed the possibility of achieving SDWP ranging from 4.27 m³/(tonne day) at 50 °C driving temperature up to 13.46 m³/(tonne day) at 85 °C. Those results were only achieved when the new control strategy was applied. More recently, other adsorbent materials were proposed, such as innovate composites based on silica gel and ionic liquids, which could dramatically reduce the driving temperature of the process down to 50 °C [46,47]. Further investigations will be needed at large scale, to validate the applicability of such a class of materials under real operating conditions.

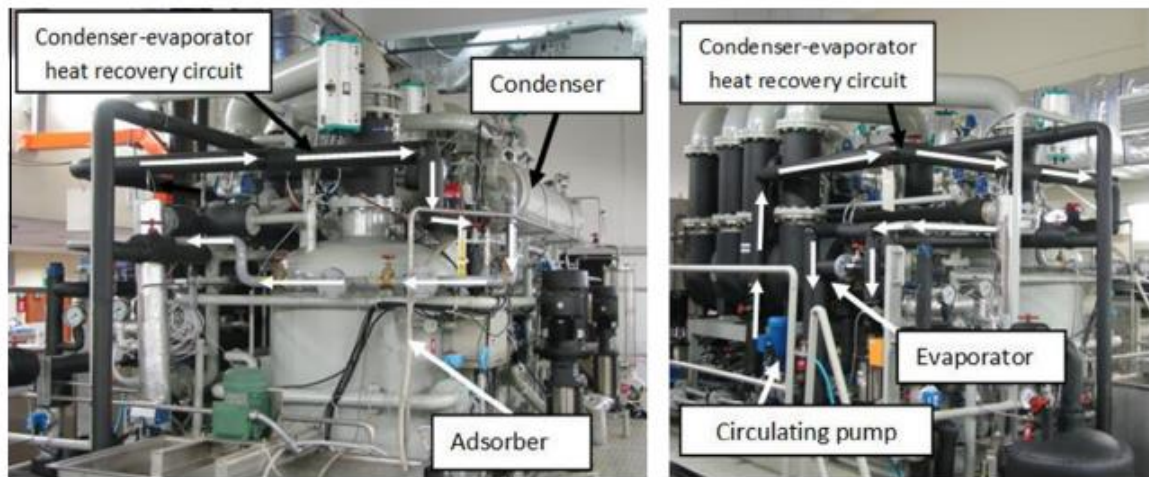


Figure 25 Overview of the four-beds AD cycle showing the heat recovery between the condenser and the evaporator [45]

2.2.5 Techno-economics

Simultaneous sorption desalination and cooling in the same device is a novel developmental technology, and therefore techno-economic data is largely absent. The most viable strategy to evaluate the techno-economic performance is to consider the device primarily as a refrigeration/cooling device, with desalinated water as a secondary added benefit, and derive the techno-economics from pure sorption cooling / refrigeration. It should be mentioned however that the desalination feature would imply (a) an increase in initial investment due to higher device complexity and due to maintenance (to remove precipitated salt from the sorbent), and (b) the added benefit of saving fuel / power on other desalination technologies, such as powering multi-flash desalination.

Table 2 CAPEX and power rating for different adsorption chillers

| Model | Cooling Power [kW] | CAPEX [€/kW] | Ref |
|-------------------------------------|--------------------|--------------|------|
| InvenSor LTC30 e plus | 10 - 35 | 1,327 | [48] |
| SorTech eCoo 2.0 Silica Gel IP20 | 16 | 1,188 | [49] |
| Unnamed Silica gel / water adsorber | 8 | 1,331 | [50] |

According to adsorption technology experts, current cooling adsorption devices in Europe go up to a maximum power rating of 100 kW. Due to the system being based on sorbent beds, the technology is more feasibly scaled down than scaled up (differently from absorption chillers where larger volumes of liquid for absorption are more economically viable). Typical investment costs and cooling power rating for various adsorption chillers are shown in Table 2.

2.2.6 Modelling adsorption refrigeration & desalination

Due to the lack of experimental data on a prototype developed both for cooling and desalination provision, for the first stage of the project a simplified modelling approach was selected, by exploiting experimental outcomes obtained on an adsorption chiller tested at CNR ITAE lab in the framework of a previous EU-funded project, HYBUILD [51]. The tested machine was based on a two-bed configuration with zeolite SAPO-34 as adsorbent material. It was tested under lab-scaled controlled conditions as reported in [52]. For the specific case of ZHENIT, the experimental dataset was considered limiting the driving temperature of the process at 85 °C, since on-board of a vessel this driving temperature should be guaranteed. Once this operating condition was fixed, the experimental data were fitted with linear and polynomial equations, using as a fitting parameter the temperature difference between the inlet temperature at the condenser/adsorber (MT_{in}) and the outlet temperature from the evaporator (LT_{out}), also defined as evaporator-condenser temperature lift: ΔT_{ec} .

The obtained equations to characterize an adsorption cooling and desalination machine are as follows (coefficient of performance in **equation (10)**, specific cooling power in **equation (11)** and specific daily water production in **equation (12)**):

$$COP = -0.0004 \Delta T_{ec}^2 - 0.0023 \Delta T_{ec} + 0.65 \quad (10)$$

$$SCP \left[\frac{kW}{kg} \right] = -0.0082 \Delta T_{ec} + 0.473 \quad (11)$$

$$SDWP \left[\frac{kg_w}{kg_{sor} \text{ day}} \right] = -0.2952 \Delta T_{ec} + 17.028 \quad (12)$$

While the water production is maximised for lower ΔT_{ec} values, the minimum feasible temperature difference is around 5 K. The practical operational value for ΔT_{ec} in the on-board energy system is in the range 20 K to 25 K, based on discussions with the technology developers at CNR-ITAE.

The amount of energy absorbed by the SCD, $F_{SCD}(t)$, is expressed as a linear function (or piecewise linear function) of the net power drawn from the waste heat exiting the engine, $P_{SCD}(t)$, using the coefficient of performance (COP) of the system (equation (13)). $\delta_{SCD}(t)$ is a binary decision variable which indicates whether the SCD is on or off at time t .

$$F_{SCD}(t) = \frac{1}{COP} P_{cool,SCD}(t) \delta_{SCD}(t) \quad (13)$$

The cooling power produced by the SCD is constrained in Equation (14) using a rated design for SCD, D_{scd} , with upper and lower bounds indicated with variables $k_{3,SCD}$ and $k_{4,SCD}$. $x_{SCD}(t)$ is a binary decision variable which indicates whether the SCD is included or excluded in the energy system.

$$k_{3,SCD} P_{cool,scd}^{min} x_{SCD}(t) \leq P_{cool,SCD}(t) \leq k_{4,SCD} P_{cool,scd}^{max} x_{SCD}(t) \quad (14)$$

2.3 Thermal Energy Storage

2.3.1 Introduction

Thermal energy storage (TES) is a technology designed to resolve the mismatch between the availability of thermal energy at a certain heat source, and the heat demand elsewhere. Time discrepancy between the supply and demand for heat is a non-negligible source of system-level inefficiency. For example, renewable thermal energy sources such as solar or waste heat are often characterised by their intermittency, and without storage their potential is limited to the immediate heat demand, with any unstored energy being lost [53]. Aboard marine vessels, the time-profiles of available waste heat from the engine exhaust, and of the on-board energy demand are very likely to be mismatched, and TES is an obvious solution to smooth out the fluctuations of the engine thermal losses. In this way TES can be a key element to the synergistic implementation of multiple WHR technologies within an energy system.

Broadly speaking there are three classes of TES each based on their own physical phenomenon: sensible thermal energy storage (STES) relies on increasing the temperature in the thermal mass of a material, latent thermal energy storage (LTES) leverages the phase change enthalpy during a phase transition of a so-called phase-change material (PCM), and thermochemical energy storage (TCS) relies on the enthalpy of reaction of reversible endo/exothermic reactions [53]. TCS is at an early development stage and still displays too many technical barriers for demanding applications such as WHR. STES is the most mature TES technology (TRL \sim 7 - 8 [54]), features some of the cheapest and simplest designs, and can

be performed with a wide range of materials that cover a broad temperature range. LTES combines a good technology readiness level (TRL~ 6 to 8 [54]), energy storage density (100 - 300 kWh/m³ [55]), and a wide variety of potential materials suited to different temperature ranges. Thus STES and LTES are suitable TES candidates for on-board waste heat recovery, and are the focus of this entry in this WHR catalogue.

2.3.2 Technology overview

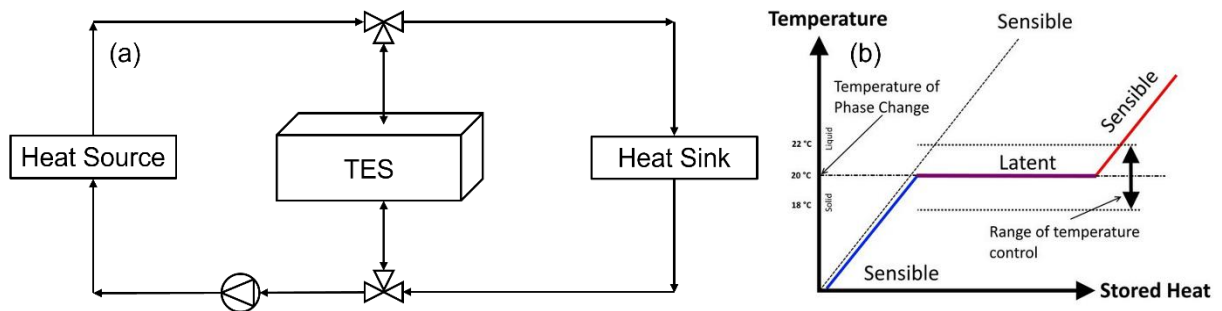
2.3.2.1 Sensible Thermal Energy Storage

With STES, heat is stored by raising (during charge) or lowering (during discharge) the temperature of a solid or liquid phase [56]. Typical materials used for STES are water, rocks, sand, concrete, molten salts, more recently metallic materials – their selection mainly depends on the temperature level of the application. STES is a mature technology with applications ubiquitous across society: water storage for domestic heating applications, underground STES for large storage capacities for district heating networks, molten salts TES for medium temperature heat storage (~250°C) in waste heat applications or concentrated solar power (CSP) plants, among others. Water-based STES is widely used in domestic applications for the delivery of hot water, and is a simple and cost-effective way of storing heat below 120°C [57]. In STES systems, heat is generally transferred by direct contact between the Heat Transfer Fluid (HTF) and the storage medium [58]. The main weaknesses of STES are the relatively low energy storage densities below 100 kWh/m³, the fluctuating power output during discharge, and heat losses which limit storage duration and enforce good insulation [53].

2.3.2.2 Latent Thermal Energy Storage

LTES leverages the constant temperature thermal energy absorption during the phase change of a storage medium, generally in a solid-to-liquid or solid-to-solid transition. During **charge**, a HTF brings heat to and melts the PCM, with the total chargeable energy being determined by the phase-change enthalpy of the storage medium. The charging temperature has to be higher than the melting point of the PCM for the heat transfer to occur. During **discharge**, the HTF extracts the thermal energy from the PCM, causing it to solidify and revert to its original state before charging. The main disadvantage of LTES is the low thermal conductivity of PCMs, generally below 1 W/m/K [59], which enforces heat transfer enhancement methods such as fabrication of composite materials, increasing heat transfer surface with fins etc.. which are all methods with high physical footprint therefore decreasing the energy storage

density of the final system; i.e. A tradeoff between improving charge/discharge power and lowering energy storage density



The choice of PCM is generally predicated on the temperature of the available heat source. Solid/solid and solid/liquid transition PCMs can broadly be categorised into organic paraffins, organic non-paraffins, inorganics, and eutectics. A selection of PCMs that have been proposed to be used for various WHR applications and spanning a range of temperatures applicable to the temperatures of on-board waste heat streams can be seen in Table 3. Organic fatty acids, inorganic salt hydrates and paraffins are typically the selected PCM for low to medium temperature (0 to 300°C) applications. Paraffins are a very common type of organic PCM used commercially, available from many suppliers such as Rubitherm, PCM products, and others. They are a waxy, soft solid obtained as a byproduct of petroleum treatment processes. Their melting point is generally found between 23°C and 67°C [61], they present good cyclability (heat storage performance is maintained over many storage cycles) and stability, which is counterbalanced by the tendency to volumetrically expand during melting and by a low thermal conductivity. Molten salts and other relatively novel metallic PCMs are inorganics used for medium to high temperatures (170 to 560°C [62]), particularly in the case of industrial waste heat and solar applications [53]. Inorganic salt hydrates are another major class of PCM. They are characterised by melting points in the 15°C to 150°C temperature range [63], higher thermal conductivity than other PCMs (approx. 0.5 to 1 W/K/m), low cost and relative abundance. The main drawback is stability and cyclability. Inorganic salts will tend to aggregate into large blocks, can hydrate in chemical sorption reactions which changes their crystalline structure and can result in deliquescence, and their energy storage density tends to degrade with multiple heat storage cycles.

Finally, eutectics are generally binary or ternary mixtures of existing PCMs, with the mass ratios of the components designed to tailor the thermophysical properties of the mixture, in particular melting temperature and storage density. Eutectics based on inorganic salts mixtures are particularly well studied [64].

Table 3 PCMs, and their thermophysical properties, used for internal combustion engine waste heat recovery, list originally compiled in [65]

| PCM Compound | PCM type | Melting Temperature [°C] | Heat of Fusion [kJ/kg] | Thermal Conductivity [W/m/°C] | Density [kg/m ³] | Ref |
|--|-----------|--------------------------|------------------------|-------------------------------|------------------------------|------|
| Na ₂ SO ₄ .10H ₂ O | Inorganic | 32.4 | 254 | 0.544 | 1,485 | [66] |
| Na ₂ HPO ₄ .12H ₂ O | Inorganic | 36 | 265 | - | 1,522 | [67] |
| Lauric Acid | Organic | 41-44.2 | 211.6 | 0.192 | 1,007 | [68] |
| Stearic Acid | Organic | 55.1 | 160 | 0.172 | 848 | [69] |
| NaOH.H ₂ O | Inorganic | 58 | - | - | - | [70] |
| Paraffin wax | Organic | 58-60 | 214 | 0.167 | 790 | [71] |
| Climsel C70 | Inorganic | 70 | 144 | 0.65 | 1,700 | [71] |
| D-Sorbitol | Organic | 89-95 | 185 | - | 1,525 | [72] |
| Xylitol | Organic | 92-94 | 256 | - | 15,030 | [73] |
| Na | Inorganic | 91 | 113 | 85 | 930 | [74] |
| Erythritol | Organic | 117.6 | 339.8 | 0.72 | 1,480 | [75] |
| 73%NaOH/23%NaNO ₃ | Eutectic | 237 | 280 | 0.63 | 2,241 | [64] |
| 59%LiCl/41%KCl | Eutectic | 352.7 | 251.5 | - | 1,880 | [76] |
| NaNO ₃ | Inorganic | 307 | 172 | 0.5 | 2,257 | [77] |

2.3.2.3 Thermochemical energy storage

Thermochemical energy storage (TCS) is a heat storage technology that leverages reversible chemical reactions which are endothermic (i.e. absorb heat) in one direction and exothermic (i.e. release heat) in the other. Equation (15) shows the generic form of such a thermochemical reaction. Combining two previously separated compounds *A* and *B* results in the formation of product *AB* and release of enthalpy of reaction ΔH – the reaction in this direction constitutes the heat discharge step. Conversely,

compound AB can absorb enthalpy of reaction ΔH which will cause A and B to separate, constituting the heat charge step. As long as the two products are kept separate, heat is stored indefinitely and without losses, assuming no material degradation by some other physical mechanism.



Compared to the other two TES technologies, LTES and STES, TCS shows the highest energy storage density, virtually lossless storage by keeping the constituting compounds separate with energy stored as chemical bonds in the so-called thermochemical material (TCM), and allows for some degree of control over the discharge power by acting on the rate of reaction (the rate of reaction is controlled through the rate and amount of compound B put into contact with A). The main limitations of TCS are a low technological maturity which translates into very few commercially available devices, with most working prototypes currently at the lab / bench top scale, and some system complexity associated with having to transport both heat and mass in/out of the TCS device.

Table 4 TCM characteristics. List originally compiled in [78]

| Reaction Type | Thermochemical Material Type | Volumetric Storage Density [kWh/m ³] | Temperature Range [°C] |
|---------------|------------------------------|--|------------------------|
| Sorption | Zeolites | 136-200 | 25-230 |
| | Silica Gels | 31-41 | 130-150 |
| | Metal-Organic Framework | 0.17 kWh/kg | 30-100 |
| | Aluminophosphates | 0.13 kWh/kg | 30-277 |
| | Salt Hydrates | 361-867 | 24-214 |
| | Composites | 166-308 | 30-250 |
| Reaction | Ammonia Based | < 830 | 350-750 |
| | Metal Based | 803 – 2,050 | 300-1,400 |
| | Carbonates | 300-889 | 500-1,730 |

Energy storage density, and charge and discharge temperature strongly depend on selection of the thermochemical reaction. A wide variety of reversible exothermic/endothermic reactions can be used as a TCS mechanism, and selection should be carried out according to the target application. Broadly speaking, most thermochemical reactions for TCS are either gas-gas or solid-gas, and are categorised as

either ‘sorption TCS’ or ‘reaction-based TCS’. Table 4 provides a selection of TCS reactions from both categories.

2.3.2.4 Performance metrics

The primary performance metric of TES systems is energy storage density [kWh/m³], calculated as the ratio of energy storage capacity over storage volume (equation (16)):

$$E_d = \frac{E_{stored}}{V_{storage}} \quad (16)$$

Where E_{stored} [J or kWh] is the stored energy, and $V_{storage}$ [m³] the storage volume. The power output/input during either discharge or charge is generally calculated relatively to the storage size, using discharge and charge power densities [kW/m³], respectively calculated with equations (17) and (18).

$$P_{v,charge} = \frac{\bar{P}_{charge}}{V_{storage}} \quad (17)$$

$$P_{v,discharge} = \frac{\bar{P}_{discharge}}{V_{storage}} \quad (18)$$

Where \bar{P}_{charge} [W] and $\bar{P}_{discharge}$ [W] are the average charge and discharge powers during the charge and discharge cycles, respectively. The economic performance of TES can be quantified with the cost per installed unit of energy storage capacity, the specific capacity cost [€/kWh] as calculated with (19).

$$SCC = \frac{C_{TES}}{E_{stored}} \quad (19)$$

2.3.3 Architecture and implementation

Fundamentally, all thermal energy storage devices revolve around the same underlying concept of some heat storage medium, and the necessary devices for heat transport during storage and heat extraction during discharge [55]. In many cases the heat storage medium can be some naturally occurring area e.g. aquifer, cavern, underground storage [79]. However, for the storage of low to medium temperature industrial waste heat, and specifically marine vessel engine exhaust heat, the heat storage medium is generally contained within, or is, a man-made engineered structure with some insulating component to

minimise heat losses during the storage period. Typical options for sensible or latent heat storage media structures at [50-350 °C] temperature range are packed beds, tanks, and heat exchanger layouts.

2.3.3.1 Hot and Cold Two tank layout

Ideally, excess thermal energy is transported to the TES without any losses which can be achieved by having the HTF transporting the excess thermal energy also act as the heat storage material. HTF containing excess thermal energy is stored in a so-called hot tank, while HTF that has extracted heat from the TES and relieved it to the target application is stored in a separate container called the cold tank, before being pumped back to the heat source when needed. This layout is represented schematically in Figure 27.

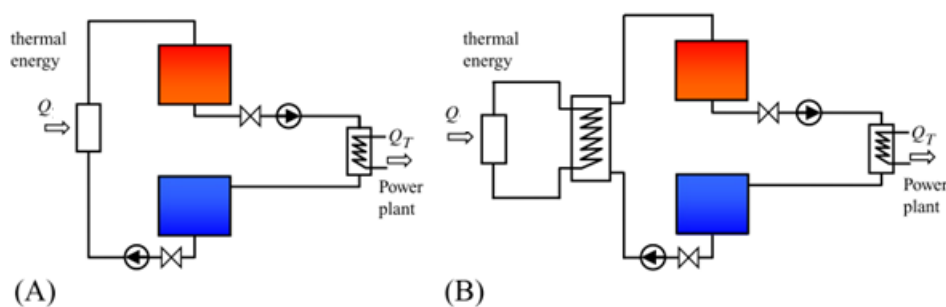


Figure 27 Schematic representation of hot and cold two-tank TES layout, with (A) configuration where the HTF at the heat source is also the TES material, and (B) configuration where the HTF at the heat source is different from the TES material with an intermediate heat exchanger [80]

2.3.3.2 Thermocline layout

The main issue with two-tank layouts is the physical footprint of such a system resulting in low system-scale volumetric energy storage density. A similar process can be performed, except that both hot and cold fluids are stored in a single tank, with hot fluid systematically stored or removed from the top of the tank, and cold fluid from the bottom the tank [80]. Due to the density difference of the single fluid at high and low temperatures, the hot and cold regions of the tank are separated by a temperature gradient [58]. Such a layout is a well established technology in TES and called thermocline (see Figure 28).

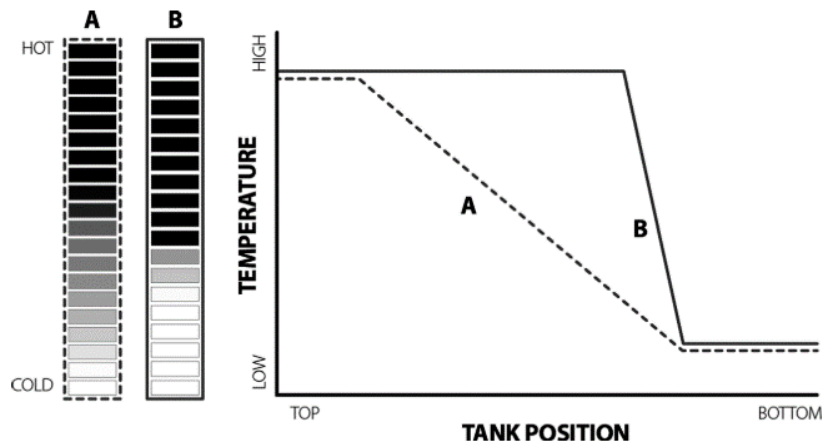


Figure 28 Schematic representation of thermocline TES with the temperature gradient shown as a function of its position along the thermocline, with A: a diffuse temperature gradient and B: a sharp temperature gradient [58]

2.3.3.3 Packed bed storage layout

Packed bed thermal energy storage is a typical architecture consisting in a storage container, a storage material and a heat transfer fluid. The TES material is packed into a porous medium within the storage tank, generally supported by a screen, and a heat transfer fluid is flown through the interstitial void caused by the natural bed porosity. This layout is represented schematically in Figure 29. In the case of STES, typical storage materials are pebbles, rocks and sand [81]. For LTES, PCM is generally encapsulated into spheres for containment purposes and is therefore prevented from leaking during heat charge induced melting. Packed bed storage is characterised by the use of generally cheap storage materials and a direct heat exchange between HTF and storage material resulting in a simple design. The properties of the porous medium need to be carefully designed to avoid significant pressure drop when flowing the HTF and minimise fan electrical energy consumption with directly impacts system efficiency [82].

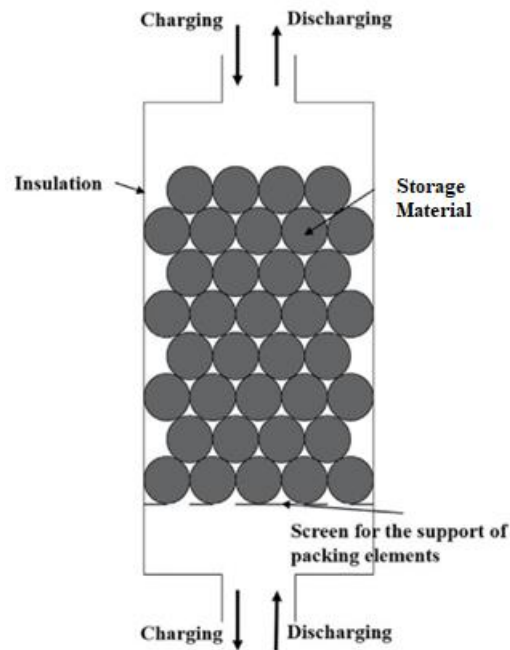


Figure 29 Schematic representation of packed bed thermal energy storage, adapted from [83]

2.3.3.4 Thermal energy storage in a heat exchanger layout

For LTES applications, PCMs are typically deployed in tubes within cylindrical or cubical containers in so-called 'pipe-layouts'. The PCM can be either within these tubes or in the interstitial space between the tubes, with the heat being injected or extracted by a fluid flow in the space not occupied by the PCM. Agyenim et al. [84] suggested a classification of different PCM-bases storages dependent on the container geometry and the PCM layout (see Figure 30). This type of pipe-layout is also relevant for sensible TES, as high thermal capacity metallic rods can be laid in this fashion for high packing efficiency, as demonstrated by Energy Nest with their developed Thermal Battery [85], which will be discussed in more detail in the next section.

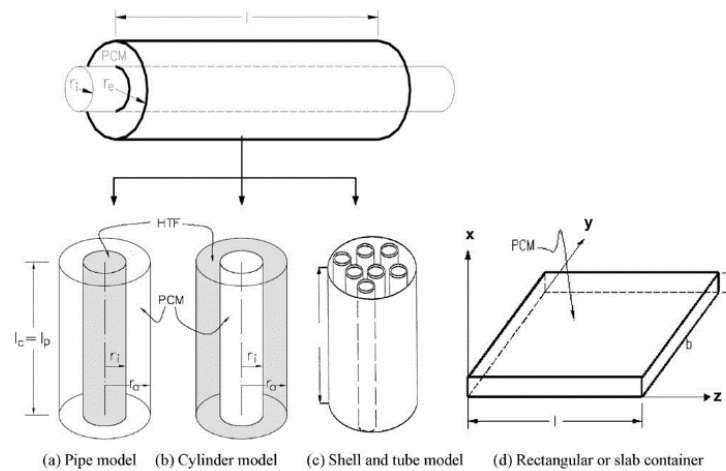


Figure 30 Schematic classification of LTES PCM-based storages in pipe layout based on container geometry and inner material distribution, proposed by Agyenim et al. [84]

2.3.4 Applications and uses

While not an active application for the direct use of waste heat, TES aboard vessels can be seen as a technological enabler used to better connect in time and space the highly intermittent available waste heat from the engine with the energy demands on board. One of the technical specificities of on-board WHR, in addition to the intermittent nature of waste heat availability, are the multiple temperature levels at which waste heat is available. Waste heat streams are present in engine exhaust gases, cooling circuits, lubricating oil, and charge air, all available at temperatures anywhere between 50°C and 300°C. Recovery of the waste heat is further complicated by the variation in these temperature levels with the ships's operational profile: main engines load, geographical location which impacts ambient air temperature and sea-water temperature.

As a way to address the flexibility constraint, Pandiyarajan et al. [86] suggested, from their first and second law analysis of on-board energy systems, a cascaded LTES with multiple PCMs with decreasing melting points. From the thermodynamic analysis they found that theoretically 15.2%/14.2%/11.4%/10.4% of total energy from fuel input could be recovered at 100%/ 75%/50%/25% main engine loads respectively. However, cascaded PCMs have mainly been investigated theoretically through simulation, will only a limited number of experimental demonstrators at lab-scale, and have not been optimised for dynamic heat sources [87]. Thus, current conceptual designs for marine TES aim for a particular location within the on-board energy system, to couple a specific waste heat stream with a relatively narrow temperature range with another WHR technology

TES appears to be well suited to the production of hot water. At certain critical points of the ship's operation, such as in port and other hoteling periods (hoteling periods are periods when hoteling energy needs i.e. crew and passenger energy needs are high), the waste thermal energy produced by the main engines is insufficient to meet the immediate hot water needs, which is matched by additional fuel use in the auxiliary systems. On merchant ships which use auxiliary boilers for the on-board heating demand, Baldi et al [88] in their preliminary analysis concluded that a 1,000 m³ TES could reduce boiler fuel consumption by 80%, saving approximately 268,000 US\$ (271,360€) per annum. The schematic diagram of a similar layout for hot water production on a cruise ship with a comparison to the conventional system is shown in Figure 31 [89].

Other WHR technologies can be synergistically combined with TES. In a report on a prior project for implementing energy efficient technologies on ships [61], the combination of storing engine waste heat in a TES which can then be used to drive an ORC is suggested as a promising concept. In the analysis was assumed the integration of a PCM based TES device storing approximately 450 MJ / 125 kWh; depending on the material, the TES volume was between 1,600 and 3,000 m³ and mass between 1,870 and 2,910 tons, equivalent to a 5,580 m³ water sensible heat storage. It was assumed that the ORC uses the latent heat of the PCM during LTES discharge, to heat the working fluid with a boiling point 100°C.

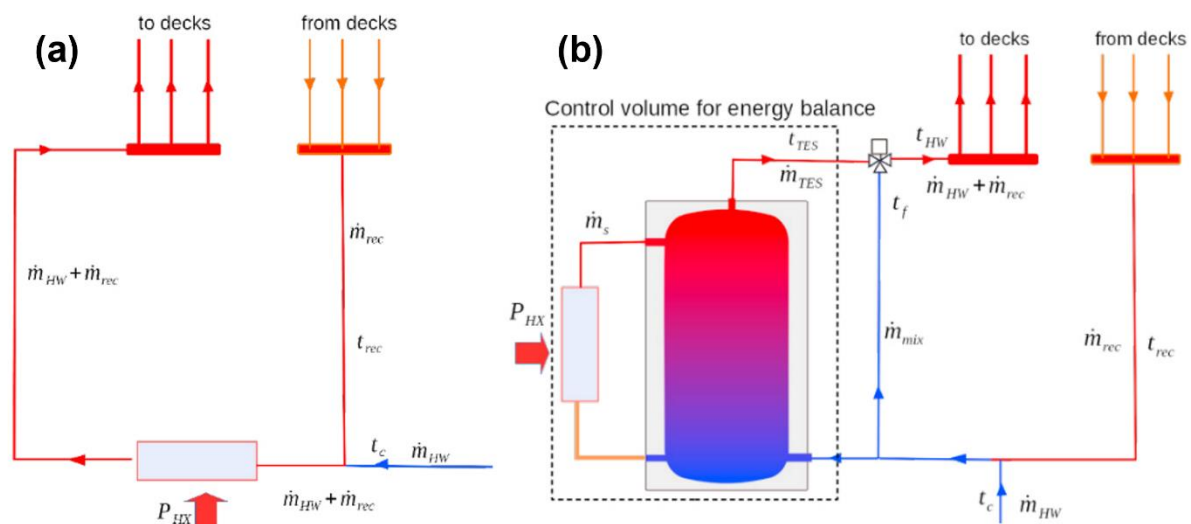


Figure 31 (a) Conventional hot water system on a cruise ship (b) modified with TES [89]

As discussed previously, the technological readiness level of TES depends on the TES subclass of interest. The storage devices of interest in this report are those which can store heat at the available temperature

ranges of Diesel 2-stroke engines waste heat (exhaust gases around 285°C, and seawater, cooling water, scavenge air and lubricating oil in the range 50°C-100°C), that can store heat with large fluctuations, a consequence of the high engine load variation, and that display a high enough energy storage density (above 50 kWh/m³ should be a minimum requirement at system-level i.e. including all TES equipment such as pumps, piping and complete container volume) since on-board installation of WHR devices is constrained by space.

2.3.4.1 STES

To this day, a large number of commercial STES devices can be found on the market for wide-ranging applications. Compact low to medium temperature STES devices that can be charged with fluctuating charge powers are reasonable candidates, such as STES targeted toward industrial waste heat recovery. Various options can be found commercially available on the market. Energy Nest developed a modular STES device (Figure 32a), Thermal Battery (temperatures up to 400°C), based on concrete storage with metallic components for structural rigidity and enhanced heat transfer [85]. EcoTech Ceram also developed a modular STES system (Figure 32b), EcoStock (temperatures up to 1,000°C), based on ceramo-metallic materials for the storage of industrial waste heat or heat converted from electricity (via power-to-heat) generated from intermittent sources such as solar PV [90]. Lumenion [91] have developed a steel-based commercial STES solution for industrial waste heat, shown in Figure 33.

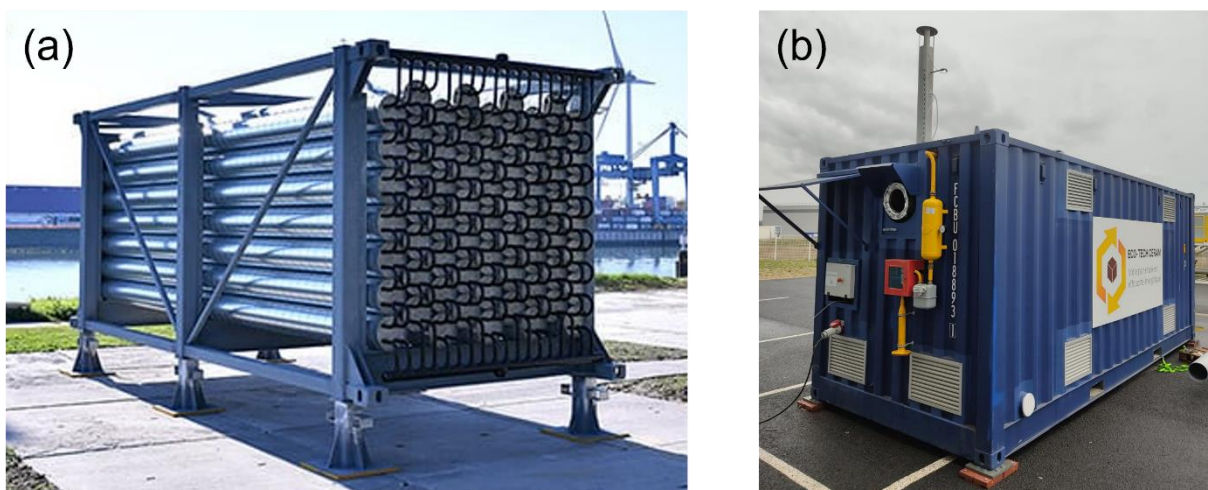


Figure 32 (a) Thermal Battery by Energy Nest [85], (b) Eco Stock by EcoTech Ceram [90]

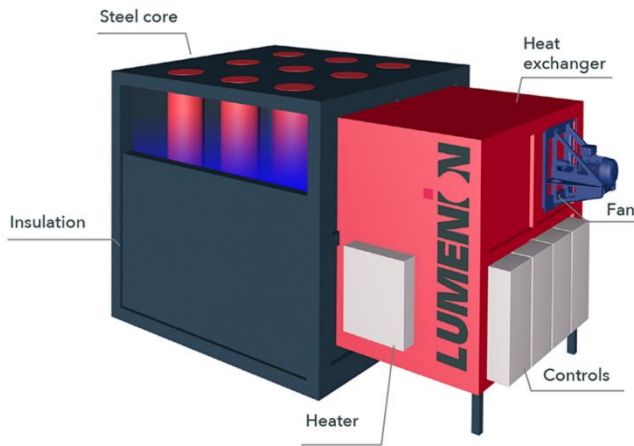


Figure 33 Lumenion steel-based thermal energy storage, left: conceptual design, right: actual 450 kWh implementation in University of Applied Sciences (HTW) laboratory [91]

2.3.4.2 LTES

LTES is at a lower technology readiness level than STES, and as such fewer commercial devices suitable for marine applications are available, with most of the relevant LTES designs being at the pilot-project scale or even at the R&D scale. The main commercial solution based on PCMs is the Sunamp Central Bank thermal battery (Plentigrade P58 PCM formulation) [92], shown in Figure 34. The storage material P58, modified sodium acetate trihydrate [93] which has a latent heat density of approximately 264 kJ/kg (~106 kWh/m³) [94], has an adaptable melting point up to ~120°C that is tailored upon formulation.



Figure 34 Sunamp PCM-based LTES [92]

An example of TES specific to on-board applications is the lab-scale hybrid sensible/latent TES designed by Frazzica et al. [95], targeted towards hot water production on ships (requires a minimum temperature of 50°C to prevent legionella). Based on the study by Baldi et al. [96], they established that two available waste heat streams, one around 40°C-60°C and the other between 70°C and 90°C which are the high and low temperature water cooling flows typical of a cruise ship energy system, are available to charge a TES. From the requirements of the heat load and the available heat sources, they selected a PCM called S58 which is a salt hydrate-based material developed by company PCM Products with melting point 58°C. The device is pictured in Figure 35. It contains 20 tubes of macro-encapsulated PCM contained in polypropylene tubes (total PCM volume 40 dm³ for a total device volume of 100 dm³) arranged as a bundle in a cylindrical stainless steel tank. The system is designed for heat to be transported to and from the TES during charge and discharge by circulating water, to mimic the potential integration of the system with a cruise ship water-based cooling circuits, with flow rates of 10 to 15 kg water/min during charge and 9 to 12 kg water/min during discharge. Average discharge powers between 15 kW and 20 kW were achieved depending on the discharge temperature, which was in the 65°C to 85°C range.

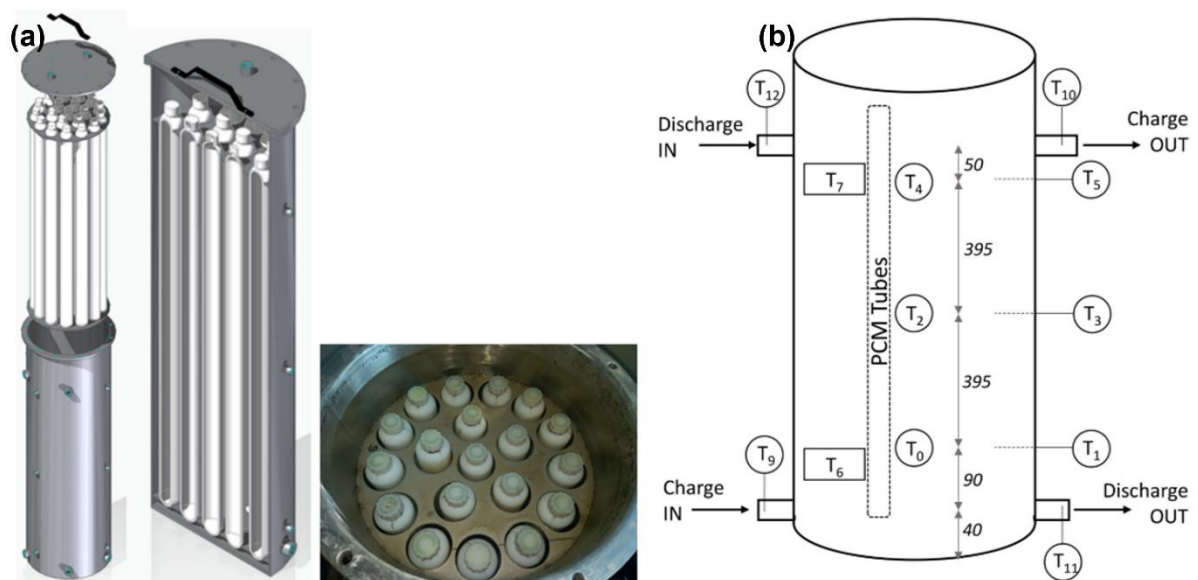


Figure 35 Hybrid STES/LTES for on-board waste heat storage, targeted towards hot water production (a) detailed exploded tri-dimensional view and (b) schematic representation with sensors and flow direction [95]

2.3.5 Techno-economics

Table 5 reports techno-economic performance indicators for a variety of TES applications (sensible and latent), including energy storage density, efficiency and volume, and installation costs specific to storage capacity (both in €/m³ and €/kWh). Most of the presented TES systems cost between 3 €/kWh (water and gravel tanks as STES) and 250 €/kWh (Paraffin RT82 tube-in-tank LTES). The costs presented in this section are system-level costs, i.e. they include the cost of the thermal energy storage medium, the non-negligible cost of the container / heat exchanger, and installation.

Table 5 Techno-economic properties of thermal energy storage. Storage costs are system-level i.e., cost of the entire process, material, and installation. Data originally synthesised in [97]

| Type | Material | Storage Density [kWh/m ³] | η | Typical Volume [m ³] | Cost [€/m ³] | Cost [€/kWh] |
|-------------------------------------|--|---------------------------------------|---------------|----------------------------------|--------------------------|--------------|
| Tank | - | 60 - 80 | 50% - 90% | 0.05 - 0.5 | 1,220 – 3,550 | 34.8 - 101.5 |
| | - | | | 300 | 470 | 15.5 |
| | - | | | 5,700 – 12,000 | 120 - 150 | 3.4 - 4.3 |
| Pit | - | 60 - 80 | < 80% | 1,000 – 200,000 | 30 - 148 | 0.9 - 4.2 |
| Borehole | - | 15 - 30 | 6% - 54% | > 5,000 | 14 - 60 | 0.9 - 4.0 |
| Aquifer | - | 30 - 40 | 70% - 90% | 5,000 – 100,000 | 25 - 40 | 0.83 - 1.33 |
| Shell and tube LTES | NaNO ₃ | 42.8 | - | 700 | - | - |
| Shell and tube LTES | KNO ₃ / NaNO ₃ | 38.8 | - | 58.3 | - | - |
| Packed bed LTES | Li ₂ CO ₃ /K ₂ CO ₃ /Na ₂ CO ₃ | 65.7 | 77.4% - 86.1% | 1.9 | - | - |
| Packed bed LTES | NaNO ₃ | 85.5 | - | 1.1 | - | - |
| Shell and tube LTES | Al-Si (88-12) | 28.7 | - | 13.9 | - | - |
| Shell and tube LTES with heat pipes | Al-Si (88-12) | 34.6 | - | 13.1 | - | - |
| Packed bed LTES | Li ₂ CO ₃ /K ₂ CO ₃ /Na ₂ CO ₃ | 114.8 | 0.6 | 83,333 | - | - |
| Packed bed LTES | KNO ₃ | 189.5 | - | 50,000 | - | - |

| | | | | | | |
|---------------------|--------------------------------------|-------|---------------|---------------|---|---------------|
| Packed bed LTES | Al-Si (75-25) | 82.5 | 32.5% - 44.1% | 0.4 | - | - |
| Shell and tube LTES | KNO ₃ / NaNO ₃ | - | 0.7 | - | - | - |
| - | Sodium Nitrate | - | - | 77,161 | - | 50.04 - 79.92 |
| - | Chloride + Carbonate Salts | - | - | - | - | 17.64 - 18.72 |
| - | KOH | - | - | 83,333 | - | 18.36 - 19.80 |
| Shell and tube LTES | Sodium acetate trihydrate | 68.1 | 90% - 95% | 6.7 | - | - |
| Packed bed LTES | D-mannitol | 100.6 | - | 14,805 | - | - |
| Tube in tank LTES | Paraffin | - | 95.3% | - | - | 37.4 |
| - | Paraffin RT82 | - | - | 6.0 | - | 259.9 |
| - | Sodium acetate trihydrate | - | - | 2,500 | - | 58.3 |
| - | Erythritol | - | - | 1,400 – 2,700 | - | 36.72 - 41.76 |
| - | Erythritol | - | - | 2,400.0 | - | 16.6 |

2.3.6 Modelling thermal energy storage

A methodology for TES modelling suggested in [98] is to express the stored heat as the equivalent heat stored in a volume of hot water in a thermocline between temperature of the hot part and the cold part, as shown in equation (20).

$$V_{TES}^{(t)} = V_{TES}^{(t-1)} + \frac{1}{\rho_{TES} C p_{TES} (T_{TES,hot} - T_{TES,cold})} (\eta_{TES} F_{TES}^{(t)} - \frac{Q_{TES}^{(t)}}{\eta_{TES}}) \quad (20)$$

Equation (20) expresses the volume of hot water stored at time t $V_{TES}^{(t)}$ as a function of the volume of hot water stored at the previous time $V_{TES}^{(t-1)}$, the volume of hot water added or drawn between those time steps, and the amount of heat lost (using a thermal efficiency term η_{TES}). The volume of the storage is constrained for the optimisation between the minimum and maximum allowable volume of stored hot water (equation (31))

$$SOC_{min}V_{TES}^{max} < V_{TES}^{(t)} < SOC_{max}V_{TES}^{max} \quad (21)$$

A constraint is added to ensure the amount of water stored at the first time step is equal to the amount stored at the final time step (equation (22)).

$$V_{TES}^{(t=t_0)} = V_{TES}^{(t=t_f)} \quad (22)$$

2.4 Isobaric Expansion Engines

2.4.1 Introduction

Isobaric Expansion (IE) Engines are unconventional heat to mechanical power converters, that can essentially be described as heat engines without a polytropic gas/vapour expansion [99]. Work is extracted from a theoretically isobaric gas expansion occurring within a cylinder. IE engines are the oldest type of heat engines. It will suffice to mention that Savery, Newcomen, and Watt pumps fit into this group [100,101]. Worthington direct-acting steam pump [102] and the Bush compressor [103] also represent this type of engines. These machines were later replaced by more efficient well-known water steam expansion machines such as piston steam engines as well as steam turbines. Over the past decades, many IE engines have been proposed and studied again under different names and for different applications. The current status of the IE technology and important modifications to make IE machines competitive and cost-effective alternatives to state-of-the-art heat conversion technologies are presented in [99].

One of the main advantages of the isobaric expansion engine is the potential for work extraction from small temperature differences ($\Delta T \geq 30 \text{ }^\circ\text{C}$) and using low temperature heat sources ($\geq 40 \text{ }^\circ\text{C}$) [104,105]. In these temperature regions, the techno-economic performance of other waste heat to power converters, such as ORCs or other types of heat engines, is insufficient to justify their use. Another feature of isobaric expansion engines are their relatively simple design due to the isobaric / near-isobaric nature of the expansion process, enabling their use as simple compressors, pumps and other converters with specific speeds and torques [99].

2.4.2 Technology overview

2.4.2.1 Thermodynamic cycle and basic operation

Encontech proposed significant changes to the original concepts of the Worthington steam pump and the Bush thermo-compressor, aiming to increase their efficiency to levels comparable or even superior to modern heat engines, above of all ORC power plants. These modifications include the application of dense working fluids with high thermal expansion at high process temperature and low compressibility at low temperature instead of gases, new concepts for efficient heat regeneration/recuperation and further technical improvements. The working principle of isobaric expansion engines is based on the continuous isobaric expansion and compression of a working fluid. The two basic implementations of the isobaric expansion engine, Worthington steam pumps (higher TRL) and Bush thermocompressors (higher theoretical efficiency) [99,105] are illustrated schematically in Figure 36.

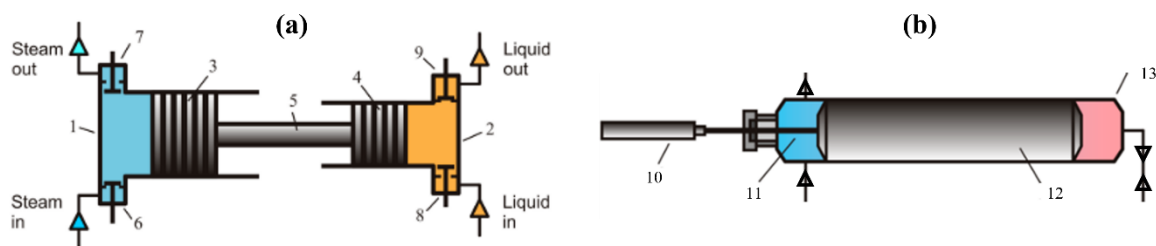


Figure 36 Basic layout of isobaric expansion engines, (a) in the Worthington steam pump configuration. 1: steam cylinder, 2: pumping cylinder, 3: steam piston, 4; pumping piston, 5: connecting rod, 6: steam inlet valve, 7—steam outlet valve, 8—liquid inlet valve, 9—liquid outlet valve.and (b) in the Bush thermocompressor configuration. 10: linear actuator, 11: cold side cylinder, 12: sealed piston, 13: hot side cylinder [99]

A working fluid is heated and cooled using heat exchangers, a heater and a cooler. The pistons of the Worthington pump are rigidly connected by rod 5 and move together as a unit. The steam cylinder is equipped with steam inlet/admission valve 6 and outlet/exhaust valve 7 shown at the top. Accordingly, the pumping cylinder has inlet/suction valve 8 and outlet/discharge valve 9. The inlet and outlet valves of the steam cylinder are forcedly actuated; the valves of the pumping cylinder are self-acting. When the inlet valve of the steam cylinder opens, steam enters the cylinder and moves the piston performing pumping stroke in the pumping cylinder. The valve remains open during the whole stroke, i.e., steam enters the cylinder at constant pressure and does not expand in the cylinder. Therefore, during the whole stroke, the pressure in the steam cylinder remains constant. The pump uses a very simple valves actuation system without a cut-off mechanism and has no crank gear and no flywheel. Pumping of the

working fluid in liquid phase from the cooler to the heater is performed by a feed pump. The Bush thermo-compressor, Figure 36b, does not use a feed pump which is necessary for the Worthington type IE engines. The linear actuator of the Bush type IEE sets the piston into a reciprocating motion. Moving to the left, the piston displaces some part of the working fluid from the cold to the hot part of the cylinder. The working fluid passes the cooler, the regenerator and the heater and heats up. Pressure in the cylinder rises, and a part of the working fluid is displaced to produce useful work. Moving to the right, the piston displaces the hot, compressed working fluid through the heater, regenerator and cooler back to the cold part of the cylinder. The pressure in the cylinder drops down. As soon as it becomes lower than the set pressure the working fluid returns back to the cylinder. Afterwards, the cycle repeats.

2.4.2.2 Performance metrics

The main performance metric for isobaric expansion engines is the thermal efficiency defined by the ratio of net produced work W [J] over the thermal energy input $Q_{heat\ source}$ [J] used to heat the hot side fluid (equation (23)).

$$\eta_{th} = \frac{W}{Q_{heat\ source}} \quad (23)$$

The cycles of the Worthington and Bush type engines are different. Their performance metrics are presented below.

Worthington-Type Engine.

The net produced work W is the difference between the raw pumping work output W_{dc} [J] from the driving cylinder and the work provided to pump the working fluid W_{fp} [J] to the IEE (equation (24)):

$$W = W_{pc} - W_{fp} \quad (24)$$

The raw work output of the driving cylinder can be theoretically estimated with (equation (25)):

$$W_{dc} = (P_{high} - P_{low})\Delta V_{dc} \quad (25)$$

Where P_{high} and P_{low} [bar] are the high and low pressure levels at the beginning and end of the expansion process, respectively, and ΔV_{dc} [m³] the change in steam volume in the driving cylinder. The pumping work W_{fp} is calculated with equation (26):

$$W_{fp} = m(h(P_{high}, T_{p,out}) - h(P_{low}, T_{p,in})) \quad (26)$$

Where m [kg] is the mass of working fluid pumped per cycle, h is the specific fluid enthalpy [kJ/kg], and $T_{P,out}$ and $T_{P,in}$ [°C] are the temperatures at the pump outlet and inlet, respectively. The thermal energy input $Q_{heat\ source}$ [J] is calculated with equation (27):

$$Q_{heat\ source} = m(h(P_{high}, T_{high}) - h(P_{high}, T_{R,out})) \quad (27)$$

Where T_{high} and $T_{R,out}$ [°C] are the temperatures at the heater outlet and inlet, respectively. The temperature at the heater inlet is determined by the heat exchange process in the recuperator. A method for the determination of the heater inlet (or the temperature at the recuperator outlet) was developed by Encontech. This method is presented in the publications [99,106].

Bush-Type Engine

The useful work generated during the cycle is:

$$W = \oint PdV_{tot} = \oint PdV_H + \oint PdV_C \quad (28)$$

where the total engine volume V_{tot} consists of the volumes of the hot space, V_H , the cold space, V_C and the regenerator V_R which does not change during engine operation. The interdependence of temperatures and volumes of the individual engine compartments and the pressure is expressed by the equation for the total mass of the working fluid:

$$m_{tot} = \rho(P, T_H)V_H + \rho(P, T_C)V_C + \rho(P, T_R)V_R \quad (29)$$

The heat supply to the hot part is determined from the energy balance of this space, neglecting changes of kinetic and potential energies:

$$Q_H = \oint PdV_H + \Delta Q_H \quad (30)$$

$Q_{heat\ source}$ is the energy required to heat the displaced working fluid from the regenerator outlet temperature (or low cycle temperature T_C , if there is no regenerator) to the high cycle temperature T_H . A method to estimate the performance of the regenerator is the same as for the Worthington-type engine. With equations (28) and (30), the thermal efficiency, equation (23) can be evaluated. The modelling of the Bush-type engine is explained in more detail in [107].

2.4.3 Architecture and implementation

2.4.3.1 Worthington Direct-Acting Steam Pump Architectures

In the Worthington steam pump configuration, two pistons are rigidly connected by a connecting shaft. The hot steam is produced by evaporating water using the heat source. The two cylinders (steam/power cylinder and pumping cylinder) feature inlet and outlet valves, with the steam inlet/outlet valves being forcibly actuated, and the liquid inlet/outlet valve being self-actuated. Opening steam inlet valve lets steam enter the cylinder and moves the steam piston / driving piston towards volume expansion, and results in the pumping piston performing its stroke and pumps liquid out of the pumping cylinder through the liquid outlet valve. During this entire process the steam inlet valve remains open, resulting in the expansion process occurring without pressure variation, i.e. isobaric expansion. Once the stroke is completed, the steam inlet valve is closed while the steam outlet valve is opened. Steam exits the steam cylinder and the piston moves back under the pressure of liquid entering the pump cylinder through the liquid inlet valve, which completes the cycle.

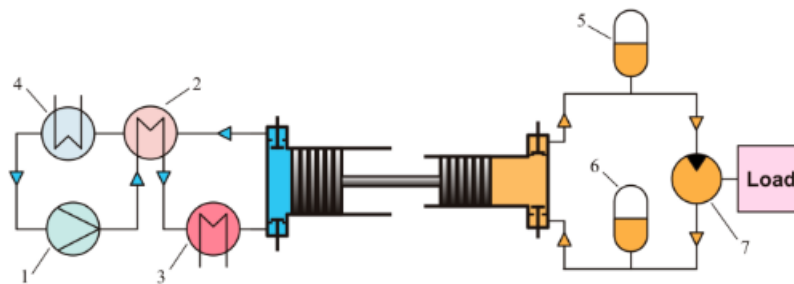


Figure 37 Integration of the Worthington steam pump IEE into a power cycle. 1: feedwater pump, 2: internal heat recovery, 3: evaporator, 4: condenser, 5: low-pressure hydraulic accumulator, 6: high-pressure hydraulic accumulator, 7: hydraulic motor [99]

According to Glushenkov et al. [99], the simplest way to leverage the work produced by a Worthington steam pump IEE is by connection to a hydraulic circuit and generator, as shown in Figure 37. Water is transported by the feedwater pump (1) through a recuperative heat exchanger (2) and evaporator (3) which functions using the thermal energy source, upstream of the steam inlet valve. Exhausted steam is cooled down in the recuperative heat exchanger and condensed back to liquid water in a condenser (4). The work produced by the cycle is transported by the hydraulic circuit to the generator to produce electrical power.

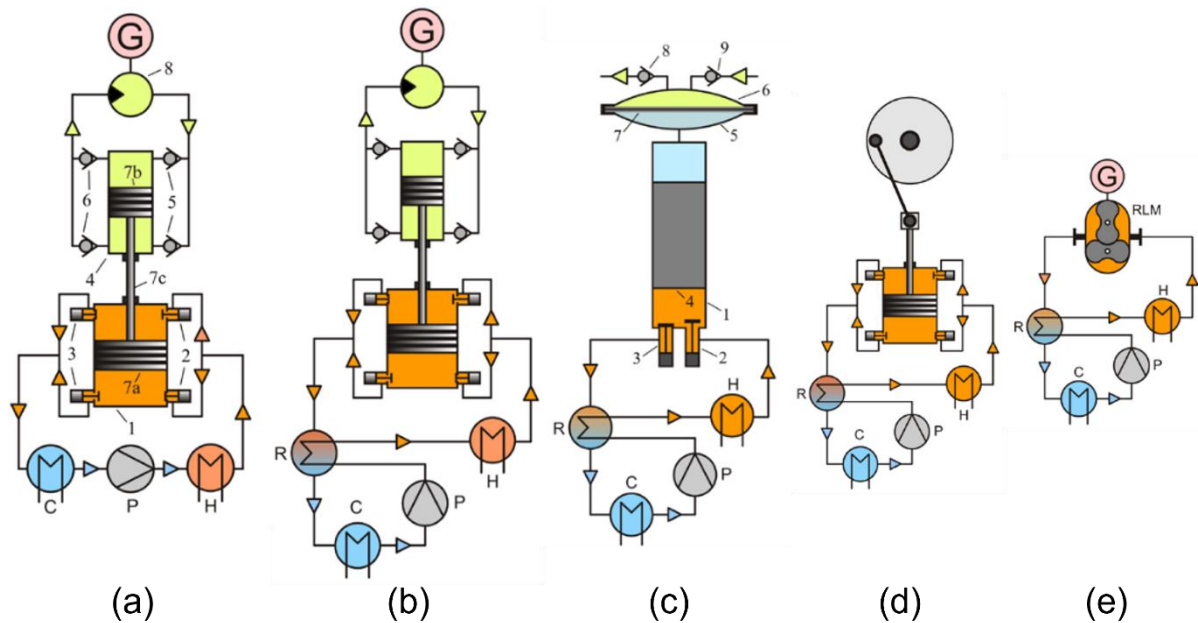


Figure 38 Various implementations and architectures of Worthington-type IEEs. (a) Simple non-regenerative with hydraulic motor and generator, (b) regenerative with hydraulic motor and generator, (c) regenerative with thermal barrier piston and diaphragm, (d) regenerative with crank-gear, (e) regenerative with rotary lobe-machine [105]

As illustrated by **Figure 38**, various options exist [105] to improve on the cycle performance or alter the useful work extraction compared to the basic layout (**Figure 38a**). The efficiency of the cycle can be improved through the use of a regenerative heat exchanger to preheat the inlet steam using the outlet (**Figure 38b**). The regenerative heat exchanger also lowers the thermal load on the condenser thereby reducing its size and exchange area. If high temperatures are present, a single acting free piston (which acts as a thermal barrier piston) can be used in conjunction with a diaphragm (**Figure 38c**), which, depending on the final configuration, can act as either a pressure transmitter between the piston and the working fluid, or as both the pump and driver for the cylinders. The diaphragm provides practical advantages such as reducing friction and leakage potential. The useful work can be extracted from the IEE's driving piston through kinematic mechanisms such as crank-gear (**Figure 38d**) or a rotary lobe machine (**Figure 38e**) when shaft power or electrical power generation are needed.

2.4.3.2 Bush Thermocompressor Based Expansion Machines Architecture

Isobaric expansion engines in the Bush thermocompressor layout distinguish themselves from the Worthington steam pumps by using a single sealed piston which separates a single cylinder into a cold

side and a hot side. A simple integration of Bush-type IEE in a power cycle is illustrated in **Figure 39**. The two sides of the cylinder are connected and communicate to one another through a heater, a regenerator and a cooler in series. The piston can be set in motion downwards through a linear actuator. Part of the cold fluid is displaced from the cylinder towards the hot side, being heated and evaporated by the regenerator and heater before entering the hot side cylinder. Pressure in the hot side of the cylinder rises, which forces the rest of the cold fluid out of the cylinder cold side into a diaphragm unit which transfers this pressure to a hydraulic circuit. The hydraulic circuit transfers the mechanical work to some power generation process (hydraulic motor for example)[108].

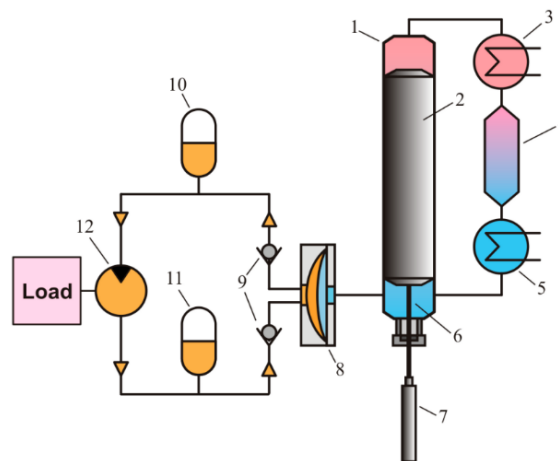


Figure 39 Integration of the Bush thermo-compressor-based IEE into a power cycle. 1: cylinder, 2: piston, 3: heater, 4: regenerator, 5: cooler, 6: connecting rod, 7: linear actuator, 8: diaphragm unit, 9: non-return valves, 10: high-pressure accumulator, 11: low-pressure accumulator, 12: hydraulic motor [99]

During its return upwards motion, the piston displaces the hot fluid out of the hot side cylinder, through the heater/regenerator/cooler series, back into the cylinder cold side. The pressure inside the cylinder cold side drops, and once that pressure is below the suction pressure the cold fluid in the diaphragm unit is forced back into the cold side cylinder. The cycle is completed and can be repeated once the piston finishes its stroke.

2.4.4 Applications and uses

The IEEs are particularly attractive as vapor-driven pumps and compressors due to their lack of complex kinematics and multiple energy conversion steps. In such applications, heat can be efficiently used to

provide direct pumping and compression, that is, without intermediate generation of shaft power or electricity, its transmission and then conversion back to mechanical energy typical of today's industry. The energy from the pumped liquid flows can be converted to shaft power (rotary motion) or electricity using off-the-shelf hydraulic motors. Another option is the so-called pump as turbine (PAT) technology, which uses mass-market centrifugal pumps that operate in reverse mode i.e. as turbines. In this case, the installation is turned into a heat-to-power converter.

Using a differential piston arrangement (a combination of two pistons with different diameters), the IE engine-pump can deliver any pressure of the pumped liquid. This allows the engine-pump to be used for high-pressure applications such as heat-driven water desalination, oil hydraulic power units, etc. The results obtained with IEEs are very promising showing that the engine is a valuable alternative to the current technologies, especially at low temperatures ($< 100\text{ }^{\circ}\text{C}$) and low power range ($< 500\text{ kW}$). The technology is easily scalable and reproducible in all industries where there is a temperature difference $> 20\text{ }^{\circ}\text{C}$. Thus low-grade solar, geothermal, biomass energy, and industrial waste heat with a temperature above $30\text{ }^{\circ}\text{C}$ can be involved in various energy conversion processes. High-pressure pumps for water desalination and heat engines for generating mechanical energy (electricity) using geothermal, biomass, and solar energy, waste heat of diesel engines, as well as of SOFCs and LT-PEM fuel cells are examples of promising applications, which are presented below.

2.4.4.1 Up-THERM engine for micro- and mini-CHP systems

The Up-THERM heat engine (also known as Encontech, or ECT engine) is a novel Bush-type heat engine suitable as a prime mover for micro-CHP and mini-CHP systems (UpTHERM). The engine targeted characteristics are as follows:

- Electric power output: 1-3 kW with a possibility of scaling up to a few MW.
- Fuel or heat source: natural gas and concentrated solar thermal power.
- Thermal efficiency: not less than 40% of the Carnot efficiency, i.e. higher than $0.4 (1 - \text{TC}/\text{TH})$ where TC and TH are the temperatures of the cooler and heater, respectively.
- Engine cost in mass production: several times less than the cost of the available Stirling type engines of the same power (200-500 €/kW versus 2.500 – 4.500 €/kW).
- Projected maintenance free interval: 50.000 hours.
- Environmentally safe working fluid, such as water, air, carbon dioxide.

- Applicable for micro-CHP systems for houses.

The Up-Therm engine was studied in a small power range (< 30 W) and in a broad range of heat source temperatures, up to 600 °C. Schematic overview of the Up-THERM engine principle, assembly drawing of the engine and its picture are shown in **Figure 40** [109].

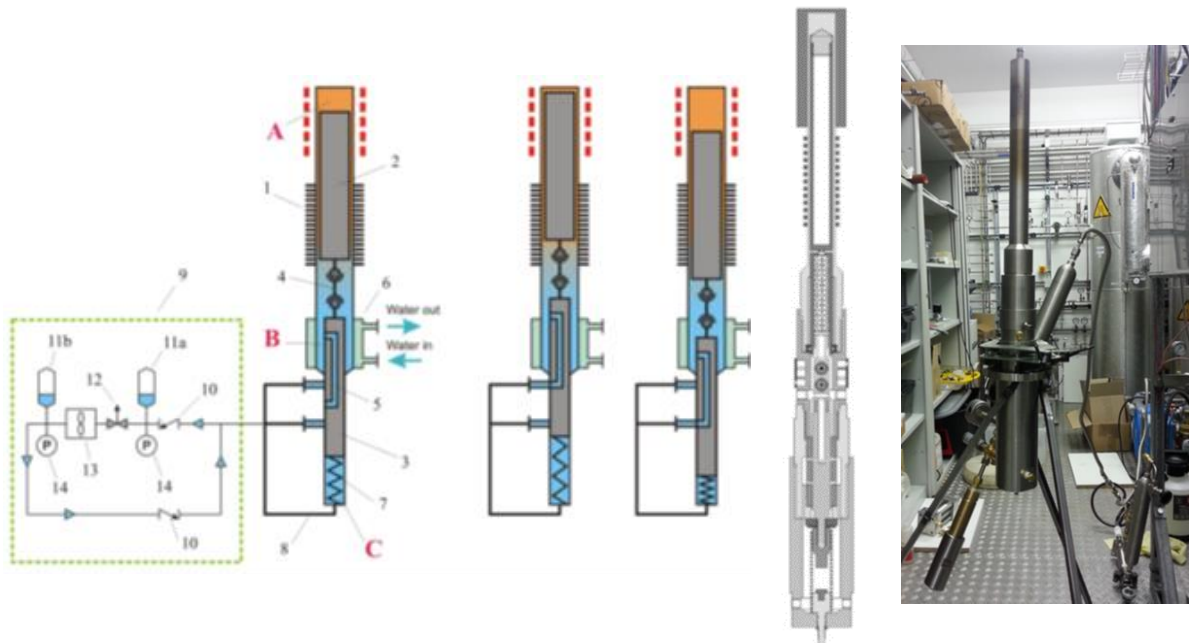


Figure 40 Schematic overview of the Up-THERM engine principle, assembly drawing and picture of the engine.
For details, see [109]

The layout of the CHP test setup used for the engine study is shown in **Figure 41**. The obtained efficiency (3 – 7%) and power density (up to 1,200 W/L) were much higher compared to the previously studied IE engines.

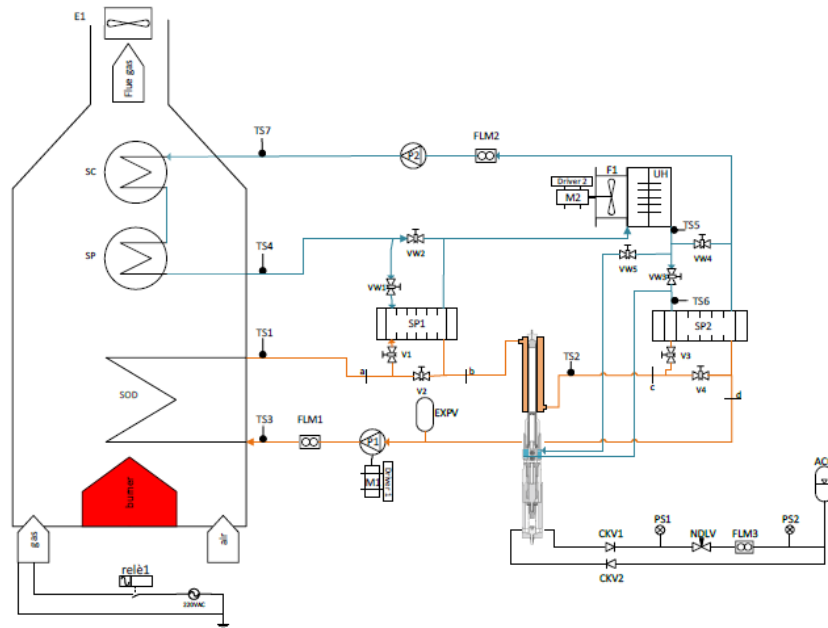


Figure 41 Layout of the CHP system engine test setup

2.4.4.2 Pump for reverse osmosis desalination

Bush-type engine was developed and tested as a high-pressure pump for reverse osmosis (RO) water desalination. Two engine versions, with a displacer actuated by an electric motor and with a self-driven displacer, were tested using hot water heated either by an evacuated tube solar collector or by an electric heater. The scheme of the experimental setup for testing the engine with self-driven displacer and its picture are shown **Figure 42**.

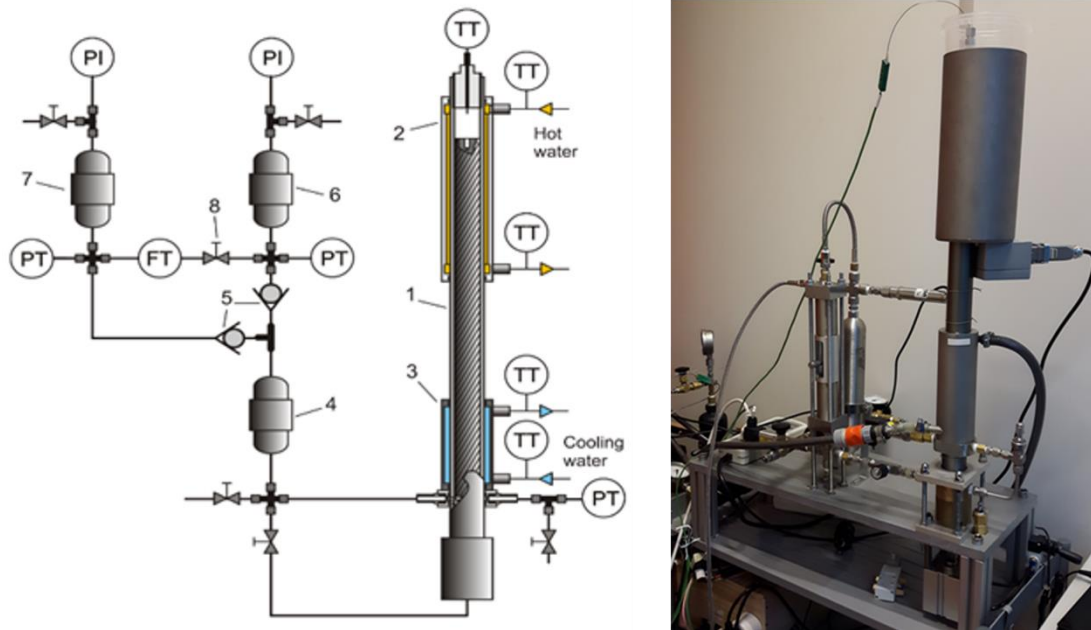


Figure 42 Scheme and picture of the experimental set up. 1: engine-pump (internal diameter 30 mm, stroke of the displacer 40 mm), 2: heating jacket, 3: cooling jacket, 4: diaphragm unit, 5: non-return valves, 6: high-pressure accumulator, 7: low-pressure accumulator, 8: throttle valve, FT: flow transmitter, PI: pressure indicators, PT: pressure transmitters, TT: temperature transmitter

Hot water (shown in yellow) with a temperature from 60 to 95°C was pumped through the heating jacket, providing the heat supply. Cold tap water (shown in blue) with temperature of 20 - 30°C was supplied to the cooling jacket for the heat rejection. Refrigerant R134a was used as a working fluid. Pictures of the solar powered test setup are shown in **Figure 43**.

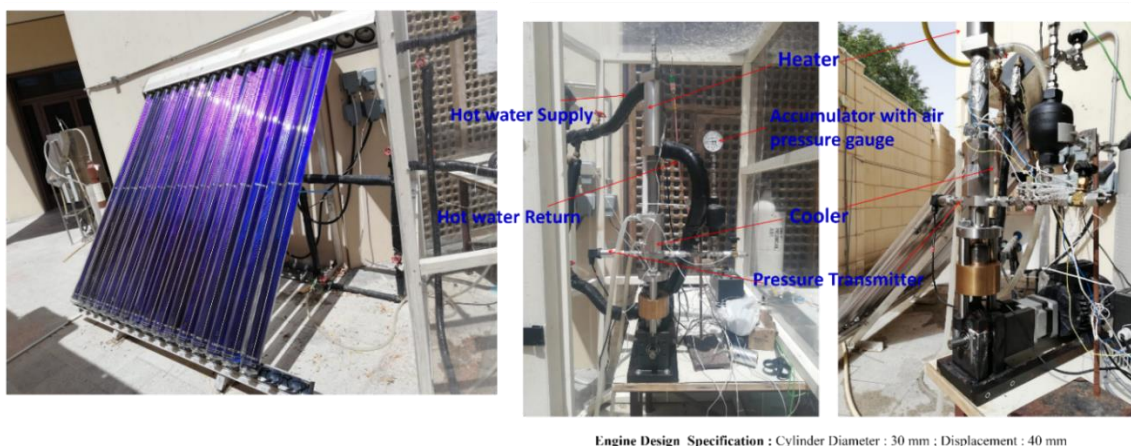


Figure 43 Solar powered test setup for water desalination

The developed engine-pump is characterized by a very high specific power (power per unit volume of displaced working fluids) up to 1.2 kW/L with a useful power of about 20 W. The obtained thermal efficiency was at least 6.4 %. This value is very high, especially when compared with the efficiency of known thermally driven pumps, which do not exceed 1 % (mostly 0.1 – 0.4 %) [110]. The engine-pump can generate very high pressure using lower grade heat (starting from 60 °C) and therefore can be used for RO processes eliminating the consumption of electricity. The efficiency of these machines can be very high even at ultra-low heat source temperatures at which all well-known energy conversion technologies are not applicable. Application of the IE engines-pumps for RO desalination promises a considerable improvement to the economics of this process because of the replacement of electricity by renewable energy and substantial reduction of the capital cost.

2.4.4.3 Vapor compressor for refrigeration

A heat driven vapor compressor for refrigeration based on Worthington type IEE was developed and tested. An assembly drawing of the IE-compressor is shown in **Figure 44**.

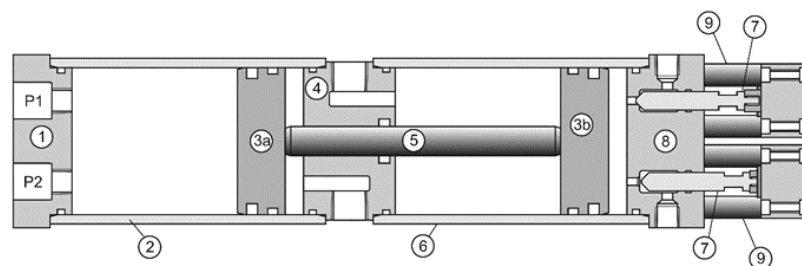


Figure 44 Assembly drawing of the IE-compressor. 1: compressor cylinder cover, 2: compressor cylinder, 3a and 3b: compressor and driving pistons, 4: guiding cover, 5: connecting rod, 6: vapor driver cylinder, 7: inlet and outlet valves, 8: valve cover, 9: pillars, P1 and P2: ports for suction and discharge valves

The guiding cover 4 is equipped with a port intended for the connection of a pressurized gas receiver providing a gas spring and a port intended for the ventilation of the compressor cylinder and lubrication of the compressor cylinder-piston pair. The volume of the driving and compression chambers is 0.502 L (internal diameter 80 mm, length 100 mm). An experimental set-up for testing the IE-compressor was developed and tested. The scheme of the experimental setup, and its picture are shown in **Figure 45**. The setup included the single-acting IE-compressor itself and power and refrigeration loops. In this scheme, a recuperator was not used due to the relatively small temperature difference between the heat source and the heat sink.

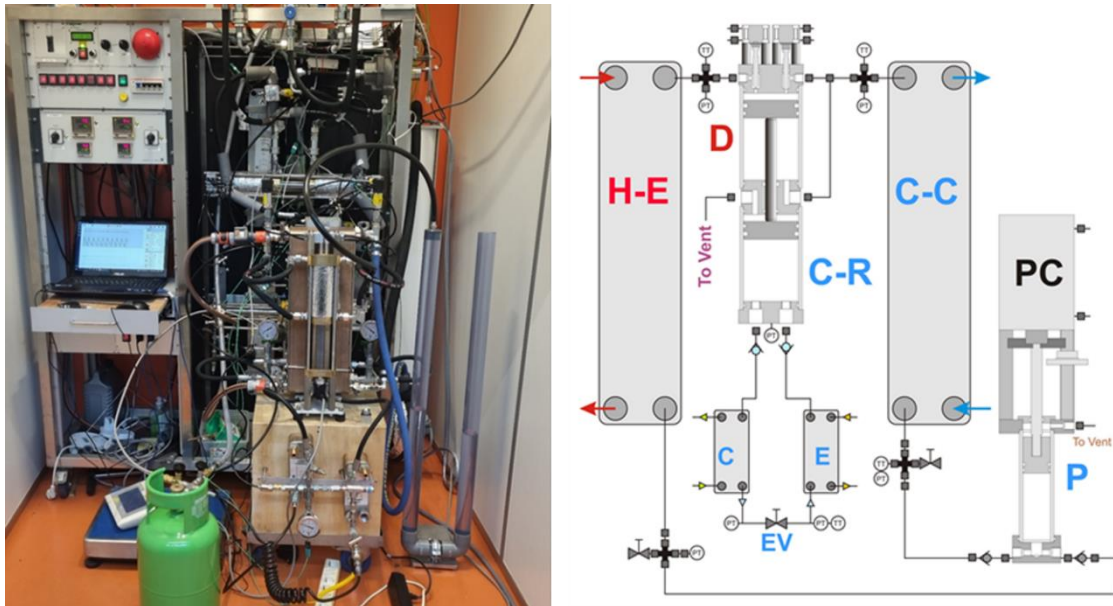


Figure 45 Experimental Worthington-type IEE-compressor schematic representation and picture of the experimental test rig. D: driving chamber, C-R: compression chambers, H-E: heater, P: feed pump, C-C: cooler, C: condenser, E: evaporator, EV: expansion valve/throttle. (Kronberg & Glushenkov 2022; Kronberg et al. 2022; Encontech IE-engine refrigerator)

In the experiments, the R134a refrigerant was used as the working fluid in both the power and refrigeration cycles. The IE-compressor was heated with hot water in the temperature range 30–80 °C and cooled with tap water at 15 - 20 °C. The operating frequency was in the range of 0.2–1 Hz. The minimum temperature obtained in the evaporator reached -14 °C. The most stable operation was observed when the temperature in the evaporator was a little higher. At temperatures of the heat source and heat sink of 55 °C and 20 °C the engine-compressor produced cold down to -11 °C. The developed compressor works perfectly even at a heat source temperature below 50 °C. No other energy conversion technologies are known to compete with the developed compressor.

2.4.4.4 Heat to electricity converter

The energy from the pumped liquid flows provided by the Worthington-type engine pump can be converted to shaft power (rotary motion) or alternatively to electricity by means of well-known commercial hydraulic motors. The second option is so-called pump as turbine (PAT) technology, which uses commercially available centrifugal pumps working in reverse regime i.e. as turbines. In this case the installation is turned into a heat-driven electric generator. In contrast to the conventional well-

known generators it can produce electricity using very low-grade heat ($> 40\text{ }^{\circ}\text{C}$). The available hydraulic motors require a rather high pressure drop of about 80 bar for the most efficient operation. Therefore, to demonstrate this application of the engine it was at first modified and then coupled with a hydraulic motor (MI04 Var-Spe radial pistons hydraulic motor, efficiency 96%) and a wind turbine alternator. Schematic representation of the IEE for production of shaft power, its picture and a picture of the test rig for electricity generation from low-grade heat is shown in **Figure 46**. The modified engine-pump (**Figure 46**) contains a differential piston reciprocating inside a differential cylinder (pumping cylinder). Compared to the engine-pump diameter of the pumping cylinder was decreased four times. This simple design without transmission or crank gear etc. allowed to increase the generated pressure up to 80 bar.



Figure 46 Experimental Worthington-type IEE coupled with hydraulic motor, HM, its picture and picture of the test rig

The engine-generator was tested at the same conditions as the engine-pump (Encontech: IE engine generates electricity). The achieved electric power was up to 400 We. This power was limited by the heat exchangers and could have been increased.

2.4.4.5 IEEs for electricity generation in geothermal plants

Engine heating is performed directly by hot water from a geothermal well with a temperature of $70\text{ }^{\circ}\text{C}$, $120\text{ }^{\circ}\text{C}$ and $180\text{ }^{\circ}\text{C}$. Cooling the IE engine is performed by $20\text{--}30\text{ }^{\circ}\text{C}$ cooling water. The hot water flow rate is $100\text{ m}^3/\text{hour}$. The generated electricity is used by households. If the temperature of the hot water is high, say $120\text{--}180\text{ }^{\circ}\text{C}$, then engine cooling can be performed instead with hot water at a temperature

60 -100°C, which can be used for house heating purposes. This highly energy efficient process (no energy losses due to engine cooling) is not considered here, but certainly deserves attention.

Working fluids and efficiencies. Refrigerant R134a can be used as a working fluid at hot water temperatures of 70°C, 120°C. At 10 - 20 bar pressure differences and a temperature of 80-120°C, the cycle efficiency is about 8%, see Figure 49, in **section 2.4.6** on the modeling of IEE performance. Refrigerant R32 can be used as a working fluid at a temperature of the hot water of 120 - 180°C. Efficiency of the IE cycle with R32 as a function of temperature and pressure difference generated by the engine is shown in **Figure 47** (left). At 100 – 200 bar pressure difference and a temperature in the range of 120 - 180°C, the average cycle efficiency is about 15%.

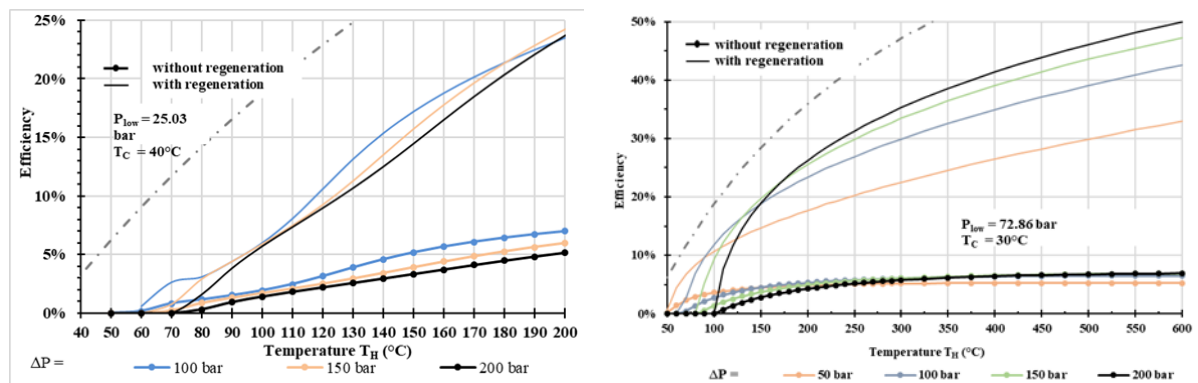


Figure 47 Efficiency of IE cycle as a function of temperature and pressure difference generated by engine.
Working fluids: R32 and CO₂

At high water temperatures (approximately above 120°C) carbon dioxide could be an interesting working fluid. The efficiency of the IE cycle with CO₂ as a function of temperature and pressure difference generated by the engine is shown in **Figure 47** (right). At 100 – 200 bar pressure difference and a temperature in the range of 150 - 180°C, the cycle efficiency can be higher than 20%. Some results of the calculations are presented in Table 6.

Table 6 Electricity generation in geothermal plants

| Hot water temperature, °C | 70 | | 120 | | 180 | |
|-----------------------------------|-----|-----|-----|-------|-------|-------|
| Water temperature drop, °C | 10 | 20 | 40 | 60 | 80 | 100 |
| Generated mechanical power, kW | 35 | 186 | 372 | 1,050 | 1,400 | 1,750 |
| Energy production, GWh/year times | 0.3 | 1.6 | 3.3 | 9.2 | 12.2 | 15.3 |
| Cost, k€** | 18 | 93 | 186 | 524 | 700 | 870 |

*number of houses was estimated assuming annual electricity consumption of 4,000 kWh (family with 1 child)

**cost of the installation was calculated based on the estimate of the specific cost of 500 €/kW. So low cost is justified by the fact that compared to ORC installations (with specific cost of 2,000 – 4,000 €/kW) the most expensive components – expander (turbine) and high pressure pump - are eliminated. These specific costs also follows from the costs of small scale engines made so far extrapolated to mass production.

2.4.4.6 Heat driven high-pressure pump for ORC system

Glushenkov et al. [104] developed an experimental Worthington type IEE as a high-pressure feed pump of the ORC unit of 10 kWe (IE engine pump in ECT’s laboratory). A picture of the engine test setup is shown in **Figure 48b**, and a schematic focused on the actual IEE setup is shown in **Figure 48a**. The layout consists in particular of two driving cylinders, each with their own piston, connected to a pumping cylinder that is divided into two by a single piston. The three pistons are interconnected by two rods, and therefore move together as unit, operating with R134a as the working fluid.

In the layout, the device is a dual acting IEE. Hot working vapour is sequentially fed to the driving cylinders on either side of the pumping piston. If vapour is admitted and expanded in the right driving cylinder, this drives the right-sided driving piston to the left, pumping liquid out of the left side of pumping cylinder, and forcing exhaust working fluid vapour out of the left sided driving cylinder. At the end of this half cycle the reverse operation is carried out, completing the full stroke. Asynchronous opening of the relevant valves allows for continuous pumping.

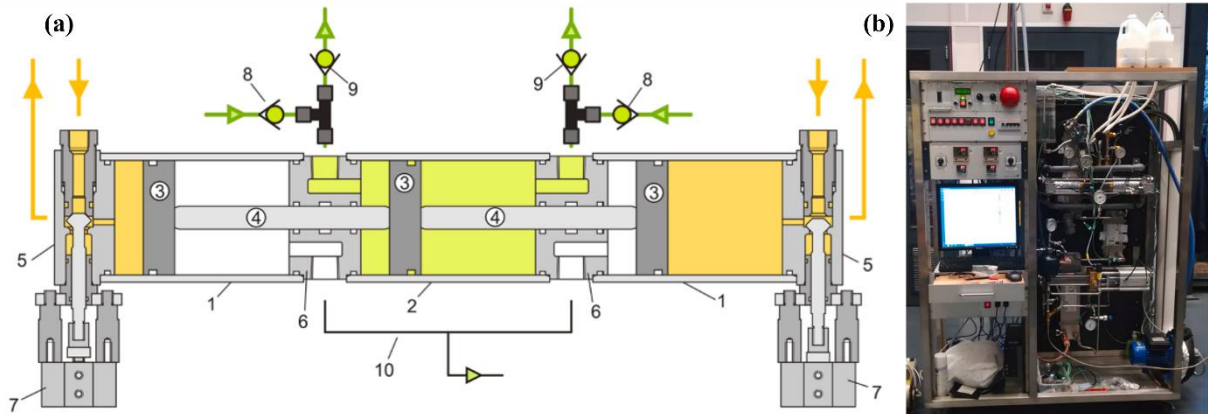


Figure 48 Experimental Worthington-type IEE (a) schematic representation 1: driving cylinder, 2: pumping cylinder, 3: pistons, 4: connecting rods, 5: driving valve covers, 6: pumping valve covers, 7: valve actuators, 8: inlet suction valves, 9: discharge valves, 10: manifold. (b) picture of the experimental test rig [104]

The performance of the device for three operating conditions (hot water temperatures 86.5°C, 60°C and 40°C at a heat source consisting 2 x 12 kW heaters) features in

Table 7. The heat input, work of the feed pump and the net work presented are per cycle.

Table 7 Performance and key properties of the dual-acting Worthington IEE.[104]

| P_{high} | P_{low} | T_{high} | T_{low} | Q_{heat} | W_{fp} | W | η |
|------------|-----------|------------|-----------|------------|----------|------|--------|
| bar | bar | °C | °C | kJ | kW | kJ | % |
| 28 | 5.5 | 86.5 | 11 | 29.13 | 0.19 | 1.58 | 5.4 |
| 15.4 | 5.2 | 59.7 | 12.5 | 14.23 | 0.09 | 0.71 | 5 |
| 10 | 4.9 | 40 | 10.8 | 8.78 | 0.06 | 0.33 | 3.8 |

The results obtained can be compared with the results for similar systems used for pumping water in the same temperature range of the heat source and heat sink (80 – 90 oC and 10 – 30 oC respectively). For comparison, a water pump based on the thermal power pump (TPP) was taken [111]. Its performance, according to the authors, is on par with or better than the performance obtained by similar existing systems. Error! Reference source not found. shows the main performance data of the compared engines.

Table 8 Comparison of nonconventional heat engines [104]

| Heat engine | Volume power cylinder(s), L | Pressure difference, bar | Cycle period, s | Power, W | Efficiency, % | Power density, W/L |
|----------------------------------|-----------------------------|--------------------------|-----------------|----------|---------------|--------------------|
| TPP system | 1.8 | 2 | 200 | 1 | 0.5 | 0.6 |
| IE engine-pump, Bush type | 0.02 | 15 | 2.5 | 20 | 6.4 | 1,200 |
| IE engine-pump, Worthington type | 1 | 23 | 4 | 500 | 5.4 | 500 |

The significant advantages of the Bush and Worthington type IE engines over similar existing systems can be seen in terms of efficiency and power output. Compared to conventional heat engines (diesel, Rankine cycle, ORC, gas turbines), the presented IE engine can be used at low heat source temperatures (< 100 °C) and has a very simple design.

2.4.4.7 Implementation of the IEEs in marine energy systems

Waste heat recovery from diesel engines, and especially marine diesel engines (cooling can be done relatively easily by ambient water), is one of the most promising applications of the IEEs. Among various techniques for low-temperature waste heat recovery, the Organic Rankine Cycle (ORC) is one of the best heat recovery option [112]. However, despite extensive research, there are virtually no stories of successful practical use of the ORC system to recover diesel engine waste heat.

Compared to ORC systems the IEEs have the following advantages:

- All sources of waste heat can be used (exhaust gases, exhaust gas recirculation, coolant and even charge air with a temperature of 40-50 °C)
- Can operate at variable diesel engine power efficiency losses, since the efficiency of the IEE is not sensitive to its speed (frequency of the reciprocating movement of the piston).
- The thermal efficiency is independent of the engine size. This allows multiple small engines to be used instead of a single large engine, providing additional flexibility with variable diesel power and the ability to use different small engines for different applications.
- Power output can be hydraulic, pneumatic or shaft power. Therefore, the engine can be used for any application where mechanical power is needed. Pumping, compression and injection of the diesel fuel is an interesting application. All applications of the IEEs

presented in this document can be implemented on board (prime mover of CHP system, water pumping, reverse osmosis desalination, vapor compression for cooling or air conditioning, electricity generation).

- Simpler and cheaper.

Also, IEE can be proposed as an autonomous engine (main marine engine). The study shows that when using carbon dioxide as a working fluid, the heat source with temperature above 600°C and the pressure drop of 200 bar created by the engine, the efficiency of the engine can reach 50%.

2.4.5 Techno-economics

An IEE system can be constructed out of commercially available heat-exchangers and simple machineable parts. Over 90% of initial investment costs will consist of the heater-, cooler- and regenerator-heat exchangers. However the costs of these components will vary greatly depending on the chosen working fluid, available temperature difference, overall power output required among other design parameters. As such it is difficult to provide a single figure based simply on a power rating. Furthermore any return on investment will depend almost solely on the application which initially generated the heat. Therefore to provide a general levelized cost of energy is challenging. To still provide an estimate; a 1 kW IEE unit may have an initial investment between €30.000,- to €40.000,- whilst a 5 kW IEE unit may require an investment between €50.000 and €95.000. The performed techno-economic evaluation of earlier versions of the IEEs (Up-Therm engine) are quite promising.

Table 9 taken from an overview of micro CHP systems [113] (added and corrected), reports the performance of known technologies, compared with the expected characteristics of Up-THERM engine:

Table 9 Performance of known CHP technologies

| Type | Fuel | Efficiencies, % | | Power electrical, kW _e | Specific Power, kg/kW | Cost, €/kW* | Service interval [hours] | Lifetime, [hours] |
|-----------------------|--------------------------------------|-----------------|------------|-----------------------------------|-----------------------|-------------|--------------------------|-------------------|
| | | total | electrical | | | | | |
| Diesel engine | Gas, biogas, fuel oils, rapeseed oil | 65-90 | 35-45 | 5-20,000 | 2-3 | 340-2,000 | | 10,000 |
| Spark ignition engine | Gas, biogas | 70-92 | 25-43 | 3-6,000 | 2-3 | 450-2,500 | | 5,000 |
| Micro turbine | Natural gas, gas oils, diesel, | 65-90 | 15-30 | 15-300 | | 900-2,500 | | |

| | | | | | | | | |
|--|--|-------|---------------------------------------|-----------|-----|-------------|-------|---------------|
| ORC, Bosch WHR OR 75-375 | Waste heat, 120-150 °C | 12-17 | 12-17 | 40-375 | | 3,000 | | |
| Stirling engine | Natural gas, gas oils, any heat, > 500 °C. | 65-96 | 25 | 3-1,000 | 1-5 | 2,500-4,500 | | 10,000-50,000 |
| Stirling engine SD ₄ -E ¹ | Heat at 1000 °C | 98 | 28 | 35 | 70 | | 4,000 | 100,000 |
| Stirling engine in micro-CHP Vitotwin 300-W ² | Natural gas | 96 | 14 | 1 | | 10,000 | MF** | |
| Up-THERM engine | Any heat, > 100 °C | | 40(1-T _c /T _H) | 0.01-1000 | 1-5 | 200-500 | MF | 50,000 |

¹ increases rapidly with decreasing power

** MF = maintenance free

Performance and costs reported in the table concern only the engine (heat-to-electricity converter), and not the entire CHP system. It is worth mentioning that for micro power range (< 50 kW_{el}) the electrical efficiency of the innovative engine is incomparable. Making a comparison with the commercially available system Vitotwin 300-W of the German company Viessmann, with an electrical efficiency of 14%, assuming a cooler and heater temperatures of 300 K and 800 K, respectively, for a power < 3 kW_{el}, the efficiency of the innovative engine would be 25%, almost double than actual technologies. The theoretical study by Kirmse et al. [114] showed that the Up-THERM engine can be regarded as an attractive alternative to the ORC engine at certain temperatures of the heat-source as the power output is comparable to or even higher than the power output of the equivalent ORC engine, while the specific costs are much lower.

¹ http://www.stirling.dk/page_content.php?menu_id=40&type=submenu

² http://www.viessmann.com/com/en/press/press_releases/combined_heating_and_power/shk-107024.html

2.4.6 Modelling the isobaric expansion engine

2.4.6.1 MILP model

The amount of energy absorbed by the IEE, $F_{IEE}(t)$, is expressed as a linear function (or piecewise linear function) of the net power drawn from the IEE, $P_{IEE}(t)$, using the thermal efficiency of the engine (equation (31)). $\delta_{IEE}(t)$ is a binary decision variable which indicates whether the IEE is on or off at time t .

$$F_{IEE}(t) = \frac{1}{\eta_{IEE}} P_{IEE}(t) \delta_{IEE}(t) \quad (31)$$

Where η_{IEE} is the thermal efficiency of the isobaric expansion engine. The work produced by the IEE is constrained in Equation (32) using a rated design for IEE D_{IEE} , with upper and lower bounds indicated with variables $k_{3,IEE}$ and $k_{4,IEE}$. $x_{IEE}(t)$ is a binary decision variable which indicates whether the IEE is included or excluded in the energy system.

$$k_{3,IEE} D_{IEE} x_{IEE}(t) \leq P_{IEE}(t) \leq k_{4,IEE} D_{IEE} x_{IEE}(t) \quad (32)$$

2.4.6.2 ENCONTECH model

Based on the experimentally validated performance maps of the laboratory scale IE engine-pumps we can propose to estimate the real efficiency as 80 % of the theoretical. Shown in Figure 49 (left) is the predicted efficiency of an IEE system running on R134a at varying high cycle pressures. Points where the efficiency sharply drop off are where the high cycle temperature is insufficient to boil the fluid at the set high cycle pressure. R134a is only one of the fluid available to use in an IEE, it is not necessarily the most optimal choice for efficiency. Some mixtures can provide higher efficiency in certain temperature and pressure ranges as shown in Figure 49 (right).

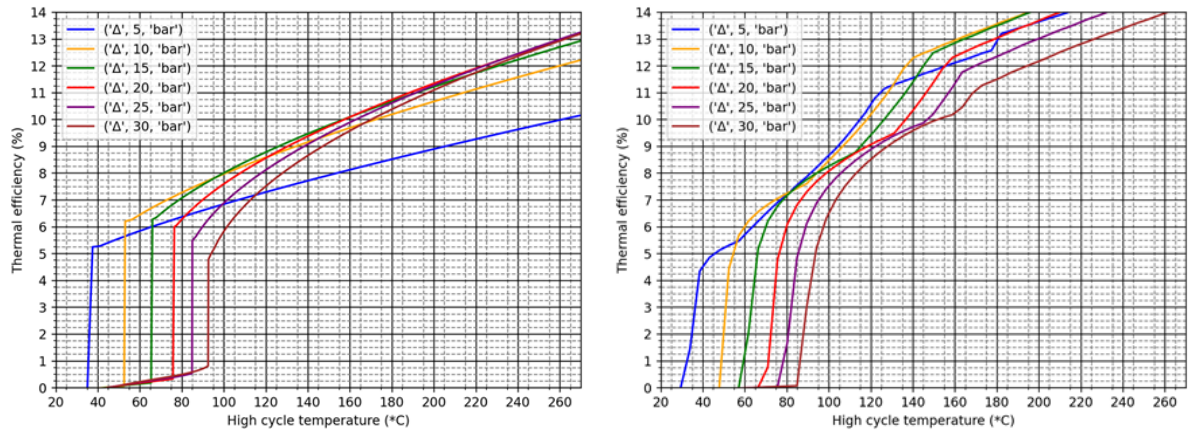


Figure 49: Thermal efficiency of model IEE running on R134a (left) and a mixture of 80 mol% ammonia and water (right)

Net power output of an IEE system running on R134a may be approximated via the following formula wherein T is the high cycle temperature in celcius and Q is the heat input in watt:

$$W_{net} = Q(0.000361T + 0.0383) \quad (33)$$

The power density (defined as the work performed by the engine-pump per unit volume of the engine cylinder) for different heat sink temperatures is shown in Figure 50 as a function of the heat source temperature.

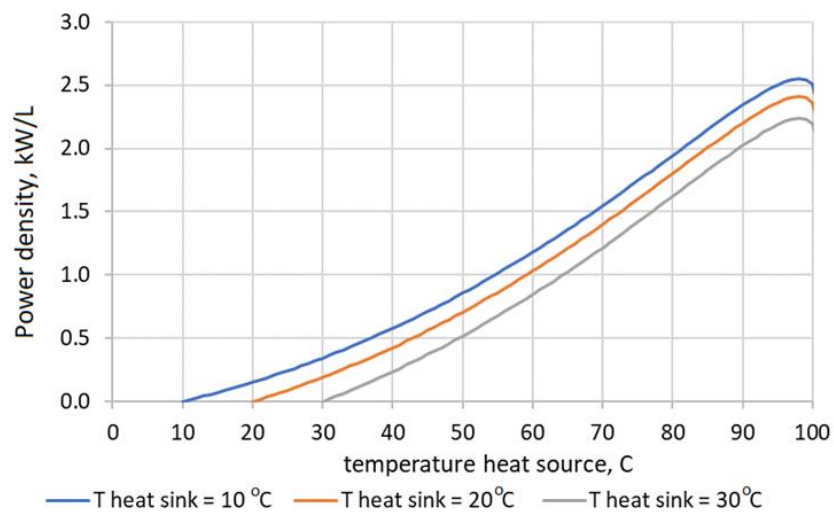


Figure 50 Power density of IE engine-pump

The developed engine-pump can be implemented in a wide power range reaching from 1 kW to several MW. Figure 49 and **Figure 50** can be used as a guideline for performance of the real size IE engine-pumps.

3 Consolidated and other developmental on-board WHR technologies

3.1 Turbo-compounding

3.1.1 Introduction

According to MAN Diesel and Turbo documentation (as of 2014-2016) on existing WHR technologies for marine Diesel engines [1,115], the main options for efficiency improvement are turbine-driven energy systems using engine exhaust gases. This type of WHR is also referred to as turbocompounding. While in automotive applications the recovered power can be directly transferred to the crankshaft as mechanical power (mechanical turbocompounding), in marine applications it is generally recovered for electricity production using a generator and gearbox (electrical turbocompounding), due to the large rotational speed differential between turbines and the slow 2-stroke engine crankshafts [116].

3.1.2 Technology overview

3.1.2.1 Power turbine and generator (PTG) systems

The simplest turbocompounding system are Power Turbine and Generator (PTG) systems: a power turbine is directly driven by exhaust waste gases and connected to a generator via a gearbox. Part of the exhaust gas (~8% to 12%) bypasses the usual turbochargers using a secondary gas connection from exhaust gas receiver (EGR) and is directly used to run the PT. While running at SMCR, a PTG system can be expected to produce electrical power equivalent to 3% to 5% SMCR [115].

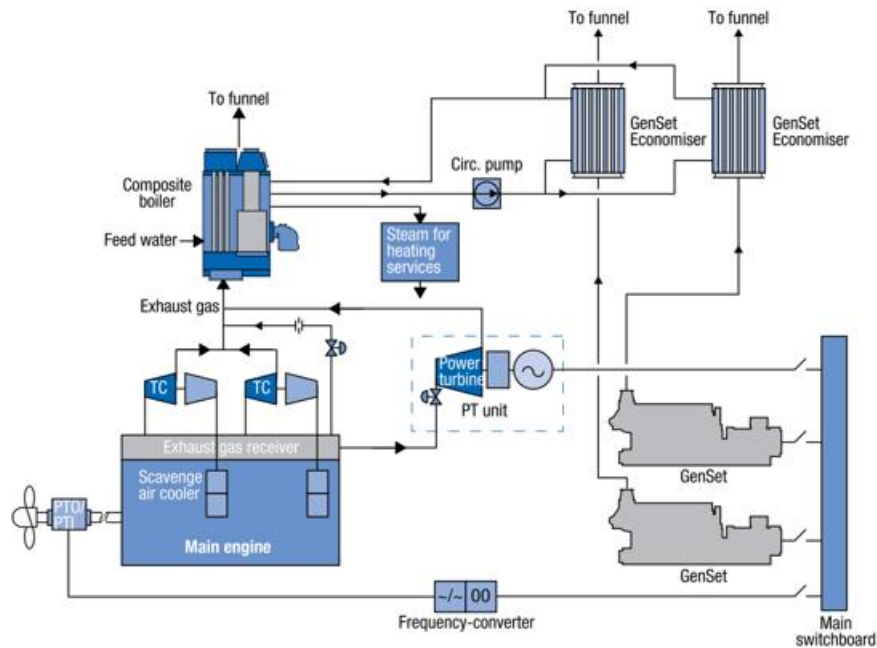


Figure 51 Example layout of power turbine and generator PTG WHR system (MAN [1])

PTGs are suitable for a total main engine power below 15,000 kW, and are the cheapest and smallest option for turbocompounding systems, since the only components needed are the power turbine and a new exhaust gas line. The design of the power turbines are generally derived from the turbocharger designs [117,118]. A standard layout for the PTG WHR system is shown in Figure 51.

3.1.2.2 Steam turbine and generator (STG) systems

Building upon the previous system, the next system in terms of complexity is the Steam Turbine and Generator (STG) system: a steam-driven turbine is connected to a generator via a gearbox. Steam is produced from large single or dual-pressure boilers driven by the engine exhaust gases. To run the STG, bypassed exhaust gases are mixed with exhaust gas exiting the turbocharger train, to increase the temperature of the exhaust gas flow (+50°C approx.). While running at 100% SMCR, STG system can be expected to produce electrical power equivalent to between 5% and 8% SMCR [115]. STGs are suitable for main engine power below 25,000 kW. Differently from the PT system, the ST system is relatively expansive and requires more space for installation. The existing boiler system would likely need expansion, along with installation of multiple pipes for exhaust gas, steam, and condensed water. A

condenser needs to be installed with the steam turbine, and can in some cases be as large as the turbine itself.

3.1.2.3 Combined steam turbine / power turbine and generator (ST-PT) systems

The third and most complex turbocompounding system consists in a combined Steam Turbine, Power Turbine and Generator (ST-PT): a combination of the two above systems. In the usual configuration, the power turbine connected to the generator via a gearbox, with the steam turbine further connected to the same generator by another gearbox, all on the same shaft, with the exhaust gases first being used to produce steam in a dual-pressure exhaust gas boiler, then expanding through the power turbine. A schematic example of the specific layout of this turbomachinery on a single shaft can be seen in Figure 52 [118]. If space in the onboard machinery is limited, the two systems may be found on separate shafts, with each their own dedicated generators [119].

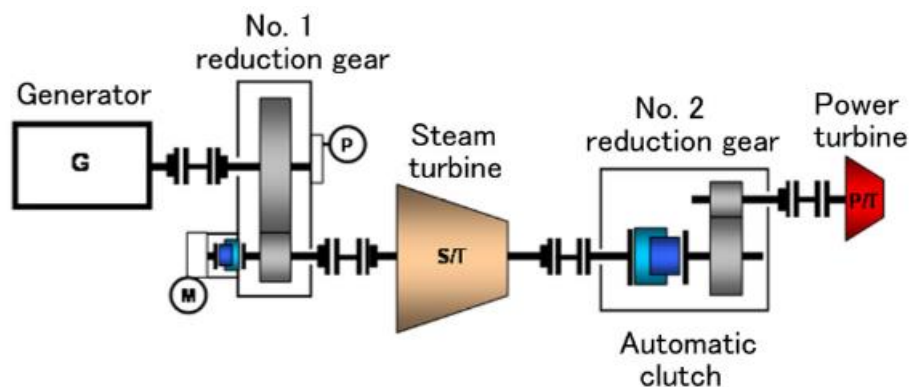


Figure 52 Example of a steam turbine, power turbine, gearboxes and generator interconnected on the same shaft [118]

This solution can be used for marine systems with high electrical power demand. The combined system has the most potential of the three systems. While running at specified maximum continuous rating (SMCR), ST-PT system can be expected to produce electrical power equivalent to approximately 10% SMCR [115]. Combined ST-PT systems are suitable for main engine power above 25,000 kW.

Wartsila developed and presented the performance results of a combined PT-ST system [117]. The WHRS was integrated to energy system with a Sulzer 12RT-flex96C engine (68,640 kW SMCR) and features a dual-pressure steam turbine (called 'steam turbogenerator' in Figure 53) a high-pressure

section at 8.5 to 9.5 barg, low-pressure section at 3 to 3.5 barg and running at 6750 rev/min which is reduced down by the gearbox to 1800 rev/min for the generator. Approximately 10% of engine SMCR was recovered as electrical power, depending on engine operating conditions and load, with ~6,500 kW recovered at 100% SMCR. Yagi et al. for Mitsubishi Heavy Industries [118] developed a combined PT-ST WHRS integrated to an engine with 47,740 kW SMCR featuring a single pressure Mitsubishi ATD52CLM steam turbine rated at 2,500 kW, using steam at 267°C / 5.88 bar (8,700 rpm), a 1,700 kW rated Mitsubishi MPT42 power turbine (20,000 rpm). The WHR system recovered 7%-9% of engine load as electrical power, with 4,159 kW recovered at 100% SMCR.

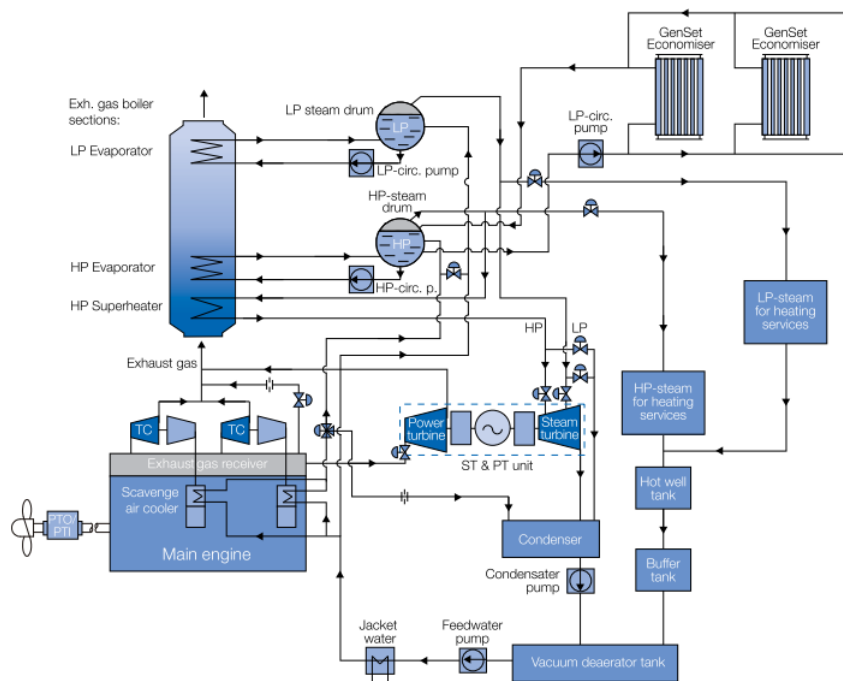


Figure 53 Example of combined PT-ST system suggested by MAN [1]

Ma et al. simulated the performance of a combined PT-ST system for a 1000 ton container ship [120]. They assumed a MAN 9K98ME-C7 engine (54,180 kW SMCR), single pressure steam turbine using 270°C / 7 bar steam. Depending on engine load, 8% to 12% of engine load was recovered, with 6,700 kW recovered at 100% SMCR. MAN present the performance of the combined PT-ST system in their WHR document [1], applied to a MAN B&W 10S90ME engine (48,510 kW SMCR), with a dual pressure steam turbine, the low pressure steam at 4.5 bar / 148 °C, and high pressure steam varying from 10 bar / 259°C

at 100% engine load, to 6.5 bar / 256°C at 50% load. 7% to 9% recovery was achieved depending on engine load, with 4,315 kW recovered at 100% SMCR.

3.1.3 Techno-economics

3.1.3.1 Technical Performance maps

Figure 54 shows the complete performance maps of these combined ST-PT systems as a function of engine load. Above ~50% engine load, the combined systems can recover approximately 7% to 14% of engine load as generated electricity for on-board demand. The performance is dependent on many factors such as engine conditions, weather, ship condition etc. However, a clear trend points towards system efficiency improving with the power rating of the main engine and the engine load. A significant drop-off is observed below 50% engine load for Ma et al.'s system and below 45% main engine load for Yagi et al.'s system; at those engine loads the by-pass valve to the power turbine is closed, and a minimum engine load is required to start operating the combined PT-ST system.

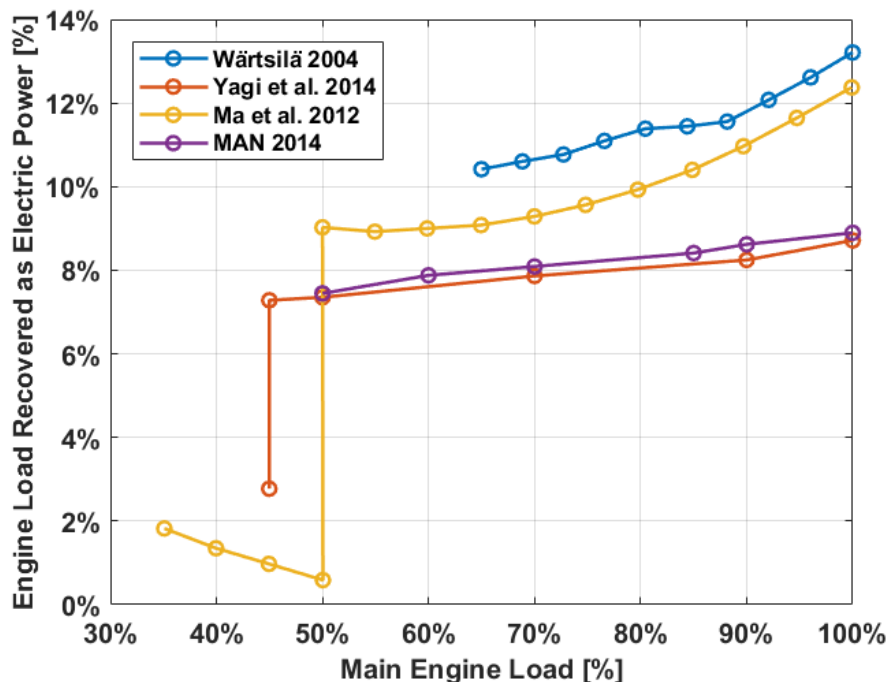


Figure 54 Performance of combined PT-ST WHRS: fraction of engine load recovered as electrical power as a function of engine load. The total recovered energy is counted as the sum of electrical power outputs of the steam turbine and power turbine

3.1.3.2 Economic Performance

The economic performance of on-board WHR depends obviously on the size of the ship, but also on the operational profile which depends strongly on the type of ship. The operational profile gives a frequency distribution of ship load operation over the course of a year, which, in combination with performance diagrams of the WHR system as a function of engine load (as shown in Figure 54), yields the total amount of generated electricity. The quantity of recovered electricity yields the total heavy fuel oil (HFO) savings (HFO cost = 150 \$US/ton), from which annual savings can be calculated. Annual savings should also account for secondary savings incurred by reducing total engine usage: maintenance and lubrication savings primarily. Operation costs of the WHRS should also be accounted for. Olaniyi et al. [121] collected data from various manufacturers including MAN, and provide the following initial investment costs for turbocompounding WHR:

- 420 €/kW installed for ST-PT systems, which can drop down to 150-200 €/kW on ships with main engine power above 50,000 kW due to economics of scale, with 32,000 €/year maintenance costs.
- 320 €/kW installed for STG systems, with 21,000€/year maintenance costs.
- 105 €/kW installed for PTG systems, with 10,500 €/year maintenance costs.

Figure 55 shows the economic performance of various turbocompound WHRS using the above methodology and assumptions. Systems with higher complexity (combined ST-PT systems) display the largest initial investment (lowest point of intersect with vertical axis at year 0) and high return rate (slope of the cash flow curve). Payback times around 5 years can be expected for these types of WHRS.

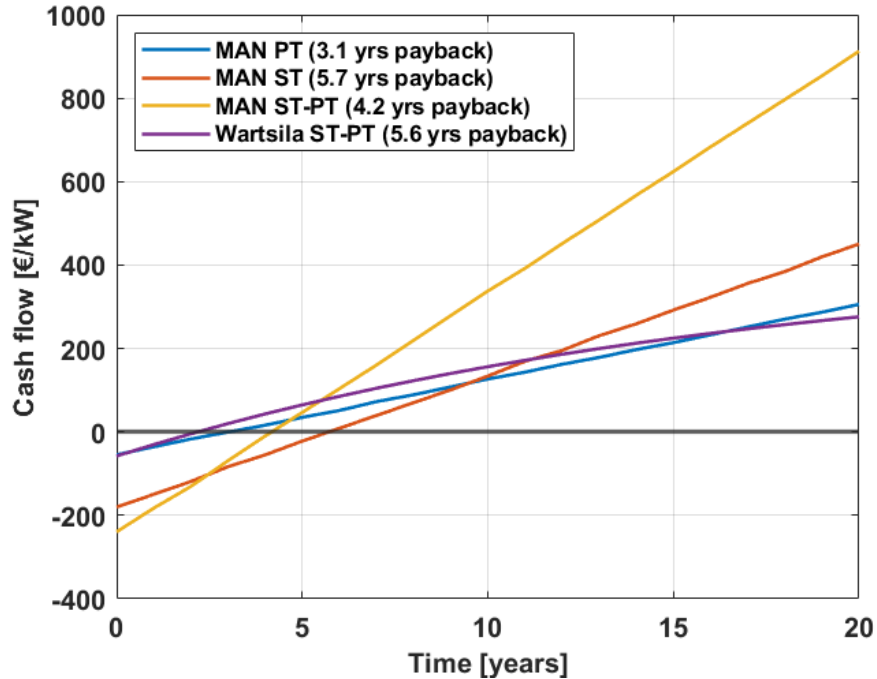


Figure 55 Economic performance of various turbo compounding WHRS, cash flow normalised for engine power rating at 100% SMCR, 20 years system lifetime assumed, 6% interest rate

3.1.4 Modelling turbocompounding systems

The amount of energy absorbed by the turbocompounding system, $F_{TC}(t)$, is expressed as a linear function (or piecewise linear function) of the net power drawn from the TC, $P_{TC}(t)$, using the thermal efficiency of the system (equation (31)). $\delta_{TC}(t)$ is a binary decision variable which indicates whether the TC is on or off at time t .

$$F_{TC}(t) = \frac{1}{\eta_{TC}} P_{TC}(t) \delta_{TC}(t) \quad (34)$$

Where η_{IEE} is the efficiency of the turbocompounding system. The work produced by the TC is constrained in Equation (32) using a rated design for TC D_{TC} , with upper and lower bounds indicated with variables $k_{1,TC}$ and $k_{2,TC}$. $x_{TC}(t)$ is a binary decision variable which indicates whether the TC is included or excluded in the energy system.

$$k_{1,TC} D_{TC} x_{TC}(t) \leq P_{TC}(t) \leq k_{2,TC} D_{TC} x_{TC}(t) \quad (35)$$

3.2 Steam Rankine Cycles

3.2.1 Introduction

The Rankine cycle is the basic working cycle used in vapour power plants [11]; its main function is the conversion of thermal energy into electrical energy. Heat is used to evaporate a working fluid, and the vapour is expanded in a turbine to produce mechanical work. Steam Rankine cycles (SRC) are conventional versions of this cycle using water as the working fluid. SRCs are a mature technology with multiple examples of applications for industrial WHR in steel, cement, chemical and power production industries, which range from ~50 kW to several hundreds of MWs [122].

3.2.2 Technology Overview

3.2.2.1 Working principle

The simplified layout of a SRC is shown in Figure 56 [11]. A subcooled liquid water flow is pumped and supplied to a boiler, using an electrical work supply to the pump \dot{W}_p [J]. In the boiler, water is heated up to its boiling point, evaporated and generally superheated beyond the boiling point, using thermal energy \dot{Q}_{in} [J] from the heat source. At the outlet of the boiler, water vapour is supplied to a turbine, where it is expanded to a lower pressure, providing a net work output as mechanical energy \dot{W}_t [J]. The main turbine shaft is generally connected to an electric generator. At the turbine outlet, the water vapour is condensed back to the liquid phase by extracting heat \dot{Q}_{out} [J] before returning to the pump, thus completing the cycle [123].

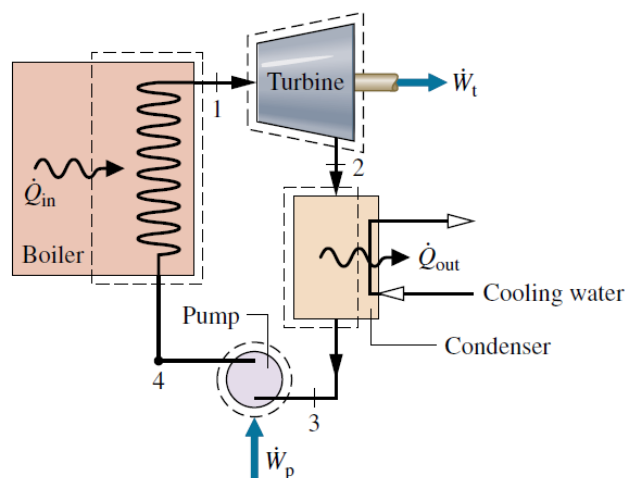


Figure 56 Basic layout of a Steam Rankine Cycle with energy and work flows [11].

SRCs require a high temperature waste heat source in order to evaporate and superheat liquid water to steam. Steam at around 17 bar will typically be superheated up to ~280-290°C [61,124]. Superheating the steam is often required to prevent water condensation which causes damage to the turbine blades by erosion. Thus, due to the pinch point in the heat exchange, the boiling and superheating process in the SRC requires a heat sources at temperatures beyond 300°C, which can be obtained from exhaust gas flows from fossil fuel plants or large diesel engines.

Typical SRC cycles can generally be separated into single pressure systems and dual-pressure systems [125]. The heat exchange between exhaust gases and the water flow for each of the two systems are compared in Figure 57, which shows a heat transfer diagram typically used when analysing SRCs. For single pressure systems, a minimum steam pressure of 7 bar with boiling point 165 °C is chosen to prevent acid condensation in the boiler as recommended by manufacturers.

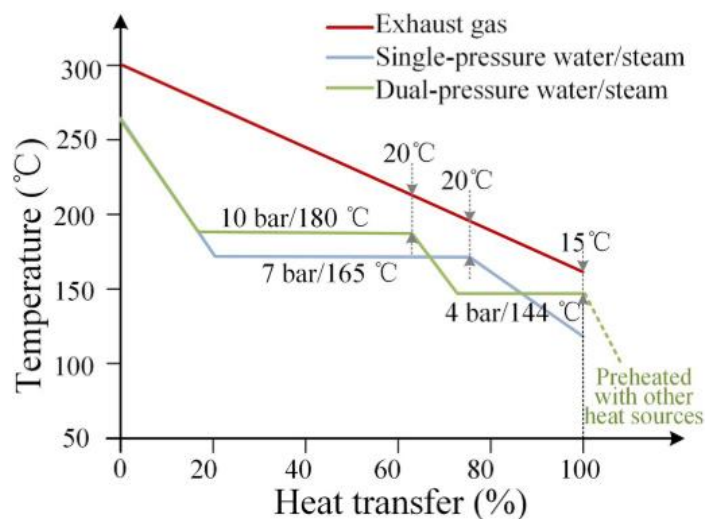


Figure 57 Heat transfer diagrams for single and dual-pressure SRC systems [125]

3.2.2.2 SRC configurations and on-board integration

The simplest integration of the SRC to marine energy systems is to directly use the exhaust gases in a boiler heat exchanger to vaporise the water flow. Senary et al. [124] estimated with a thermodynamic model that the integration of a SRC aboard a LNG carrier can recover up to 16% of the waste heat (i.e. 8% fuel efficiency increase with a 50% engine efficiency) at 100% SMCR, generating ~7 MW electrical power. In this configuration steam is generated at 17 bar, superheated to 280°C in a SRC layout where

water is preheated in economiser, evaporated and superheated using exhaust gases as the heat carrier as shown in Figure 58 [124]. This layout is relatively simple as the Rankine cycle is in the most basic layout (single loop, no regeneration) and uses a single temperature heat source, for electrical power generation without any coupling with other WHR technologies.

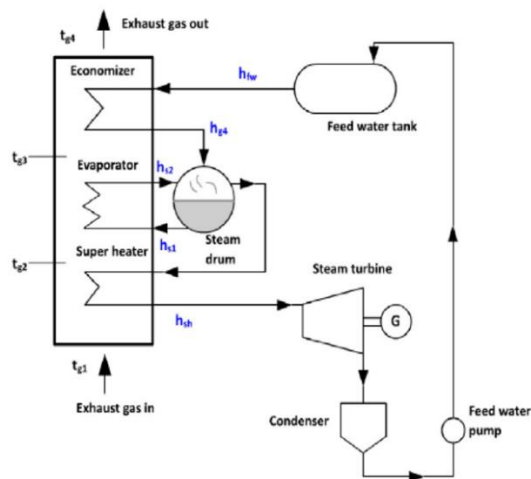


Figure 58 Simplified steam Rankine cycle layout using exhaust gases to heat, evaporate and superheat a flow of water [124]. The steam turbine is commonly connected to a generator to convert the mechanical power output to electrical power.

Indeed, coupling the SRC with other WHR technology which can leverage the heat recovered during steam condensation has been investigated in various configurations. Furthermore in some layouts multiple waste heat sources are used in series to generate steam. Rivera-Alvarez et al. [126] suggest coupling a SRC with a conventional turbocompounding steam turbine, a typical currently implemented WHR technology for marine energy systems (see previous **section 3.1** on Turbocompounding), in a so-called combined cycle system. The layout is shown in Figure 59. In their analysis, they evaluate the trade-off of increasing the efficiency of the two coupled turbine systems which increases system weight and therefore technical complexity, space required on-board and results in increased fuel consumption.

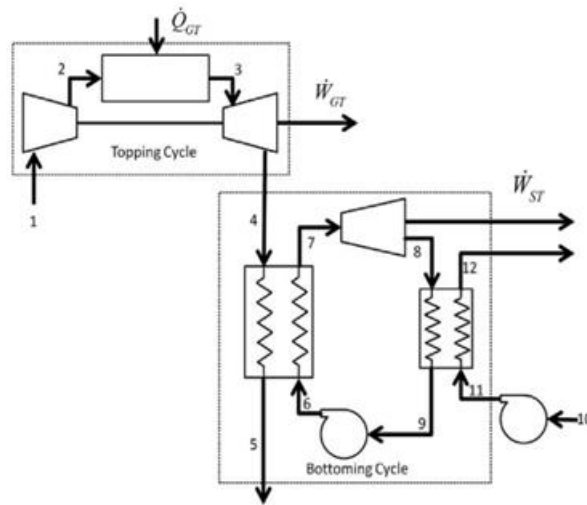


Figure 59 Combined gas turbine cycle with steam Rankine cycle for marine energy systems [126]

Liang et al. [127] used a thermodynamic model to evaluate the performance of a SRC coupled to an ammonia-water pair based absorption refrigeration cycle (absorption refrigeration cycles are reviewed in more detail further in this report in section 0). The condenser of the SRC serves as the evaporator in the absorption refrigeration cycle, with water condensation occurring in the 52°C to 82°C temperature range at 0.7 bar absolute pressure. SRC working fluid is preheated with jacket cooling water (JCW, temperature around 315°C) from the engine cooling systems, and evaporated and superheated by heat from the exhaust gases which are available around 325°C. At 100% SMCR, they calculated a cycle net power output of 128 kW_e and cycle efficiency of approximately 19%.

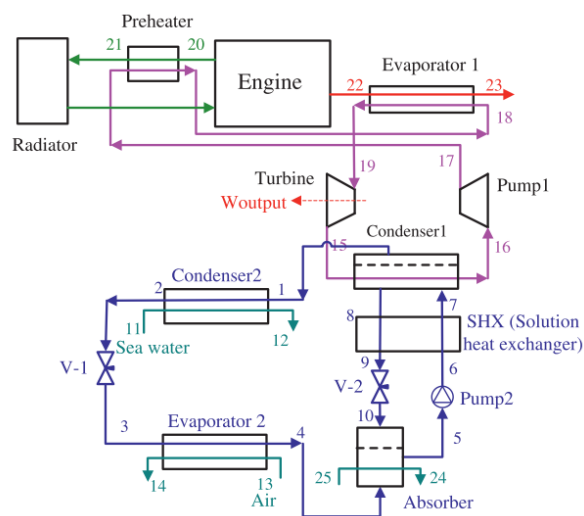


Figure 60 On-board steam Rankine cycle coupled with absorption refrigeration [127]

In their comparison of various power cycles for marine WHR, Larsen et al. [128] suggest using engine JCW and charge air successively to preheat the water circuit of a SRC before carrying out evaporation in a dual-pressure boiler system (3.4 bar and 9.8 bar) using the exhaust gases. The integrated cycle at 100% SMCR increased the fuel efficiency of the system from 49.4% (engine and turbu-charger without WHR), to 51.1% with the SRC, equivalent to a 3.44% cycle thermal efficiency.

On a bulk carrier, Vanttola and Kuosa [61] from VTT Technical Research Centre of Finland, evaluated via pinch analysis that the integration of a SRC could lower auxiliary fuel expenditure 18.8%, which effectively corresponds to a total fuel consumption decrease of 4.7%. The methodology used aimed to identify the maximum energy recovery (MER), while also accounting for the various ship operating conditions relating to its yearly operational profile.

3.2.3 Techno-Economics

3.2.3.1 SRC Technical performance

The performance of the SRC is generally measured with the cycle thermal efficiency, defined as the ratio between the net work production (equal to the difference in work produced at the turbine and work provided to power the pump) and the thermal energy provided, see equation (36).

$$\eta = \frac{\dot{W}_t - \dot{W}_p}{\dot{Q}_{in}} \quad (36)$$

There are little to no examples of currently integrated SRCs in on-board energy systems. As has been seen in the previous section, most studies involve the theoretical integration of SRCs and the evaluation of their behaviour and performance through modelling. The technical performance of these SRC systems proposed in the literature is shown in

Table 10. The proposed systems use either a single heat source for the entire boiling process (exhaust gases, marked as 'EG' in the heat source types), or multiple heat sources from the exhaust gases, jacket cooling water (JCW), and charge air (CAC). In the latter case the type, temperature and extracted power from each heat source are indicated.

Table 10 Technical performance of proposed on-board integrated SRCs

| ICE Power [MW][| T heat source [°C] | Heat Source Type | P heat source [kW] | W net [kW] | η src | Ref |
|-----------------|--------------------|---------------------|--------------------|------------|------------|-------|
| 11.7 | 373.0 | EG | - | 7,016.4 | 16%-20% | [124] |
| 51.5 | 325.4 / 89.9 | EG / JCW | 654.7 | 127.8 | 19.5% | [127] |
| 19.7 | 234.0 | EG | 3426.9 | 864.0 | 3.4% | [128] |
| - | 300-200 / 148 / 85 | EG (AE) / CAC / JCW | 1000.0/359.3/242.8 | 162.7 | 16.3% | [61] |

3.2.3.2 SRC costing elements

Oak Ridge National Laboratory reported [122] the findings of consulting and technology company ICF which feature cost estimates for the installation and maintenance of SRCs as a function of the cycle net power output, which can be seen in **Table 11**. In-house data, commercially available systems and discussions with industrial stakeholders helped develop these cost estimates. Capital costs for SRC range from ~ 3,500 €/kW at low capacities to 1,400 €/kW for the largest systems. The authors of the initial study specify that these values do not account for contingency for site-specific characteristic, and actual costs could potentially be higher; however these values provide a reasonable estimate and inform how the cost could scale with installed capacity.

Table 11 ICF's steam Rankine cycle cost estimates (capital investment and O&M) as a function of installed capacity, reported by Oak Ridge National Laboratory (ORNL) [123], costs converted to euros and annualised

| Capacity (kW) | Capital Costs (€/kW) | O&M Costs (€/kW) | Ref |
|----------------|----------------------|------------------|-------|
| 50 - 500 | 3,500 | 0.015 | [122] |
| 500 - 1,000 | 2,900 | 0.01 | |
| 1,000 - 5,000 | 2,100 | 0.009 | |
| 5,000 - 20,000 | 1,750 | 0.007 | |
| > 20,000 | 1,400 | 0.006 | |

3.2.4 Modelling the steam Rankine cycle

The amount of energy absorbed by the SRC, $F_{\text{SRC}}(t)$, is expressed as a linear function (or piecewise linear function) of the net power drawn from the SRC, $P_{\text{SRC}}(t)$, using the thermal efficiency of the system (equation (31)). $\delta_{\text{SRC}}(t)$ is a binary decision variable which indicates whether the SRC is on or off at time t .

$$F_{\text{SRC}}(t) = \frac{1}{\eta_{\text{SRC}}} P_{\text{SRC}}(t) \delta_{\text{SRC}}(t) \quad (37)$$

Where η_{SRC} is the efficiency of the SRC. The work produced by the SRC is constrained in Equation (32) using a rated design for SRC D_{SRC} , with upper and lower bounds indicated with variables $k_{1,\text{SRC}}$ and $k_{2,\text{SRC}}$. $x_{\text{SRC}}(t)$ is a binary decision variable which indicates whether the SRC is included or excluded in the energy system.

$$k_{1,\text{SRC}} D_{\text{SRC}} x_{\text{SRC}}(t) \leq P_{\text{SRC}}(t) \leq k_{2,\text{SRC}} D_{\text{SRC}} x_{\text{SRC}}(t) \quad (38)$$

3.3 Thermoelectric Generation (using Seebeck effect)

3.3.1 Introduction

Thermoelectric generators (TEG) are devices based on solid-state semi-conductors designed to convert thermal power into electrical power. A set of thermoelectric modules are arranged between two heat exchangers, with each thermoelectric module being composed of up to hundreds of thermoelectric pairs (electrically in series and thermally in parallel) [129]. The rugged, reliable nature of TEG has made it a technology of choice in extreme environments. The traditional field of applications of TEGs was/is the space industry, used on-board long distance satellites due to the compact, continuous, reliable supply of electricity [129]. Nowadays TEG is increasingly being investigated for heat recovery in various transport and industrial sectors, including the maritime sector.

3.3.2 Technology overview

3.3.2.1 Working principle

A temperature difference between two different semiconductors yields a voltage gradient between the two materials via the so-called Seebeck effect. The magnitude of the generated voltage gradient

depends mainly on the temperature difference and the material constituting the two semiconductors, see equation (39).

$$V = S(T_h - T_c) \quad (39)$$

Heat is provided on one side of the semiconductors, and rejected on the other side. TEG devices are assembled by combining semiconductor pairs: one n-type semiconductor (with excess electrons i.e. negative charge) and one p-type semiconductor (with a missing electron i.e. positively charged). A typical arrangement is shown schematically in Figure 61 [130]. A metallic, conducting stripe (gold or nickel) acts as the junction between two semiconductors. Examples of semi conductor material could be bismuth telluride (Bi_2Te_3) or lead telluride (PbTe) [131,132],

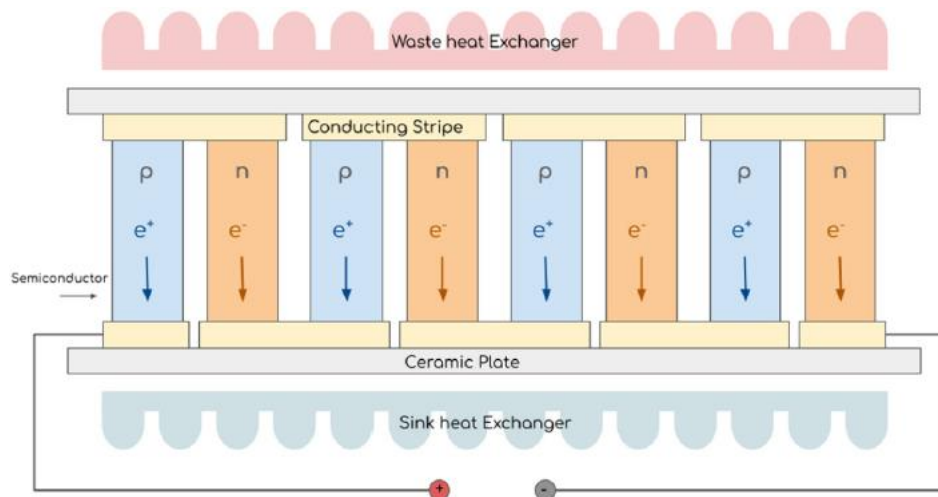


Figure 61 Typical layout of a thermoelectric generator [130]. Pairs of semiconductors are arranged electrically in series, and thermally in parallel

In the context of marine applications, the main advantages of TEG are silent operation, no moving parts which reduces maintenance requirements and results in a long lifespan, low weight and physical footprint, and direct conversion between thermal and electrical power (different from most heat-to-electric converter with an intermediate mechanical energy conversion using an alternator). The main disadvantages are the low conversion efficiency (below 5%) and low power ratings which result in poor cost-efficiency [130].

3.3.2.2 Performance Metrics

The performance of TEG devices is evaluated using efficiency η , which depends mainly on the cold side / hot side temperature difference, calculated with equation (40):

$$\eta = \frac{T_h - T_c}{T_h} \cdot \frac{\sqrt{1 + ZT} - 1}{\sqrt{1 + ZT} + \frac{T_c}{T_h}} \quad (40)$$

Where T_h is the hot side temperature, T_c cold side temperature, T the average temperature ($T = (T_h + T_c)/2$) and ZT is an overall dimensionless figure of merit for TEG devices with Z being the factor of merit. The factor of merit Z depends on the properties of the semi-conducting materials constituting the TE device, as is shown in equation (41), where α , ρ , and λ are Seebeck coefficient, electrical resistivity and thermal conductivity of positively (p) and negatively (n) charged semiconductors, respectively. ZT typically ranges between 0.5 and 2 [133].

$$Z = \frac{(\alpha_p - \alpha_n)^2}{((\lambda_p \rho_p)^{1/2} + (\lambda_n \rho_n)^{1/2})^2} \quad (41)$$

Figure 62 shows the graphical representation of equation (40), i.e. the effect of source/sink temperature difference on thermoelectric efficiency for various figures of merit ZT , along with the theoretical Carnot efficiency. Outside of very large temperature differences ($\Delta T > 200$ °C), thermoelectric generation can be expected to show an efficiency below 10%.

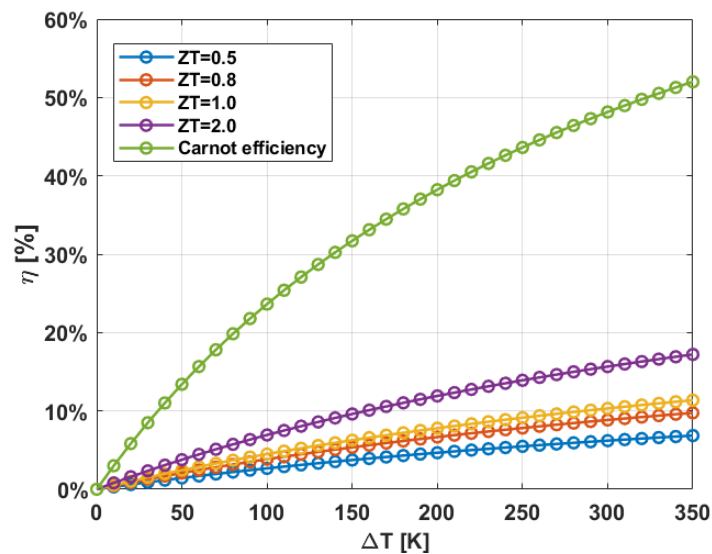


Figure 62 Thermoelectric efficiency values for various figures of merit ZT , compared to theoretical Carnot efficiency, with heat sink temperature $T_c = 50$ °C, adapted from [129]

3.3.3 Applications

Figure 63 and Figure 64 show examples of designs of TEG devices for marine waste heat recovery. These designs were made specifically for the recovery of heat from flue gases from on-board waste incinerators. The TEG in Figure 63 uses sea water (5°C to 30°C) as heat sink. The device geometry was optimised for maximum efficiency, maximum net power gain or cost per unit power [$\$/\text{W}$] minimisation, with module thickness and spacing as the optimisation variables. Devices were obtained with net work outputs between 27.4 kW_e and 57.7 kW_e depending on the objective function for the optimisation, which cost between $2.46 \text{ \$/W}_e$ and $7.42 \text{ \$/W}_e$.

The TEG device in Figure 64 is designed for waste heat recovery in a ship waste incinerator plant, which is a type of on-board waste and pollution management device that operates at temperature range $850\text{--}1200^{\circ}\text{C}$ with exhaust gases that are typically cooled down to below 350°C by heating the ship's fresh water supply [134]. The dimensions of the device are 500 mm length, 100 mm inner diameter with 6 mm pipe thickness, and the system is constituted of 42 individual TEG modules arranged into a hexahedron. With a maximum hot side temperature of 520°C (cold side at 30°C), a 882 W_e power output can be achieved, which corresponds to 4.32% efficiency according to the authors. This efficiency is likely to be lower since pumping power for cold side cooling was not added to the final energy balance.

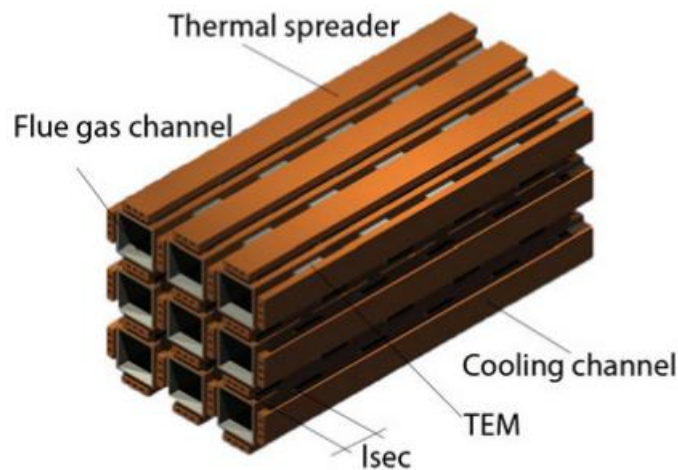


Figure 63 TEG heat exchanger example [135]. TEM = thermoelectric module, L_{sec} = section length

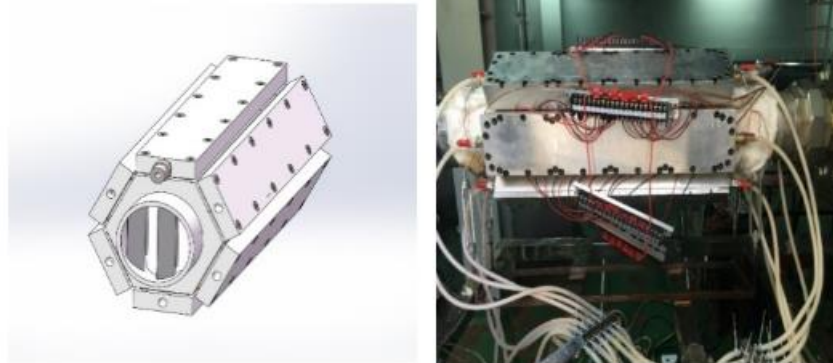


Figure 64 TEG designed for recovering waste heat from ship incinerator exhaust gas [134]

Due to small size as demonstrated in the preceding figures and low net power output, TEG installation is typically envisioned as arrays of TEG modules arranged onto the surfaces of suitable ducts carrying waste heat, such as exhaust ducts in ICE-driven ships. In this applications a probable pitfall is cooling the TEG on the cold side, which could require pumping thus making overall efficiency negligible. Armenakis et al. suggest attaching TEG arrays to the inner surface of the ship hull, below the lower water line. The inner side of the wet hull metal plates is almost always cooler than 30°C; thus when considering the potential temperature range of exhaust gases and TEG performance based on temperature difference, overall efficiency should be reasonable, especially with cooling without pumping and with an infinite heat sink [136]. This infinite cooling capacity is generally highlighted as one of the main reasons why TEG could be particularly suited to marine applications [129]. Another aspect supporting TEG is the ability to convert difficult to recover heat, such as in the case of radiated heat energy; TEG needs simply to be installed on the machinery surface. According to Freer and Powell [133], the main current limitation to TEG in marine applications are the high cost / low availability of the best performing semiconductor materials, and efforts should be focused on developing new high performance materials for economic viability to be achieved.

3.3.4 Techno-economics

Thermoelectric generators and modules are available from various manufacturers including Tegmart [137], Hi-Z [138], Tecteg [139], and Marlow Industries [140]. The following section analyses costing elements of TEG based on the commercial modules provided by these manufacturers. The absolute cost of thermoelectric modules tends to increase as the power output of the module increases (see **Figure**

65). All of the analysed TEG modules cost between 10 € and 70 €, for absolute power outputs in the range 1 W_e to 80 W_e . However, as can be seen from Figure 66 the specific cost of modules with increasing power density tends to decrease, incentivising purchases of high power TEG modules, above 5 kW_e/m^2 . Surface-specific power outputs can be found in the range 5 to 50 kW_e/m^2 . For TEG modules above 5 kW_e/m^2 the specific cost can be expected in the range 0 – 4,000 €/kW $_e$.

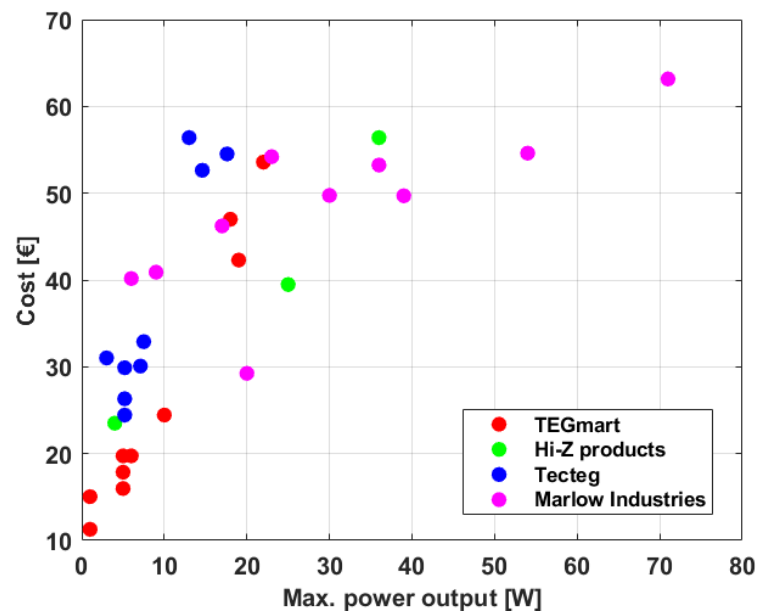


Figure 65 Absolute cost of commercial TEG modules as a function of maximum power output

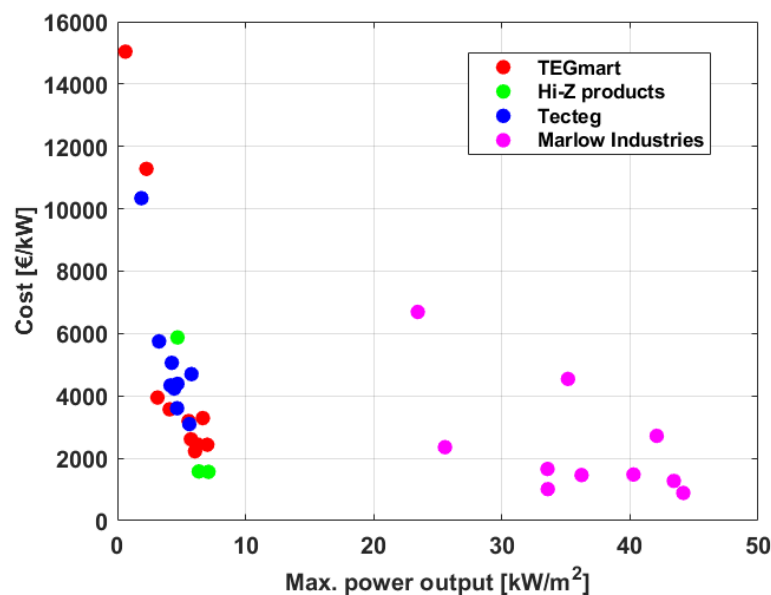


Figure 66 Specific cost of commercial TEG modules as a function of surface power output

3.3.5 Modelling thermoelectric generation

The amount of energy absorbed by the TEG, $F_{\text{TEG}}(t)$, is expressed as a linear function (or piecewise linear function) of the net power drawn from the TEG, $P_{\text{TEG}}(t)$, using the efficiency of the system (equation (31)). $\delta_{\text{TEG}}(t)$ is a binary decision variable which indicates whether the TEG is on or off at time t .

$$F_{\text{TEG}}(t) = \frac{1}{\eta_{\text{TEG}}} P_{\text{TEG}}(t) \delta_{\text{TEG}}(t) \quad (42)$$

Where η_{TEG} is the efficiency of the TEG. The work produced by the TEG is constrained in Equation (32) using a rated design for TEG D_{TEG} , with upper and lower bounds indicated with variables $k_{1,\text{TEG}}$ and $k_{2,\text{TEG}}$. $x_{\text{TEG}}(t)$ is a binary decision variable which indicates whether the TEG is included or excluded in the energy system.

$$k_{1,\text{TEG}} D_{\text{TEG}} x_{\text{TEG}}(t) \leq P_{\text{TEG}}(t) \leq k_{2,\text{TEG}} D_{\text{TEG}} x_{\text{TEG}}(t) \quad (43)$$

3.4 Absorption Refrigeration

3.4.1 Introduction

Cooling capacity is needed in maritime applications, regardless of the ship type, in the form of cabin air conditioning, medicine preservation, and food storage and transport, particularly aboard fishing trawlers etc... While most cooling power generation machinery is electrically powered, recent research has been motivated by the search for energy efficient heat-driven refrigeration systems. On ships, such refrigeration systems can be driven by the waste heat supply from diesel engine exhaust gases and cooling flows. Absorption refrigeration leverages the low boiling point of a refrigerant to remove heat from another fluid flow as the refrigerant evaporates, resulting in the intended cooling effect. A heat source is then used to regenerate the sorbent and recover the refrigerant in vapour form. Thus, absorption systems are similar to common vapour compression systems, except that rather than compressing a refrigerant between evaporator and condenser using mechanical energy, the refrigerant is absorbed by a secondary liquid to form a solution, which is later regenerated using thermal energy. One of the main advantages of absorption refrigeration is that the process of pumping the working solution that has absorbed the refrigerant requires significantly less work than compressing the equivalent vapour in the vapour-compression system, due to the lower specific volume of the liquid

solution [11]. Typical refrigerant/absorbent working pairs are ammonia/water (water is the absorbent), and water/LiBr (water is the refrigerant), with the former suited to lower temperature application (evaporation of the refrigerant occurs at sub-zero temperatures) while the latter may be targeted towards low-temperature heat sources since evaporation occurs at $\sim 5^{\circ}\text{C}$ [141].

3.4.2 Technology overview

3.4.2.1 Working principle

Three key stages form the absorption refrigeration cycle [61] which is schematically represented in Figure 67. **Evaporation** during which the liquid refrigerant flows from the condenser (state 2), through an expansion valve (state 3) and into an evaporator. The refrigerant evaporates by removing the heat at low temperature from a second flow (water), thereby producing the intended cooling effect (state 13 to 14). **Absorption** during which the refrigerant vapour is chemically absorbed in a solution tank called absorber, thereby forming the so-called strong solution. This chemical reaction is exothermic, and cooling water is circulated through the absorber to remove the excess heat (states 15 to 16) since the amount of water which can be absorbed by the refrigerant increases as the temperature of the refrigerant decreases [11]. The strong solution is then pumped to a higher pressure towards the generator (states 10, 9 and 8). The refrigerant then undergoes **regeneration**, the stage during which the heat source is used to desorb the refrigerant in the generator, thereby returning it to the vapour state, from the absorbent which is now the so-called weak solution. Weak solution is returned to the solution tank through a valve (states 7, 6 and 5), whilst the refrigerant vapour is returned to the condenser (state 1), thereby completing the cycle.

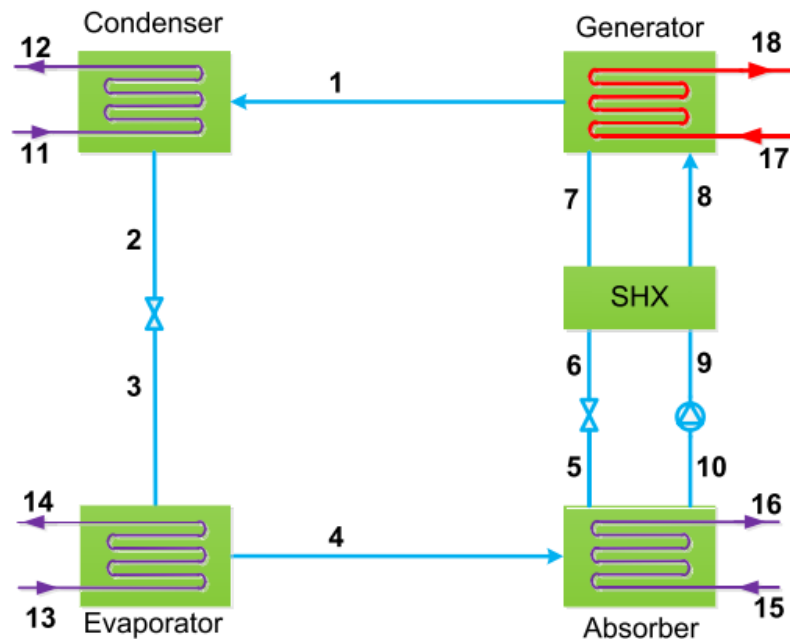


Figure 67 Basic Principle of Single-Effect Absorption Refrigeration Cycle [142]

3.4.2.2 Performance Metrics

The main performance metric for absorption refrigeration systems is the coefficient of performance (COP) which is the ratio of useful cooling power obtained at the evaporator (i.e. the phase-change enthalpy absorbed by the cycle working fluid) over the heat provided at the generator and the power required for pumping the working solution (Equation (44)):

$$COP = \frac{Q_{evap}}{Q_{generator} + W_{pump}} \quad (44)$$

3.4.2.3 Cycle configuration

In practice, two modifications are often made to the basic cycle shown previously in Figure 67. The interface between the generator and the absorber features a heat exchanger so that the strong solution entering the generator is preheated by the flow of weak solution returning to the absorber. This modification reduces the amount of heat needed at the generator to regenerate the absorbent. The other modification typically found is the addition of a rectifier between the generator and condenser; the function of the rectifier is to remove traces of absorbent from the refrigerant as it enters the condenser. The modified cycle with rectifier and intermediate heat exchanger is shown in Figure 68.

The system presented in Figure 68 can still be considered as a simple absorption cycle since it is formed of a single absorption stage. Multiple stage absorption cycles are capable of achieving refrigeration at significantly lower sub-zero temperatures [143].

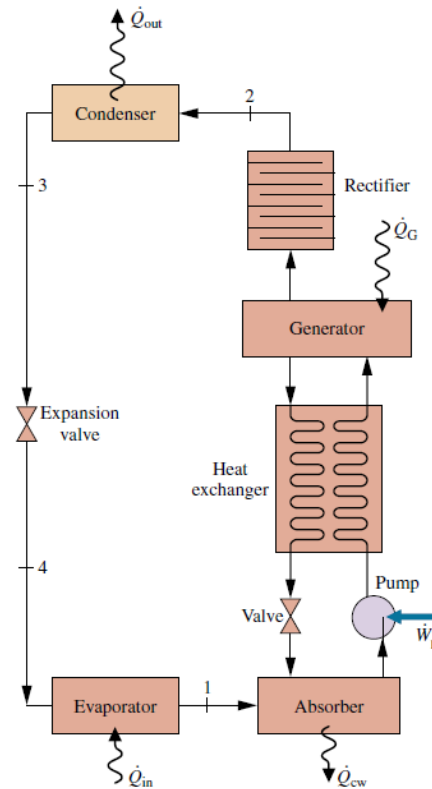


Figure 68 Single-Effect Absorption Refrigeration Cycle with Intermediate Heat Exchanger and Rectifier [11]



Figure 69 (left) 2AA WHR absorption chiller by WorldEnergy which uses hot water at approx. 70°C as the heat source. Retrieved from [144]. (right) hot water driven absorption chiller designed by Kawasaki Thermal Engineering, retrieved from [145]

3.4.3 Applications

Cao et al. [142] proposed a configuration for the integration of absorption refrigeration onboard a cargo ship targeted towards cabin air conditioning, using waste heat carried by the main exhaust gas flow. The performance of the system was evaluated with modelling and simulation. The schematic representation of the configuration can be seen in Figure 70. Heat from the exhaust gas is used to produce hot water which acts as the heat carrier into the generator. The absorber and the condenser are cooled by sea water. Clean water brings the evaporation heat to the refrigerant inside the evaporator, and this process yields chilled water which is transported to the ship's HVAC system.

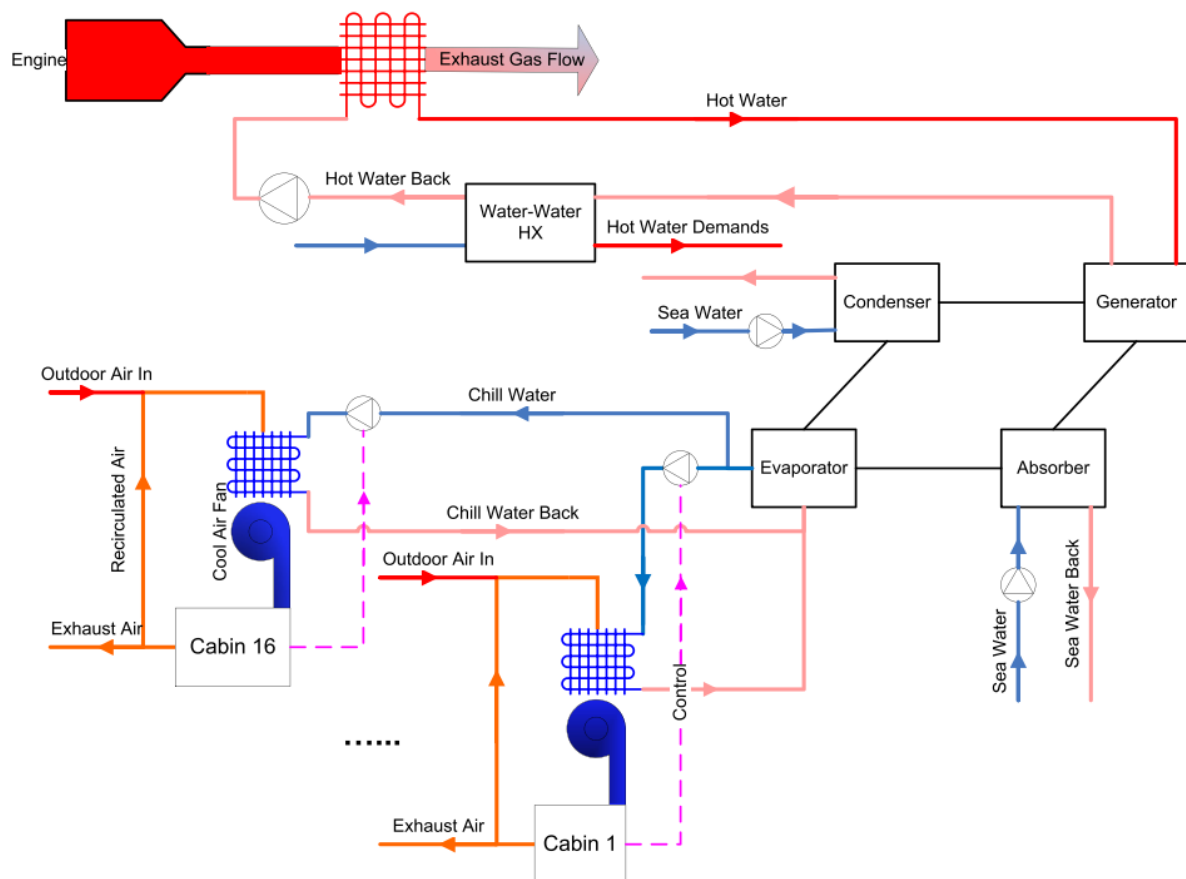


Figure 70 Integration of an absorption refrigeration cycle in a marine application, directly using exhaust gas waste targeted towards cabin air conditioning [142]

The performance and temperature level of various absorption cooling devices designed for sub-zero refrigeration using ammonia as the refrigerant are shown in Table 12. Cycles are shown with increasing

level of system complexity; single stage cycles which refrigeration up to -30°C , while with more complex systems with two stages, two cascaded stages or an additional compression step refrigeration temperatures can be brought down as low as -50°C in some cases.

Table 12 Performance and characteristics of sub-zero refrigerating absorption devices using ammonia as refrigerant, data originally synthesised in [143]

| Cycle | Evaporation Temperature | COP | Working Fluid | Ref |
|------------------------|-------------------------------|---------------|--|------------|
| Single-stage | - 30 to 5°C | 0.25 - 0.55 | $\text{NH}_3 - \text{H}_2\text{O}$ | [146] |
| | - 18 to 3°C | 0.49 - 0.58 | $\text{NH}_3 - \text{H}_2\text{O}$ | [147] |
| | - 8°C | Solar COP | $\text{NH}_3 - \text{LiNO}_3$ | [148] |
| | | 0.066 - 0.093 | $\text{NH}_3 - \text{LiNO}_3 - \text{H}_2\text{O}$ | |
| | - 10°C | 0.6 | $\text{NH}_3 - \text{H}_2\text{O}$ | [149] |
| | - 30 to 10°C | / | $\text{NH}_3 - \text{H}_2\text{O}$ | [150] |
| Double-stage cascade | - 20 to 0°C | 0.17 - 0.31 | $\text{H}_2\text{O} - \text{LiBr} // \text{NH}_3 - \text{H}_2\text{O}$ | [151,152] |
| | - 20 to 0°C | ~ 0.25 | $\text{NH}_3 - \text{H}_2\text{O} // \text{NH}_3 - \text{LiNO}_3$ | [152] |
| | - 70 to -30°C | 0.20 - 0.65 | $\text{NH}_3 - \text{H}_2\text{O}$ | [153] |
| | - 45°C | 0.25 | $\text{NH}_3 - \text{H}_2\text{O} // \text{CO}_2/\text{NH}_3$ | [154] |
| Double-stage | - 15 to 0°C | 0.32 | $\text{NH}_3 - \text{LiNO}_3$ | [155] |
| | | 0.29 | $\text{H}_2\text{O} - \text{NH}_3$ | |
| | - 15°C | 0.27 | $\text{NH}_3 - \text{NaSCN}$ | [ref] |
| | | 0.27 | $\text{NH}_3 - \text{LiNO}_3$ | |
| Absorption/Compression | - 10°C | 1 | $\text{NH}_3 - \text{H}_2\text{O}$ | [155][155] |
| | - 50°C | 0.58 | $\text{NH}_3 - \text{H}_2\text{O}$ | [155] |

3.4.4 Techno-economics

Table 13 reports key investment, installation and O&M costs for absorption chillers, based on composite values (i.e. values synthesised from various case studies which do not refer to a particular system)

provided by US department of Energy [156]. Installation costs for absorption refrigeration systems can be found in the range 500 – 2,000 €/kW. The higher costs tend to be found for the lower capacity systems. Furthermore can be seen the high share of construction and installation which are approximately up to twice the cost of purchasing the equipment.

Table 13 Composite absorption chiller investment and O&M costs, costs converted and annualised, taken from US department of Energy document [156]

| Design | Heat Source | Nominal Cooling Capacity (kW) | Equipment Cost (€/kW) | Construction and Installation (€/kW) | Installed Cost (€/kW) | O&M Costs (cts/kWh) |
|--------------|---------------|-------------------------------|-----------------------|--------------------------------------|-----------------------|---------------------|
| Single Stage | Hot Water | 175 | 652 | 1,293 | 1,945 | 0.195 |
| | | 1,540 | 301 | 444 | 746 | 0.065 |
| | LP Steam | 4,620 | 266 | 318 | 584 | 0.032 |
| Two Stage | HP Steam | 1,155 | 386 | 587 | 973 | 0.097 |
| | | 4,620 | 324 | 389 | 713 | 0.032 |
| | Exhaust Fired | 1,155 | 431 | 639 | 1070 | 0.097 |
| | | 3,500 | 301 | 347 | 648 | 0.032 |

3.4.5 Modelling absorption refrigeration systems

The amount of energy absorbed by the absorption refrigeration system, $F_{ABS}(t)$, is expressed as a linear function (or piecewise linear function) of the net power drawn from the ABS, $P_{ABS}(t)$, using the coefficient of performance of the system (equation (31)). $\delta_{ABS}(t)$ is a binary decision variable which indicates whether the ABS is on or off at time t .

$$F_{ABS}(t) = \frac{1}{\eta_{ABS}} P_{ABS}(t) COP \quad (45)$$

Where η_{ABS} is the efficiency of the ABS. The work produced by the absorption refrigeration system is constrained in Equation (32) using a rated design D_{ABS} , with upper and lower bounds indicated with variables $k_{1,ABS}$ and $k_{2,ABS}$. $x_{ABS}(t)$ is a binary decision variable which indicates whether the ABS is included or excluded in the energy system.

$$k_{1,ABS} D_{ABS} x_{ABS}(t) \leq P_{ABS}(t) \leq k_{2,ABS} D_{ABS} x_{ABS}(t) \quad (46)$$

3.5 Organic Flash Cycles

3.5.1 Introduction

Organic Flash Cycles (OFC) belong to the same class of WHR technology as ORCs, i.e. power generation cycles where a liquid flow is turned to gas by a heat source before expansion in a turbine. More specifically, OFCs are a modified variant of the ORC, developed as a result of the limitations of trilateral ORCs due to the absence of two-phase expanders, for which research is still ongoing [157]. Another limitation to conventional, single-component ORCs is the inevitable temperature mismatch between the heat source (which displays a linear temperature profile) and the working fluid (which, outside of the preheating and superheating, shows a near-isothermal temperature profile during phase change). In the OFC heat is provided to the working fluid until reaching a saturated liquid state, with a vapour phase being generated in a consecutive flash evaporation step. This method enables a narrow temperature difference between heat source and working fluid throughout the entire heat exchange [158], thus minimising irreversibilities and exergy destruction [159]. While the potential of OFCs has been extensively studied through thermodynamic modelling, practical applications are still very limited [159].

3.5.2 Technology Overview

3.5.2.1 Working Principle

The basic layout of an OFC is shown schematically in **Figure 71** [160]. In the OFC, the working fluid is heated in the heat exchanger up to a saturated liquid state. After contact with the heat source, the working fluid is throttled, or flash evaporated, to a lower pressure liquid-vapour mixture. The flow is then separated into saturated liquid and saturated vapour phases. The vapour phase expands in the turbine; as with all power cycles of this WHR class, useful cycle work is extracted at this stage. The lower pressure vapour phase at the turbine outlet is then mixed with the liquid phase exiting from the flash evaporator outlet which has bypassed the expander and had its pressure lowered to the condensation pressure by a throttling valve. The mixture is pumped to a higher pressure before returning to the heat exchanger, thus completing the cycle.

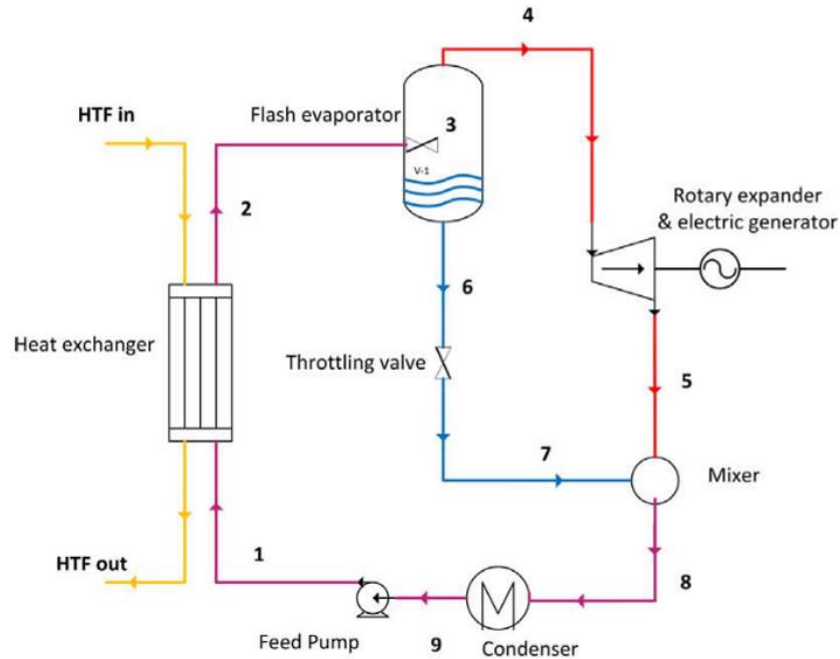


Figure 71 Schematic representation of a conventional Organic Flash Cycle layout [160]

3.5.2.2 Performance Metrics

As for most vapour expansion-based power cycles, the performance of the OFC can be quantified by the net work output as the turbine, and the efficiency of thermal energy to mechanical energy conversion. Net work output W_{net} is the different between the work output at the turbine and the work provided to circulate the working fluid through the process (equation (47)):

$$W_{net,OFC} = W_t - W_{pump} \quad (47)$$

The thermal efficiency η_{th} is the ratio between the net work output of the OFC with the thermal energy used to evaporate the ammonia-water mixture (equation (48)):

$$\eta_{th,OFC} = \frac{W_{net}}{Q_{heat\ source}} \quad (48)$$

3.5.2.3 Configurations and on-board integration

A common variation of the conventional OFC is the double-flash OFC, which is inspired from the double flash steam cycle found in geothermal power generation plants [161]. The layout of the double-flash OFC is shown schematically in Figure 72. The flash evaporation process is carried out in two steps at two

different pressure levels. The vapour phases separated from each evaporator are expanded in two different turbines (high pressure, HP, and low pressure, LP) connected to the same train. This modification is known to increase the amount of working fluid evaporated and expanded, and therefore increase power production compared to the conventional OFC.

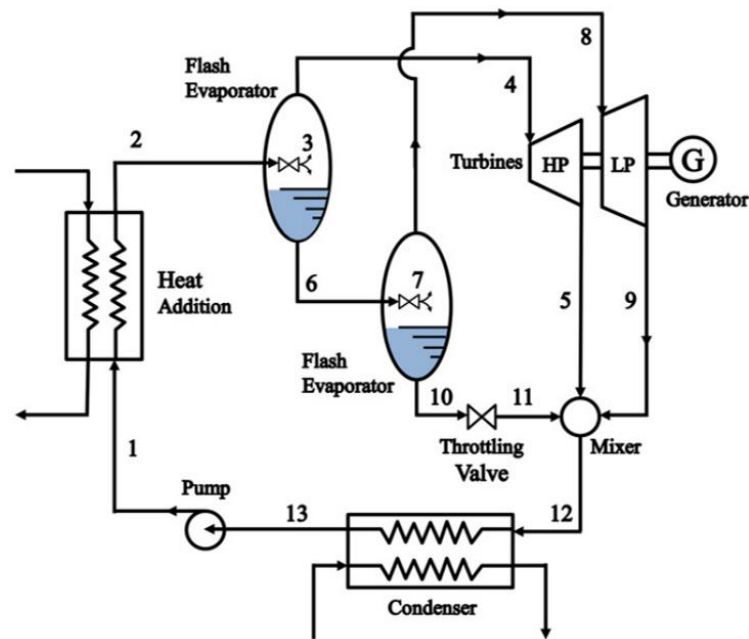


Figure 72 Schematic representation of the double flash OFC layout [161]

In practice, the temperature difference between the returning working fluid and the heat source is large enough to enforce a very large heat exchange surface area, negatively affecting cost. A commonly suggested cycle architecture improvement is to leverage the enthalpy of the working fluid liquid phase at the outlet of the flash separator by mixing it with the working fluid which has been expanded and condensed beforehand (in the conventional cycle the vapour and liquid phases are mixed before condensation). This so-called Organic Flash Regenerative Cycle (OFRC), presented schematically in Figure 73, has the benefit of reducing heat exchange surface area requirements of the condenser and of the main heat exchanger [160,162]. In their cycle analysis comparing OFRC to OFC using I-pentane as the working fluid, Baccioli and Antonelli [160] noted a surface area reduction of ~47% and ~6% for the main heat exchanger and condenser respectively, corresponding to a cost reduction of ~16% and ~6.5% for these components.

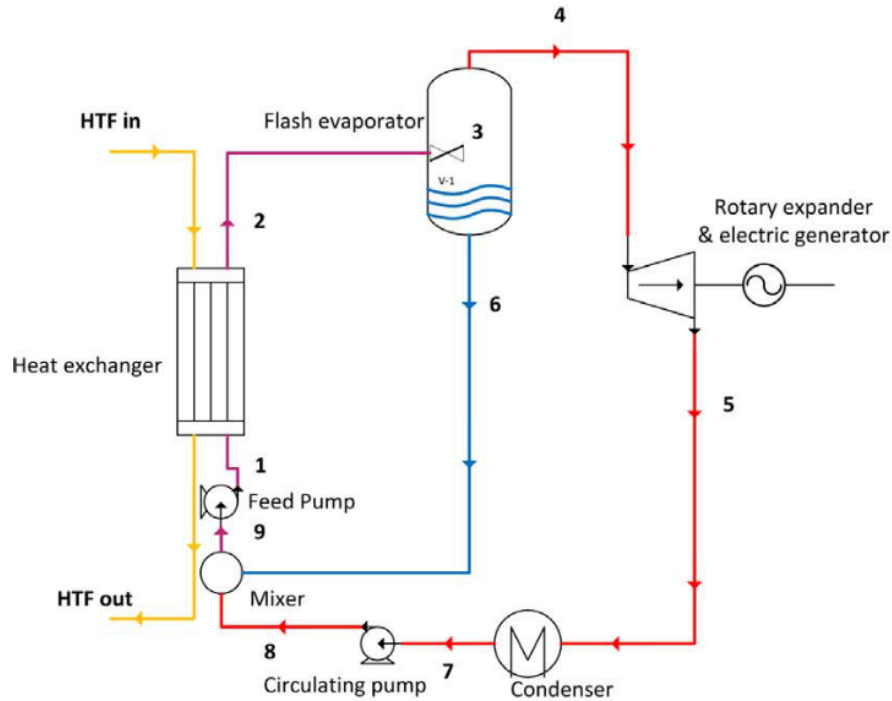


Figure 73 Schematic representation of a Organic Flash Regenerative Cycle layout [160]

3.5.3 Techno-economics

Table 14 shows a synthesis of technical performance data of proposed OFC layouts. Data was either directly extracted from the scientific literature or derived from available secondary data, while certain values were unavailable. In these suggested systems, electrical power outputs in the range 5 – 200 kW_e can be expected using heat sources with power approximately 100 to 2000 kW_{th} and with temperatures between 120°C and 200°C. As is commonly seen with power cycle-based WHR technologies, overall performance can be seen to scale with heat source temperature.

Table 14 Synthesis of technical performance data of Organic Flash Cycles in scientific literature

| Type | P _{Heat Source} [kW] | T _{Heat Source} [C°] | Working Fluid | W _{net} [kW] | η _{th} [%] | Ref |
|------|-------------------------------|-------------------------------|---------------|-----------------------|---------------------|-------|
| OFC | 530.0 | 180 | R245fa | 50.65 | 9.56% | [158] |
| OFC | 508.9 | 180 | R123 | 43.97 | 8.64% | [158] |
| OFC | 552.6 | 180 | o-xylene | 45.04 | 8.15% | [158] |

| | | | | | | |
|-----------------|-------|-----|-----------|--------|--------|-------|
| OFC | 741.3 | 150 | N-heptane | | | [162] |
| OFRC | 571.7 | 150 | N-heptane | | | [162] |
| OFC | 100 | 180 | I pentane | 7.09 | 7.09% | [160] |
| OFRC | 100 | 180 | I pentane | 6.70 | 6.70% | [160] |
| OFC | 2717 | 150 | I pentane | 144.41 | 5.31% | [163] |
| 2 phase OFRC | 2717 | 150 | I pentane | 165.52 | 6.09% | [163] |
| OFRC | | 150 | Pentane | | 15.60% | [164] |
| OFC | | 150 | Pentane | | 9.03% | [164] |
| OFRC | | 175 | Pentane | | 17.50% | [164] |
| OFC | | 175 | Pentane | | 12.40% | [164] |
| OFRC | | 200 | Pentane | | 19.02% | [164] |
| OFC | | 200 | Pentane | | 17.01% | [164] |

Baccioli et al. [162] and Bonolo de Campos et al. [164] provide data for the specific cost of OFCs and more specifically the regenerated variant, based on thermodynamic analysis, process simulation and cost functions from Turton et al. [38]. At constant heat source power, the performance, size and therefore specific cost of the constituting machinery was found to be highly sensitive to the heat source temperature (HTF inlet temperature at the main heat exchanger). Increasing HTF inlet temperature from 80°C to 170°C and therefore the temperature difference in the main heat exchanger (with a constant power of 900 kW maintained through variation of HTF flow rate) results in two counteracting effects:

- increase of required heat exchange surface area and therefore cost of the main heat exchanger and condenser;
- decrease of the flow rate entering the expander and therefore decrease in required size and cost.

The final effect of HTF temperature variation on total specific cost of the OFRCs can be seen in Figure 74. Specific costs OFRC can be seen to level out around ~2,000-3,000 €/kW for heat sources at temperatures beyond 140°C. For heat sources at temperatures below ~100-120°C specific investment costs are above 4,000 €/kW.

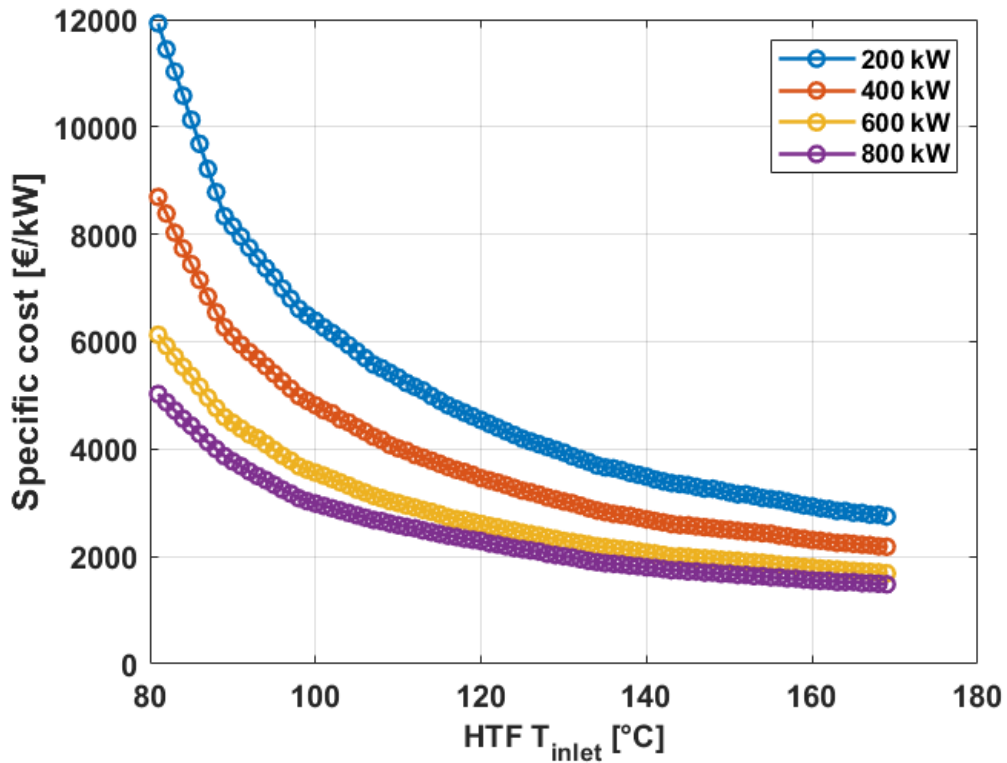


Figure 74 Effect of heat source temperature on the specific cost of regenerated OFCs, data from [162] and [164]

3.5.4 Modelling the organic flash cycle

The amount of energy absorbed by the OFC, $F_{\text{OFC}}(t)$, is expressed as a linear function (or piecewise linear function) of the net power drawn from the OFC, $P_{\text{OFC}}(t)$, using the efficiency of the system (equation (31)). $\delta_{\text{OFC}}(t)$ is a binary decision variable which indicates whether the OFC is on or off at time t .

$$F_{\text{OFC}}(t) = \frac{1}{\eta_{\text{OFC}}} P_{\text{OFC}}(t) \delta_{\text{OFC}}(t) \quad (49)$$

Where η_{OFC} is the efficiency of the OFC. The work produced by the OFC is constrained in Equation (32) using a rated design for OFC D_{OFC} , with upper and lower bounds indicated with variables $k_{1,\text{OFC}}$ and $k_{2,\text{OFC}}$. $x_{\text{OFC}}(t)$ is a binary decision variable which indicates whether the OFC is included or excluded in the energy system.

$$k_{1,\text{OFC}} D_{\text{OFC}} x_{\text{OFC}}(t) \leq P_{\text{OFC}}(t) \leq k_{2,\text{OFC}} D_{\text{OFC}} x_{\text{OFC}}(t) \quad (50)$$

3.6 Kalina Cycles

3.6.1 Introduction

Kalina cycles are a type of power cycle designed to convert heat to electricity in a similar class of WHR technology as steam and organic Rankine cycles. It was originally introduced in 1983 [165] as an alternative to the aforementioned Rankine cycles, with potentially higher efficiency and lower components cost, described as condensation supplemented by absorption, following expansion in a turbine. While, since its conception, the cycle has been extensively studied in terms of thermodynamics, energy and exergy efficiencies, few actual applications may be found, either commercially available or implemented in industry [166–168]. Thus this technology can still be considered as a developmental WHR technology, and should therefore be discussed as a potential alternative to Rankine cycles rather than an established technology.

3.6.2 Technology Overview

3.6.2.1 Working principle

Kalina cycles leverage the non-isothermal phase-change behaviour of ammonia-water mixtures, which are zeotropic mixes. Kalina cycle are thus suitable to operate using variable temperature heat sources, such as renewable heat sources (solar, geothermal, industrial or engine waste heat) [125]. The evaporation temperature of the mix varies with the water-ammonia composition of the mixture. The higher the ammonia content, the lower is the boiling temperature (**Figure 75**). Kalina cycle is composed of three main process units: boiler, turbine, and condensation/distillation system. The composition of the mixture is controlled in the condensation/distillation system in order to adapt the boiling point to the temperature of the available heat source.

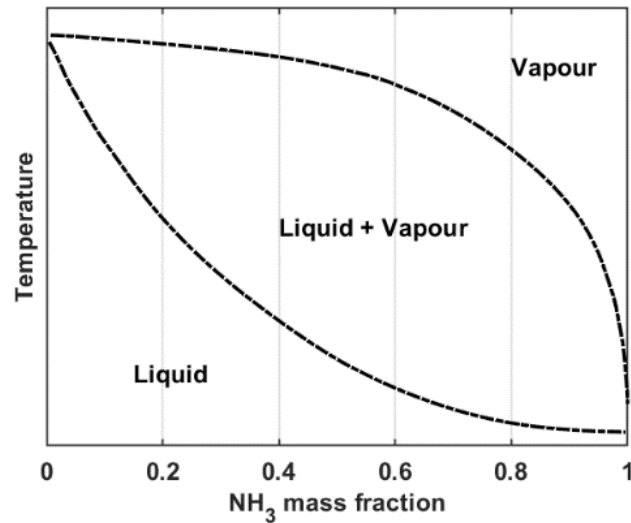


Figure 75 Bubble and dew point in phase diagram for the ammonia-water mixture as a function of ammonia mass content, for a constant pressure, adapted from [2]

The basic configuration of the Kalina cycle is shown schematically in Figure 76. Useful work is produced by expanding the superheated ammonia-water vapour flow in a turbine. The ammonia-water mixture at the turbine outlet is cooled (distiller, and reheaters 1 and 2), mixed with a weak ammonia solution returning from a separator further down the process, and condensed in an absorber. The liquid ammonia-water flow is pumped to a higher pressure, heated in three stages by the outlet of the turbine, before being separated into a weak ammonia solution and an ammonia-rich vapour (separator). The weak solution is returned to the turbine outlet as described previously, while the vapour is cooled. Some of the original water-vapour solution is added to the vapour, to obtain a ~70% ammonia-content solution, which is then cooled, condensed (water-cooled), pumped, preheated, and sent to the boiler to be turned to superheated ammonia-water vapour, thus completing the cycle. Useful work is extracted at the turbine, thermal energy is provided at the boiler, and electrical energy is spent pumping the fluid.

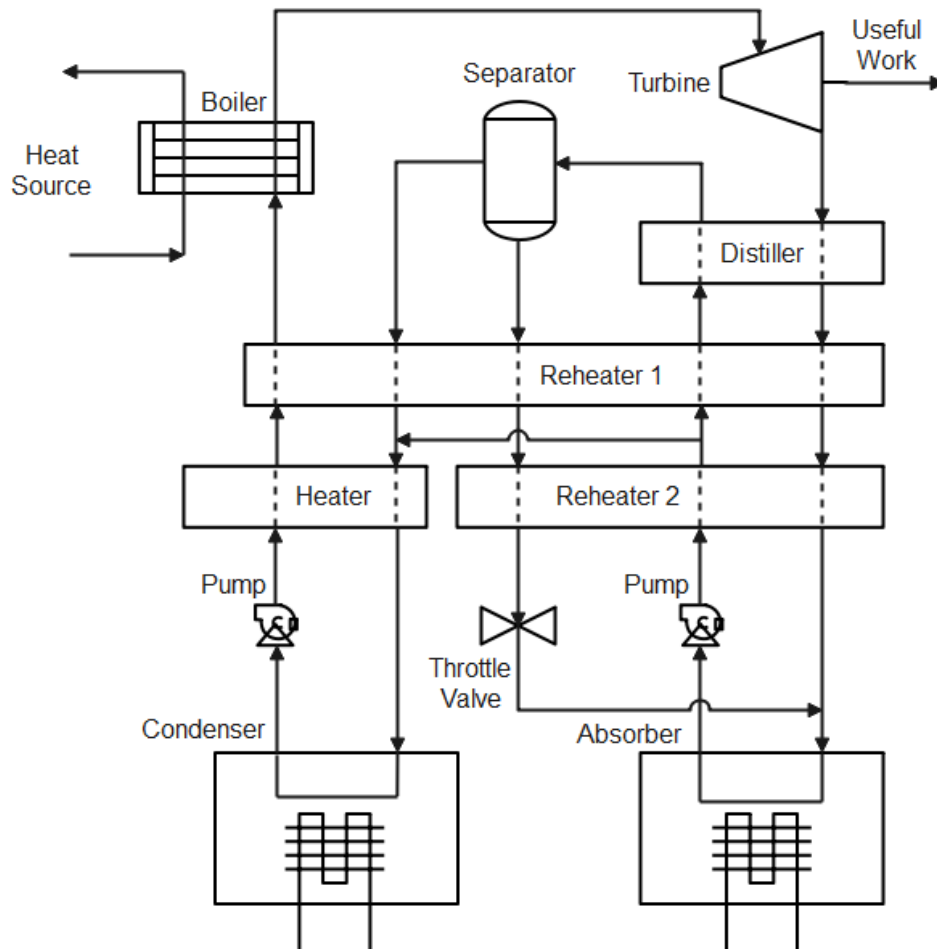


Figure 76 Schematic representation of a Kalina cycle standard layout, adapted from [167]

3.6.2.2 Configurations and on-board integration

The integration of Kalina cycles is typically envisioned to recover high temperature waste thermal flows found in energy intensive industries (steel, cement, petrochemicals, power generation), and in the exhaust flows from gas turbines and large engines. Figure 77 shows a proposed layout for a Kalina cycle as a WHR method for the exhaust gases of a 97 kW 4-stroke Diesel engine [169]. In this system, an engine cooling circuit (waste heat at temperature 87°C, flow rate 1.6 kg/s) is used to preheat the ammonia-water mix, while the thermal energy in the EG at the outlet (temperature 540°C, flow rate 0.177 kg/s) of the engine's turbocompressor turbine is used to fully evaporate and superheat to 450°C the mixture.

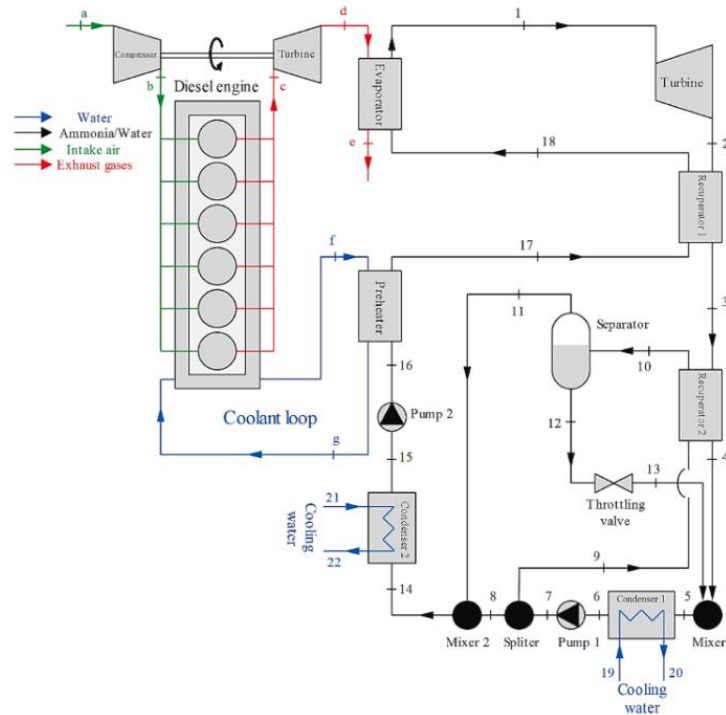


Figure 77 Integration of a Kalina cycle as a bottoming cycle to a Diesel engine, generating useful work using the exhaust gases and engine coolant loop [169]

Bombarda et al. [170] compared the potential for recovering and converting waste heat from large Diesel engines (two 17.9 MW engines with EG at 35 kg/s for both engines and temperature 346 °C) to electricity with either an ORC or a Kalina cycle. The layout for the proposed Kalina cycle integration is shown schematically in Figure 78. The results indicated that the Kalina cycle (17.5% recovery efficiency) presents a slight increase in performance over the ORC (17.3% recovery efficiency) at the cost of larger heat exchangers, a larger plant and overall more complicated layout mainly due to potential corrosion of dissolved ammonia with many metals and much higher pressure in the Kalina cycle (50 to 100 bar) compared to the ORC (10 bar). The results of this specific study indicate that the Kalina is probably not advantageous in marine energy systems, where compactness and system simplicity are major requirements, compared to ORCs.

Table 15 Synthesis of technical performance data of Kalina cycles either commercially available or found in scientific literature. Data originally synthesised in and table adapted from European project SoWhat deliverable 1.6 [166]

| Heat Source | $T_{\text{heat source}} [^{\circ}\text{C}]$ | Power [kW] | $\eta_{th} [\%]$ | Ref |
|---------------------------------|---|------------|------------------|-------|
| Gas Flow From Oxygen Conversion | 98 | 3,450 | 10.4 | [171] |
| Vapour Flow | 116 | 3,300 | 7.6 | [172] |
| Clinker EG + Cooling | 360 | 8,600 | - | [173] |
| Clinker Cooling | - | 4,750 | - | [174] |
| Vapour Flow | 179 | 1,362 | 20 | [175] |
| Thermal Oil | 200 | 278 | 11.7 | [176] |
| Generic Industrial Heat Source | 300 | 739 | 21.7 | [177] |
| Coal Combustion Flue gas | 150 | 320 | 12.3 | [178] |
| Cement Preheater EG | 390 | 3,430 | 23.3 | [168] |
| Engine EG + Cooling | 524 / 86.8 | 21.7 | 25.6 | [169] |
| Engine EG | 439 | 217 | 18.8 | [179] |
| Engine EG | 346 | 1,615 | 19.7 | [170] |
| Gas Turbine EG | 566 | 3,137 | 28.6 | [180] |
| | 550 | - | 30 | [181] |
| | 522 | 86,136 | 35.6 | [182] |
| | 550 | - | 30.7 | [183] |
| | 560 | 2,700 | 32.9 | [184] |

Consequently, economic data on costing aspects of Kalina cycles are very sparse. In most economic studies on Kalina cycles, the capital cost of such plants is stated to be expected as comparable to the cost of Rankine cycle-based power plants of the same capacity.

Table 16 shows a summary of Kalina cycle investment costs. For Kalina cycles above 1 MW costs can be found in the range 1,000 – 1,500 /kW, while below 500 kW investments costs are higher, in the 2,000 – 3,000 €/kW range [178].

Table 16 Costing elements for Kalina cycles taken from literature studies. Capacity refers to the power output of the Kalina heat recovery cycle. Costs annualised

| Application | Capacity [kW] | Cost [€/kW] | Year | Ref |
|-----------------------------|---------------|---------------|------|-------|
| Geothermal | < 500 | 2,000 – 3,000 | 2009 | [178] |
| Geothermal | 1,850 | 1,150 | 2013 | [185] |
| Cement Plant | 6,000 | 1,500 | 2005 | [186] |
| Gas Turbine Bottoming Cycle | 86,000 | 1,157 | 1991 | [182] |

3.6.4 Modelling the Kalina cycle

The amount of energy absorbed by the KC, $F_{KC}(t)$, is expressed as a linear function (or piecewise linear function) of the net power drawn from the KC, $P_{KC}(t)$, using the efficiency of the system (equation (31)). $\delta_{KC}(t)$ is a binary decision variable which indicates whether the KC is on or off at time t .

$$F_{KC}(t) = \frac{1}{\eta_{KC}} P_{KC}(t) \delta_{KC}(t) \quad (53)$$

Where η_{KC} is the efficiency of the KC. The work produced by the KC is constrained in Equation (32) using a rated design for KC D_{KC} , with upper and lower bounds indicated with variables $k_{1,KC}$ and $k_{2,KC}$. $x_{KC}(t)$ is a binary decision variable which indicates whether the KC is included or excluded in the energy system.

$$k_{1,KC} D_{KC} x_{KC}(t) \leq P_{KC}(t) \leq k_{2,KC} D_{KC} x_{KC}(t) \quad (54)$$

4 Conclusions

Ten different waste heat recovery have been reviewed in this report: the four technologies investigated in the context of the ZHENIT project, and six other meaningful waste heat recovery technologies which are either already implemented or with clear potential for marine engine waste heat recovery. Each of the investigated technologies either convert waste thermal energy into another form (electrical, cold, mechanical), provide some added value with respect to the on-board energy demands (i.e. waste heat is used for water or desalination), or support (a) the other technologies, and potentially (b) the synergistic implementation of multiple technologies (thermal energys storage) . For each technology was reported its basic working principle, the typical architectures and layouts, the implications of its specific implementation in marine diesel engine waste heat recovery and the techno-economic performance. The results presented in this report allow to:

1. understand the basic operating principles and typical implementation architectures of the waste heat recovery technologies.
2. review the specificities of integrating the waste heat recovery technologies on marine energy systems.
3. quantify the expected performance, operating conditions, size and costs of the investigated waste heat recovery technologies.
4. carry out basic modelling of each waste heat recovery technology in the context of the techno-economic assessment of the broader energy system.

The results gathered in this deliverable can support other tasks and workpackages in the ZHENIT project, notably through the provided algorithmic models and techno-economic data. The main characteristics of the investigated WHR technologies are summarised in **Table 17**.

Table 17 Summary of the investgiated WHR technologies

| Technology | Technology Type | Capacity | Performance | Cost |
|----------------------------------|-----------------|----------------|-------------------|----------------------|
| ORC | Heat-to-Power | 10 - 10,000 kW | $\eta = 5 - 25\%$ | 1,000 - 100,000 €/kW |
| Adorption Desalination & Cooling | Heat-to-Cooling | 1 - 50 kW | COP = 0.2 - 0.8 | 1,000 - 1,500 €/kW |

| | | | | |
|--------------------------|--------------------------|-----------------------------|---------------------|---------------------|
| TES | Load Matching | 50 - 200 kWh/m ³ | $\eta = 50 - 100\%$ | 1 - 100 €/kWh |
| IEE | Heat-to-Mechanical Power | 1 - 1,000 kW | $\eta = 1 - 14\%$ | 500 - 2,500 €/kW |
| Turbocompounding | Heat-to-Power | 500 - 10,000 kW | $\eta = 3 - 15\%$ | 100 - 500 €/kW |
| Steam Rankine | Heat-to-Power | 500 - 20,000 kW | $\eta = 3 - 20\%$ | 1,000 - 3,500 €/kW |
| TEG | Heat-to-Power | 1 - 80 W | $\eta = 1 - 20\%$ | 1,000 - 15,000 €/kW |
| Absorption Refrigeration | Heat-to-Cooling | 150 - 5,000 kW | COP = 0.1 - 0.6 | 500 - 2,000 €/kW |
| OFC | Heat-to-Power | 5 - 200 kW | $\eta = 5 - 20\%$ | 2,000 - 12,000 €/kW |
| Kalina | Heat-to-Power | 20 - 100,000 kW | $\eta = 7.5 - 35\%$ | 1,000 - 3,000 €/kW |

References

- [1] MAN Diesel & Turbo. Waste Heat Recovery System (WHRS). 2014.
- [2] Singh DV, Pedersen E. A review of waste heat recovery technologies for maritime applications. *Energy Convers Manag* 2016;111:315–28. <https://doi.org/10.1016/j.enconman.2015.12.073>.
- [3] United Nations. Developments in international seaborne trade. 2017. <https://doi.org/10.18356/e9e3b605-en>.
- [4] Maritime Organisation International. Cutting GHG emissions from shipping - 10 years of mandatory rules. *WwwImoOrg* 2021. <https://www.imo.org/en/MediaCentre/PressBriefings/pages/DecadeOfGHGAction.aspx> (accessed August 22, 2022).
- [5] United Nations. Take urgent action to combat climate change and its impacts. *SdgsUnOrg* 2022. <https://sdgs.un.org/goals/goal13>.
- [6] Mallouppas G, Yfantis EA. Decarbonization in Shipping industry: A review of research, technology development, and innovation proposals. *J Mar Sci Eng* 2021;9. <https://doi.org/10.3390/jmse9040415>.
- [7] Zhu S, Sun K, Bai S, Deng K. Thermodynamic and techno-economic comparisons of the steam injected turbocompounding system with conventional steam Rankine cycle systems in recovering waste heat from the marine two-stroke engine. *Energy* 2022;245:123245. <https://doi.org/10.1016/j.energy.2022.123245>.
- [8] Quoilin S, Broek M Van Den, Declaye S, Dewallef P, Lemort V. Techno-economic survey of organic rankine cycle (ORC) systems. *Renew Sustain Energy Rev* 2013;22:168–86. <https://doi.org/10.1016/j.rser.2013.01.028>.
- [9] Landelle A, Tauveron N, Haberschill P, Revellin R, Colasson S. Organic Rankine cycle design and performance comparison based on experimental database. *Appl Energy* 2017;204:1172–87. <https://doi.org/10.1016/j.apenergy.2017.04.012>.
- [10] Hipólito-Valencia BJ, Rubio-Castro E, Ponce-Ortega JM, Serna-González M, Nápoles-Rivera F, El-Halwagi MM. Optimal integration of organic Rankine cycles with industrial processes. *Energy Convers Manag* 2013;73:285–302. <https://doi.org/10.1016/j.enconman.2013.04.036>.
- [11] Moran MJ, Shapiro HN, Boettner DD, Bailey MB. *Fundamentals of Engineering Thermodynamics*. 2018. <https://doi.org/10.4324/9781315119717>.
- [12] Castelli AF, Elsidio C, Scaccabarozzi R, Nord LO, Martelli E. Optimization of organic rankine cycles for waste heat recovery from aluminum production plants. *Front Energy Res* 2019;7. <https://doi.org/10.3389/fenrg.2019.00044>.
- [13] Lecompte S, Huisseune H, Van Den Broek M, Vanslambrouck B, De Paepe M. Review of organic Rankine cycle (ORC) architectures for waste heat recovery. *Renew Sustain Energy Rev* 2015;47:448–61. <https://doi.org/10.1016/j.rser.2015.03.089>.
- [14] Song J, Song Y, Gu C wei. Thermodynamic analysis and performance optimization of an Organic Rankine Cycle (ORC) waste heat recovery system for marine diesel engines. *Energy*

- 2015;82:976–85. <https://doi.org/10.1016/j.energy.2015.01.108>.
- [15] Lion S, Taccani R, Vlaskos I, Scrocco P, Vouvakos X, Kaiktsis L. Thermodynamic analysis of waste heat recovery using Organic Rankine Cycle (ORC) for a two-stroke low speed marine Diesel engine in IMO Tier II and Tier III operation. *Energy* 2019;183:48–60. <https://doi.org/10.1016/j.energy.2019.06.123>.
- [16] Casisi M, Pinamonti P, Reini M. Increasing the energy efficiency of an internal combustion engine for ship propulsion with bottom ORCS. *Appl Sci* 2020;10:1–18. <https://doi.org/10.3390/app10196919>.
- [17] Liu P, Shu G, Tian H. How to approach optimal practical Organic Rankine cycle (OP-ORC) by configuration modification for diesel engine waste heat recovery. *Energy* 2019;174:543–52. <https://doi.org/10.1016/j.energy.2019.03.016>.
- [18] Mohammed AG, Mosleh M, El-Maghlany WM, Ammar NR. Performance analysis of supercritical ORC utilizing marine diesel engine waste heat recovery. *Alexandria Eng J* 2020;59:893–904. <https://doi.org/10.1016/j.aej.2020.03.021>.
- [19] Macchi E, Astolfi M. *Organic Rankine Cycle (ORC) Power Systems: Technologies and Applications*. 2016.
- [20] Colonna P, Casati E, Trapp C, Mathijssen T, Larjola J, Turunen-Saaresti T, et al. *Organic Rankine Cycle Power Systems: From the Concept to Current Technology, Applications, and an Outlook to the Future*. *J Eng Gas Turbines Power* 2015;137:1–19. <https://doi.org/10.1115/1.4029884>.
- [21] Leontaritis A, Pallis P, Karellas S, Papastergiou A, Vourliotis P, Kakalis NM, et al. Experimental Study on a Low Temperature ORC Unit for Onboard Waste Heat Recovery From Marine Diesel. *3RD Int Semin ORC Power Syst Oct 12-14, 2015, Brussels, Belgium* 2015:660–9.
- [22] Pallis P, Varvagiannis E, Braimakis K, Roumpedakis T, Leontaritis AD, Karellas S. Development, experimental testing and techno-economic assessment of a fully automated marine organic rankine cycle prototype for jacket cooling water heat recovery. *Energy* 2021;228:120596. <https://doi.org/10.1016/j.energy.2021.120596>.
- [23] Alfa Laval. Alfa Laval E-PowerPack 2022.
- [24] Orcan-Energy. Efficiency Pack. Orcan-EnergyCom 2017. <https://www.orcan-energy.com/en/applications-marine.html>.
- [25] Mitsubishi Heavy Industries. Hydrocurrent™ Organic Rankine Cycle Module 125EJW - Compact and High-performance Waste Heat Recovery System Utilizing Low Temperature Heat Source. *Mitsubishi Heavy Ind Tech Rev* 2015;52:53–5.
- [26] Caltenix Technologies. Hydrocurrent™ Organic Rankine Cycle (ORC) Module 125EJW What Makes Hydrocurrent™ Superior The Optimal Heat-to-Power Solution for Marine Vessels n.d.
- [27] Yuksek EL, Mirmobin P. Waste heat utilization of main propulsion engine jacket water in marine application. *Proc 3rd Int Semin ORC Power Syst* 2015:1–10.
- [28] Enogia. DATASHEET ORC ENO-180LT 2022. <https://enogia.com/> (accessed October 6, 2022).
- [29] Enerbasque. HRU-25 2022. <http://enerbasque.com/> (accessed October 6, 2022).
- [30] Rank-ORC. Rank-ORC 2022. <https://www.rank-orc.com/> (accessed October 6, 2022).

- [31] Soffiato M, Frangopoulos CA, Manente G, Rech S, Lazzaretto A. Design optimization of ORC systems for waste heat recovery on board a LNG carrier. *Energy Convers Manag* 2015;92:523–34. <https://doi.org/10.1016/j.enconman.2014.12.085>.
- [32] Ahlgren F, Mondejar ME, Genrup M, Thern M. Waste heat recovery in a cruise vessel in the Baltic Sea by using an organic Rankine cycle: A case study. *J Eng Gas Turbines Power* 2016;138:1–10. <https://doi.org/10.1115/1.4031145>.
- [33] Mondejar ME, Ahlgren F, Thern M, Genrup M. Quasi-steady state simulation of an organic Rankine cycle for waste heat recovery in a passenger vessel. *Appl Energy* 2017;185:1324–35. <https://doi.org/10.1016/j.apenergy.2016.03.024>.
- [34] Shu G, Liu P, Tian H, Wang X, Jing D. Operational profile based thermal-economic analysis on an Organic Rankine cycle using for harvesting marine engine's exhaust waste heat. *Energy Convers Manag* 2017;146:107–23. <https://doi.org/10.1016/j.enconman.2017.04.099>.
- [35] Yang MH. Payback period investigation of the organic Rankine cycle with mixed working fluids to recover waste heat from the exhaust gas of a large marine diesel engine. *Energy Convers Manag* 2018;162:189–202. <https://doi.org/10.1016/j.enconman.2018.02.032>.
- [36] Song J, Gu C wei. Performance analysis of a dual-loop organic Rankine cycle (ORC) system with wet steam expansion for engine waste heat recovery. *Appl Energy* 2015;156:280–9. <https://doi.org/10.1016/j.apenergy.2015.07.019>.
- [37] Lemmens S. Cost engineering techniques & their applicability for cost estimation of organic rankine cycle systems. *Energies* 2016;9. <https://doi.org/10.3390/en9070485>.
- [38] Turton R, Shaeiwiz J, Bhattacharyya D, Whiting W. *Analysis, Synthesis, and Design of Chemical Processes*. 2012.
- [39] Shmroukh AN, Ali AHH, Ookawara S. Adsorption working pairs for adsorption cooling chillers: A review based on adsorption capacity and environmental impact. *Renew Sustain Energy Rev* 2015;50:445–56. <https://doi.org/10.1016/j.rser.2015.05.035>.
- [40] Stefański S, Nowak W, Sztekler K, Kalawa W, Siwek T. Applicability of adsorption cooling/desalination systems driven by low-temperature waste heat. *IOP Conf Ser Earth Environ Sci* 2019;214. <https://doi.org/10.1088/1755-1315/214/1/012126>.
- [41] Woo SY, Lee HS, Ji H, Moon DS, Kim YD. Silica gel-based adsorption cooling cum desalination system: Focus on brine salinity, operating pressure, and its effect on performance. *Desalination* 2019;467:136–46. <https://doi.org/10.1016/j.desal.2019.06.016>.
- [42] Zhang Y, Palomba V, Frazzica A. Understanding the effect of materials, design criteria and operational parameters on the adsorption desalination performance – A review. *Energy Convers Manag* 2022;269:116072. <https://doi.org/10.1016/j.enconman.2022.116072>.
- [43] Palomba V, Dino GE, Ghirlando R, Micallef C, Frazzica A. Decarbonising the shipping sector: A critical analysis on the application of waste heat for refrigeration in fishing vessels. *Appl Sci* 2019;9. <https://doi.org/10.3390/app9235143>.
- [44] Sztekler K, Kalawa W, Nowak W, Mika L, Gradziel S, Krzywanski J, et al. Experimental study of three-bed adsorption chiller with desalination function. *Energies* 2020;13:1–13. <https://doi.org/10.3390/en13215827>.

- [45] Thu K, Yanagi H, Saha BB, Ng KC. Performance analysis of a low-temperature waste heat-driven adsorption desalination prototype. *Int J Heat Mass Transf* 2013;65:662–9. <https://doi.org/10.1016/j.ijheatmasstransfer.2013.06.053>.
- [46] Askalany AA, Uddin K, Saha BB, Sultan M, Santori G. Water desalination by silica supported ionic liquid: Adsorption kinetics and system modeling. *Energy* 2022;239:122069. <https://doi.org/10.1016/j.energy.2021.122069>.
- [47] Askalany AA, Freni A, Santori G. Supported ionic liquid water sorbent for high throughput desalination and drying. *Desalination* 2019;452:258–64. <https://doi.org/10.1016/j.desal.2018.11.002>.
- [48] Wyrwa A, Chen YK. Techno-Economic Analysis of Adsorption-Based DH Driven Cooling System. *IOP Conf Ser Earth Environ Sci* 2019;214. <https://doi.org/10.1088/1755-1315/214/1/012128>.
- [49] McNally J. Techno-Economic Analysis of a Solar Adsorption Cooling System for Residential Applications in Canada 2020. <https://doi.org/10.22215/etd/2020-14434>.
- [50] Reda AM, Ali AHH, Morsy MG, Taha IS. Design optimization of a residential scale solar driven adsorption cooling system in upper Egypt based. *Energy Build* 2016;130:843–56. <https://doi.org/10.1016/j.enbuild.2016.09.011>.
- [51] HYBUILD - Innovative compact hybrid storage systems for low energy buildings 2020. <http://www.hybuild.eu/> (accessed October 14, 2022).
- [52] NTUA, AIR, CNR ITAE. HYBUILD Deliverable 3.4 - Report on the experimental tests and the final design of the hybrid sub-systems. 2020.
- [53] IRENA. Innovation Outlook: Thermal Energy Storage. 2020.
- [54] Ease/Eera. European Energy Storage Technology Development Roadmap Towards 2030 – Update 2017.
- [55] Koohi-Fayegh S, Rosen MA. A review of energy storage types, applications and recent developments. *J Energy Storage* 2020;27:101047. <https://doi.org/10.1016/j.est.2019.101047>.
- [56] Alva G, Lin Y, Fang G. An overview of thermal energy storage systems. *Energy* 2018;144:341–78. <https://doi.org/10.1016/j.energy.2017.12.037>.
- [57] Ease/Eera. European Energy Storage Technology Development Roadmap - 2017 Update. 2017:128.
- [58] Stekli J, Irwin L, Pitchumani R. Technical challenges and opportunities for concentrating solar power with thermal energy storage. *J Therm Sci Eng Appl* 2013;5:1–12. <https://doi.org/10.1115/1.4024143>.
- [59] Xu C, Zhang H, Fang G. Review on thermal conductivity improvement of phase change materials with enhanced additives for thermal energy storage. *J Energy Storage* 2022;51:104568. <https://doi.org/10.1016/j.est.2022.104568>.
- [60] Skovajsa J, Koláček M, Zálešák M. Phase change material based accumulation panels in combination with renewable energy sources and thermoelectric cooling. *Energies* 2017;10. <https://doi.org/10.3390/en10020152>.
- [61] Zou Guangrong. Ship energy efficiency technologies - now and the future 2017.

- [62] Bauer T, Odenthal C, Bonk A. Molten Salt Storage for Power Generation. *Chemie-Ingenieur-Technik* 2021;93:534–46. <https://doi.org/10.1002/cite.202000137>.
- [63] Kenisarin M, Mahkamov K. Salt hydrates as latent heat storage materials: Thermophysical properties and costs. *Sol Energy Mater Sol Cells* 2016;145:255–86. <https://doi.org/10.1016/j.solmat.2015.10.029>.
- [64] Pereira da Cunha J, Eames P. Thermal energy storage for low and medium temperature applications using phase change materials - A review. *Appl Energy* 2016;177:227–38. <https://doi.org/10.1016/j.apenergy.2016.05.097>.
- [65] Omara AAM. Phase change materials for waste heat recovery in internal combustion engines: A review. *J Energy Storage* 2021;44:103421. <https://doi.org/10.1016/j.est.2021.103421>.
- [66] Becheleni EMA, Rodriguez-Pascual M, Lewis AE, Rocha SDF. Influence of Phenol on the Crystallization Kinetics and Quality of Ice and Sodium Sulfate Decahydrate during Eutectic Freeze Crystallization. *Ind Eng Chem Res* 2017;56:11926–35. <https://doi.org/10.1021/acs.iecr.7b02668>.
- [67] Feng H, Sheikh MN, Hadi MNS, Gao D, Zhao J. Mechanical properties of micro-steel fibre reinforced magnesium potassium phosphate cement composite. *Constr Build Mater* 2018;185:423–35. <https://doi.org/10.1016/j.conbuildmat.2018.07.037>.
- [68] Yadav C, Sahoo RR. Effect of thermal performance on melting and solidification of lauric acid PCM in cylindrical thermal energy storage. *J Phys Conf Ser* 2019;1240. <https://doi.org/10.1088/1742-6596/1240/1/012088>.
- [69] Li B, Liu T, Hu L, Wang Y, Nie S. Facile preparation and adjustable thermal property of stearic acid-graphene oxide composite as shape-stabilized phase change material. *Chem Eng J* 2013;215–216:819–26. <https://doi.org/10.1016/j.cej.2012.11.077>.
- [70] Khan MMA, Saidur R, Al-Sulaiman FA. A review for phase change materials (PCMs) in solar absorption refrigeration systems. *Renew Sustain Energy Rev* 2017;76:105–37. <https://doi.org/10.1016/j.rser.2017.03.070>.
- [71] Tatsidjoudoug P, Le Pierrès N, Luo L. A review of potential materials for thermal energy storage in building applications. *Renew Sustain Energy Rev* 2013;18:327–49. <https://doi.org/10.1016/j.rser.2012.10.025>.
- [72] Beemkumar N, Karthikeyan A, Saravanakumar B, Jayaprabakar J. Performance improvement of D-sorbitol PCM-based energy storage system with different fins. *Int J Ambient Energy* 2018;39:372–6. <https://doi.org/10.1080/01430750.2017.1303642>.
- [73] Hühlein S, König-Haagen A, Brüggemann D. Thermophysical characterization of MgCl₂·6H₂O, xylitol and erythritol as phase change materials (PCM) for latent heat thermal energy storage (LHTES). *Materials (Basel)* 2017;10. <https://doi.org/10.3390/ma10040444>.
- [74] Bellettre J, Ollivier E, Tazerout M. The Use of a Phase Change Material within a Cylinder Wall in order to Detect Knock in a Gas SI Engine. *J Mech Eng* 2005;51:462–9.
- [75] Agyenim F, Eames P, Smyth M. Experimental study on the melting and solidification behaviour of a medium temperature phase change storage material (Erythritol) system augmented with fins to power a LiBr/H₂O absorption cooling system. *Renew Energy* 2011;36:108–17. <https://doi.org/10.1016/j.renene.2010.06.005>.

- [76] Korin E, Reshef R, Tshernichovesky D, Sher E. Improving cold-start functioning of catalytic converters by using phase-change materials. SAE Tech Pap 1998. <https://doi.org/10.4271/980671>.
- [77] Zalba B, Marin JM, Cabeza LF, Mehling H. Review on thermal energy storage with phase change: materials, heat transfer analysis and applications. vol. 23. 2003.
- [78] Marie LF, Landini S, Bae D, Francia V, O'Donovan TS. Advances in thermochemical energy storage and fluidised beds for domestic heat. J Energy Storage 2022;53:105242. <https://doi.org/10.1016/j.est.2022.105242>.
- [79] Novo A V., Bayon JR, Castro-Fresno D, Rodriguez-Hernandez J. Review of seasonal heat storage in large basins: Water tanks and gravel-water pits. Appl Energy 2010;87:390–7. <https://doi.org/10.1016/j.apenergy.2009.06.033>.
- [80] Li PW, Chan CL. Thermal Energy Storage Analyses and Designs. 2017. <https://doi.org/10.1016/c2015-0-04678-0>.
- [81] McTigue JD, Markides CN, White AJ. Performance response of packed-bed thermal storage to cycle duration perturbations. J Energy Storage 2018;19:379–92. <https://doi.org/10.1016/j.est.2018.08.016>.
- [82] Scapino L, Zondag HA, Van Bael J, Diriken J, Rindt CCM. Energy density and storage capacity cost comparison of conceptual solid and liquid sorption seasonal heat storage systems for low-temperature space heating. Renew Sustain Energy Rev 2017;76:1314–31. <https://doi.org/10.1016/j.rser.2017.03.101>.
- [83] Cao D, Yu C, Wu S, Zhang C. Perspectives on Low-Temperature Packed Bed Latent Heat Storage Systems. Front Energy Res 2022;10:1–5. <https://doi.org/10.3389/fenrg.2022.935100>.
- [84] Agyenim F, Hewitt N, Eames P, Smyth M. A review of materials, heat transfer and phase change problem formulation for latent heat thermal energy storage systems (LHTESS). Renew Sustain Energy Rev 2010;14:615–28. <https://doi.org/10.1016/j.rser.2009.10.015>.
- [85] Energy Nest. Energy Nest - Thermal Battery 2022. <https://energy-nest.com/thermal-battery/#batterythermal> (accessed October 19, 2022).
- [86] Pandiyarajan V, Chinnappandian M, Raghavan V, Velraj R. Second law analysis of a diesel engine waste heat recovery with a combined sensible and latent heat storage system. Energy Policy 2011;39:6011–20. <https://doi.org/10.1016/j.enpol.2011.06.065>.
- [87] Li Z, Lu Y, Huang R, Chang J, Yu X, Jiang R, et al. Applications and technological challenges for heat recovery, storage and utilisation with latent thermal energy storage. Appl Energy 2021;283:116277. <https://doi.org/10.1016/j.apenergy.2020.116277>.
- [88] Baldi F, Gabriellii C, Melino F, Bianchi M. A Preliminary Study on the Application of Thermal Storage to Merchant Ships. Energy Procedia 2015;75:2169–74. <https://doi.org/10.1016/j.egypro.2015.07.364>.
- [89] Manzan M, Pezzi A, Zorzi EZ De, Freni A, Frazzica A, Vaglieco BM, et al. Potential of thermal storage for hot potable water distribution in cruise ships. Energy Procedia 2018;148:1105–12. <https://doi.org/10.1016/j.egypro.2018.08.044>.
- [90] EcoTech Ceram. EcoTech Ceram - EcoStock 2022. <https://ecotechceram.com/en/energy->

- storage/ (accessed October 19, 2022).
- [91] Lumenion. Lumenion Thermal Store 2022.
 - [92] Sunamp. Sunamp Central Bank thermal storage for heating 2022. <https://sunamp.com/en-gb/heating-central-bank-overview/> (accessed October 24, 2022).
 - [93] Oliver DE, Bissell AJ, Liu X, Tang CC, Pulham CR. Crystallisation studies of sodium acetate trihydrate-suppression of incongruent melting and sub-cooling to produce a reliable, high-performance phase-change material. *CrystEngComm* 2021;23:700–6. <https://doi.org/10.1039/d0ce01454k>.
 - [94] Ma Z, Bao H, Roskilly AP. Study on solidification process of sodium acetate trihydrate for seasonal solar thermal energy storage. *Sol Energy Mater Sol Cells* 2017;172:99–107. <https://doi.org/10.1016/j.solmat.2017.07.024>.
 - [95] Frazzica A, Manzan M, Palomba V, Brancato V, Freni A, Pezzi A, et al. Experimental Validation and Numerical Simulation of a Hybrid Sensible-Latent Thermal Energy Storage for Hot Water Provision on Ships. *Energies* 2022;15. <https://doi.org/10.3390/en15072596>.
 - [96] Baldi F, Ahlgren F, Nguyen T Van, Thern M, Andersson K. Energy and exergy analysis of a cruise ship. *Energies* 2018;11:1–41. <https://doi.org/10.3390/en11102508>.
 - [97] SoWHat. D1.9 – TECHNO-ECONOMIC DATABASE OF INDUSTRIAL WH/C RECOVERY TECHNOLOGIES AND MODELLING ALGORITHMS. 2021.
 - [98] Dall’Armi C, Pivetta D, Taccani R. On optimal integration of PEMFC and low temperature waste heat recovery in a cruise ship energy system. *Proc ECOS 2022* 2022.
 - [99] Glushenkov M, Kronberg A, Knoke T, Kenig EY. Isobaric expansion engines: New opportunities in energy conversion for heat engines, pumps and compressors. *Energies* 2018;11. <https://doi.org/10.3390/en11010154>.
 - [100] Van der Kooij BJG. The Invention of the Steam Engine. 2015.
 - [101] Whitmore M. Development of Coal-Fired Steam Technology in Britain. *Encycl Anthr* 2018:285–305.
 - [102] Nesbitt B. Handbook of Pumps and Pumping. 2006. <https://doi.org/10.1016/B978-1-85617-476-3.X5000-8>.
 - [103] Bush V. Apparatus for compressing gases. 2,157,229, 1935.
 - [104] Glushenkov M, Kronberg A. Experimental study of an isobaric expansion engine-pump – Proof of concept. *Appl Therm Eng* 2022;212:118521. <https://doi.org/10.1016/j.applthermaleng.2022.118521>.
 - [105] Roosjen S, Glushenkov M, Kronberg A, Kersten S. Waste Heat Recovery Systems with Isobaric Expansion Technology Using Pure and Mixed Working Fluids 2022:1–14. <https://doi.org/10.20944/preprints202207.0002.v1>.
 - [106] Kronberg A, Glushenkov M, Knoke T, Kenig EY. Theoretical limits on the heat regeneration degree. *Int J Heat Mass Transf* 2020;161. <https://doi.org/10.1016/j.ijheatmasstransfer.2020.120282>.
 - [107] Knoke T, Kenig EY, Kronberg A, Glushenkov M. Model-based analysis of novel heat engines for

- low-temperature heat conversion. Chem Eng Trans 2017;57:499–504.
<https://doi.org/10.3303/CET1757084>.
- [108] Encontech B.V. Isobaric expansion machines as heat driven pumps , compressors and heat-to-electricity converters 2008:7500.
- [109] Glushenkov M, Bhosale R, Kumar A, Al Momani F, Kronberg A. Heat powered water pump for reverse osmosis desalination. Adv Mater - TechConnect Briefs 2016 2016;2:201–4.
- [110] Glushenkov M, Kronberg A, Knoke T, Kenig EY. Heat Driven Pump for Reverse Osmosis Desalination. Encontech B V 2021. www.encontech.nl.
- [111] Nihill J, Date A, Velardo J, Jadkar S. Experimental investigation of the thermal power pump cycle – Proof of concept. Appl Therm Eng 2018;134:182–93.
<https://doi.org/10.1016/j.applthermaleng.2018.01.106>.
- [112] P. V, Deshmukh D. A comprehensive review of waste heat recovery from a diesel engine using organic rankine cycle. Energy Reports 2021;7:3951–70.
<https://doi.org/10.1016/j.egyr.2021.06.081>.
- [113] Simader GR, Krawinkler R, Trnka G. Micro CHP systems : state-of-the-art. Vienna: 2006.
- [114] Kirmse CJW, Oyewunmi OA, Haslam AJ, Markides CN. Comparison of a novel organic-fluid thermofluidic heat converter and an organic Rankine cycle heat engine. Energies 2019;9:1–26.
<https://doi.org/10.3390/en9070479>.
- [115] MAN. MAN B&W S90ME-C9.2-TII. 2012.
- [116] Sharp N. Recovering Waste Heat from Heavy-Duty Diesel Engines. Turbo Technol - Ed 14 2010.
- [117] Wartsila. Less emissions through waste heat recovery. Green Sh Technol Conf London 2004;28:29.
- [118] Yagi K, Motoda T. Development of Waste Heat Recovery System for Marine Diesel Engines. J Japan Inst Mar Eng 2014;49:223–8. <https://doi.org/10.5988/jime.49.223>.
- [119] Virtasalo M, Vänskä K. Achieving improved fuel efficiency with waste heat recovery. Waste Heat Recover Syst 2013:6.
- [120] Ma Z, Yang D, Guo Q. Conceptual design and performance analysis of an exhaust gas waste heat recovery system for a 10000TEU container ship. Polish Marit Res 2012;19:31–8.
<https://doi.org/10.2478/v10012-012-0012-8>.
- [121] Olaniyi EO, Prause G. Investment analysis of waste heat recovery system installations on ships' engines. J Mar Sci Eng 2020;8:1–21. <https://doi.org/10.3390/jmse8100811>.
- [122] Elson A, Tidball R, Hampson A. Oak Ridge National Laboratory - Waste Heat to Power Market Assessment. 2015.
- [123] Calise F, D'Accadia MD, Vanoli L, Vicidomini M. Polygeneration Systems - Design, Processes and Technologies. 2022. <https://doi.org/10.1016/c2019-0-01304-0>.
- [124] Senary K, Tawfik A, Hegazy E, Ali A. Development of a waste heat recovery system onboard LNG carrier to meet IMO regulations. Alexandria Eng J 2016;55:1951–60.
<https://doi.org/10.1016/j.aej.2016.07.027>.

- [125] Zhu S, Zhang K, Deng K. A review of waste heat recovery from the marine engine with highly efficient bottoming power cycles. *Renew Sustain Energy Rev* 2020;120:109611. <https://doi.org/10.1016/j.rser.2019.109611>.
- [126] Rivera-Alvarez A, Coleman MJ, Ordonez JC. Ship weight reduction and efficiency enhancement through combined power cycles. *Energy* 2015;93:521–33. <https://doi.org/10.1016/j.energy.2015.08.079>.
- [127] Liang Y, Shu G, Tian H, Liang X, Wei H, Liu L. Analysis of an electricity-cooling cogeneration system based on RC-ARS combined cycle aboard ship. *Energy Convers Manag* 2013;76:1053–60. <https://doi.org/10.1016/j.enconman.2013.08.056>.
- [128] Larsen U, Sigthorsson O, Haglind F. A comparison of advanced heat recovery power cycles in a combined cycle for large ships. *Energy* 2014;74:260–8. <https://doi.org/10.1016/j.energy.2014.06.096>.
- [129] Champier D. Thermoelectric generators: A review of applications. *Energy Convers Manag* 2017;140:167–81. <https://doi.org/10.1016/j.enconman.2017.02.070>.
- [130] Baldi F, Coraddu A, Mondejar ME. Sustainable Energy Systems on Ships: Novel Technologies for Low Carbon Shipping. 2022. [https://doi.org/10.1108/s1574-8715\(2013\)0000012002](https://doi.org/10.1108/s1574-8715(2013)0000012002).
- [131] Godoi FC, Prakash S, Bhandari BR. Thermoelectric Exhaust Heat Recovery Generator (TEG) Project Project: Final report. *Rev 3D Print Potential Red Meat Appl* 2021:1–61.
- [132] Wallace TT, Jin ZH, Su J. Efficiency of a Sandwiched Thermoelectric Material with a Graded Interlayer and Temperature-Dependent Properties. *J Electron Mater* 2016;45:2142–9. <https://doi.org/10.1007/s11664-016-4358-z>.
- [133] Freer R, Powell A V. Realising the potential of thermoelectric technology: A Roadmap. *J Mater Chem C* 2020;8:441–63. <https://doi.org/10.1039/c9tc05710b>.
- [134] Liu C, Li F, Zhao C, Ye W, Wang K, Dong Y, et al. Experimental research of thermal electric power generation from ship incinerator exhaust heat. *IOP Conf Ser Earth Environ Sci* 2019;227. <https://doi.org/10.1088/1755-1315/227/2/022031>.
- [135] Kristiansen NR, Snyder GJ, Nielsen HK, Rosendahl L. Waste heat recovery from a marine waste incinerator using a thermoelectric generator. *J Electron Mater* 2012;41:1024–9. <https://doi.org/10.1007/s11664-012-2009-6>.
- [136] Armenakis Y, Chatzis S. Waste heat recovery and electrical power production on vessels by means of TEG arrays attached on the hull below the underwater line. 2019 IEEE Electr Sh Technol Symp ESTS 2019 2019:430–7. <https://doi.org/10.1109/ESTS.2019.8847849>.
- [137] TEGmart. <https://www.tegmart.com/> 2023. <https://www.tegmart.com/> (accessed January 9, 2023).
- [138] Hi-Z. <https://hi-z.com/products/> (accessed January 9, 2023).
- [139] Tecteg. [Tecteg](https://tecteg.com/) 2023. <https://tecteg.com/> (accessed January 9, 2023).
- [140] II-VI. [II-VI](https://ii-vi.com/thermoelectrics/) 2023. <https://ii-vi.com/thermoelectrics/> (accessed January 9, 2023).
- [141] Cao T, Lee H, Hwang Y, Radermacher R, Chun HH. Modeling of waste heat powered energy system for container ships. *Energy* 2016;106:408–21.

- <https://doi.org/10.1016/j.energy.2016.03.072>.
- [142] Cao T, Lee H, Hwang Y, Radermacher R, Chun HH. Performance investigation of engine waste heat powered absorption cycle cooling system for shipboard applications. *Appl Therm Eng* 2015;90:820–30. <https://doi.org/10.1016/j.applthermaleng.2015.07.070>.
- [143] Wu W, Wang B, Shi W, Li X. An overview of ammonia-based absorption chillers and heat pumps. *Renew Sustain Energy Rev* 2014;31:681–707. <https://doi.org/10.1016/j.rser.2013.12.021>.
- [144] WorldEnergy. WorldEnergy n.d. <http://worldenergy.co.kr/> (accessed January 25, 2023).
- [145] Kawasaki Thermal Engineering. Efficio Gene-Link n.d. <https://www.khi.co.jp/corp/kte/EN/chiller/efficio-genelink/> (accessed January 5, 2023).
- [146] Lazzarin RM, Gasparella A, Longo GA. Ammonia-water absorption machines for refrigeration: Theoretical and real performances. *Int J Refrig* 1996;19:239–46. [https://doi.org/10.1016/0140-7007\(96\)00016-3](https://doi.org/10.1016/0140-7007(96)00016-3).
- [147] Clerx M, Trezek GJ. Performance of an aqua-ammonia absorption solar refrigerator at sub-freezing evaporator conditions. *Sol Energy* 1987;39:379–89. [https://doi.org/10.1016/S0038-092X\(87\)80056-7](https://doi.org/10.1016/S0038-092X(87)80056-7).
- [148] Moreno-Quintanar G, Rivera W, Best R. Comparison of the experimental evaluation of a solar intermittent refrigeration system for ice production operating with the mixtures NH₃/LiNO₃ and NH₃/LiNO₃/H₂O. *Renew Energy* 2012;38:62–8. <https://doi.org/10.1016/j.renene.2011.07.009>.
- [149] Colonna P, Gabrielli S. Industrial trigeneration using ammonia-water absorption refrigeration systems (AAR). *Appl Therm Eng* 2003;23:381–96. [https://doi.org/10.1016/S1359-4311\(02\)00212-0](https://doi.org/10.1016/S1359-4311(02)00212-0).
- [150] Bassols J, Kuckelkorn B, Langreck J, Schneider R, Veelken H. Trigeneration in the food industry. *Appl Therm Eng* 2002;22:595–602. [https://doi.org/10.1016/S1359-4311\(01\)00111-9](https://doi.org/10.1016/S1359-4311(01)00111-9).
- [151] Kaushik SC, Kumar R. Computer-Aided Conceptual Thermodynamic Design of a Two-Stage Dual Fluid Absorption Cycle for Solar Refrigeration 1985;35:401–7.
- [152] Kaushik, S.C., Kumar, Rajesh, Chandra S. Thermal Modelling and Parametric Study of Two Stage Absorption Refrigeration and Air-Conditioning Systems. *Energy Res* 1985;9.
- [153] Rogdakis, E.D., Antonopoulos KA. Performance of a low-temperature NH₃-H₂O absorption-refrigeration system. *Energy* 1992;17:477–84.
- [154] Fernández-Seara J, Sieres J, Vázquez M. Compression-absorption cascade refrigeration system. *Appl Therm Eng* 2006;26:502–12. <https://doi.org/10.1016/j.applthermaleng.2005.07.015>.
- [155] Venegas M, Izquierdo M, De Vega M, Lecuona A. Thermodynamic study of multistage absorption cycles using low-temperature heat. *Int J Energy Res* 2002;26:775–91. <https://doi.org/10.1002/er.815>.
- [156] United States Department of Energy. Absorption Chillers for CHP Systems. *Adv Manuf Off* 2017:3–6.
- [157] Ho T, Mao SS, Greif R. Comparison of the Organic Flash Cycle (OFC) to other advanced vapor

- cycles for intermediate and high temperature waste heat reclamation and solar thermal energy. *Energy* 2012;42:213–23. <https://doi.org/10.1016/j.energy.2012.03.067>.
- [158] Lee HY, Park SH, Kim KH. Comparative analysis of thermodynamic performance and optimization of organic flash cycle (OFC) and organic Rankine cycle (ORC). *Appl Therm Eng* 2016;100:680–90. <https://doi.org/10.1016/j.applthermaleng.2016.01.158>.
- [159] Kim KH. Thermodynamic performance and optimization analysis of a modified organic flash cycle for the recovery of low-grade heat. *Energies* 2019;12. <https://doi.org/10.3390/en12030442>.
- [160] Baccioli A, Antonelli M. Organic Flash Cycles: Off-design behavior and control strategies of two different cycle architectures for Waste Heat Recovery applications. *Energy Convers Manag* 2018;157:176–85. <https://doi.org/10.1016/j.enconman.2017.12.004>.
- [161] Ho T, Mao SS, Greif R. Increased power production through enhancements to the Organic Flash Cycle (OFC). *Energy* 2012;45:686–95. <https://doi.org/10.1016/j.energy.2012.07.023>.
- [162] Baccioli A, Antonelli M, Desideri U. Technical and economic analysis of organic flash regenerative cycles (OFRCs) for low temperature waste heat recovery. *Appl Energy* 2017;199:69–87. <https://doi.org/10.1016/j.apenergy.2017.04.058>.
- [163] Wang Q, Wu W, Li D, Wang J, He Z. Thermodynamic analysis and optimization of four organic flash cycle systems for waste heat recovery. *Energy Convers Manag* 2020;221:113171. <https://doi.org/10.1016/j.enconman.2020.113171>.
- [164] Bonolo de Campos G, Bringhamti C, Traverso A, Takachi Tomita J. Thermoeconomic comparison between the organic flash cycle and the novel organic Rankine flash cycle (ORFC). *Energy Convers Manag* 2020;215:112926. <https://doi.org/10.1016/j.enconman.2020.112926>.
- [165] Kalina AI. Combined cycle and waste heat recovery power systems based on a novel thermodynamic energy cycle utilizing low-temperature heat for power generation. *Proc ASME Turbo Expo 1983*;1983-Janua. <https://doi.org/10.1115/83JPGCGT3>.
- [166] SoWHat. D1 . 6 – Report on H / C Recovery / Storage Technologies 2020.
- [167] Zhang X, He M, Zhang Y. A review of research on the Kalina cycle. *Renew Sustain Energy Rev* 2012;16:5309–18. <https://doi.org/10.1016/j.rser.2012.05.040>.
- [168] Júnior EPB, Arrieta MDP, Arrieta FRP, Silva CHF. Assessment of a Kalina cycle for waste heat recovery in the cement industry. *Appl Therm Eng* 2019;147:421–37. <https://doi.org/10.1016/j.applthermaleng.2018.10.088>.
- [169] Mohammadkhani F, Yari M, Ranjbar F. A zero-dimensional model for simulation of a Diesel engine and exergoeconomic analysis of waste heat recovery from its exhaust and coolant employing a high-temperature Kalina cycle. *Energy Convers Manag* 2019;198:111782. <https://doi.org/10.1016/j.enconman.2019.111782>.
- [170] Bombarda P, Invernizzi CM, Pietra C. Heat recovery from Diesel engines: A thermodynamic comparison between Kalina and ORC cycles. *Appl Therm Eng* 2010;30:212–9. <https://doi.org/10.1016/j.applthermaleng.2009.08.006>.
- [171] Global Geothermal. Iron and Steel Industry - Waste Heat Recovery. Kalina Cycle Application in Steel Manufacturing Process n.d.

- <http://www.recurrentengineering.com/IronSteelIndustry.aspx> (accessed November 29, 2022).
- [172] Matsuda K. Low heat power generation system. *Chem Eng Trans* 2013;35:223–8. <https://doi.org/10.3303/CET1335037>.
- [173] <https://www.globalcement.com/>. DG Khan Khairpur: The ‘self-sufficient’ cement plant 2018.
- [174] <https://www.globalcement.com/>. Kalina Cycle power systems in waste heat recovery applications 2012.
- [175] Chew JM, Reddy CCS, Rangaiah GP. Improving energy efficiency of dividing-wall columns using heat pumps, Organic Rankine Cycle and Kalina Cycle. *Chem Eng Process Process Intensif* 2014;76:45–59. <https://doi.org/10.1016/j.cep.2013.11.011>.
- [176] Hua J, Chen Y, Wang Y, Roskilly AP. Thermodynamic analysis of ammonia-water power/chilling cogeneration cycle with low-grade waste heat. *Appl Therm Eng* 2014;64:483–90. <https://doi.org/10.1016/j.applthermaleng.2013.12.043>.
- [177] Hua J, Chen Y, Wu J, Zhi Z, Dong C. Waste heat supply-side power regulation with variable concentration for turbine in Kalina cycle. *Appl Therm Eng* 2015;91:583–90. <https://doi.org/10.1016/j.applthermaleng.2015.08.048>.
- [178] Ogriseck S. Integration of Kalina cycle in a combined heat and power plant, a case study. *Appl Therm Eng* 2009;29:2843–8. <https://doi.org/10.1016/j.applthermaleng.2009.02.006>.
- [179] Yue C, Han D, Pu W, He W. Comparative analysis of a bottoming transcritical ORC and a Kalina cycle for engine exhaust heat recovery. *Energy Convers Manag* 2015;89:764–74. <https://doi.org/10.1016/j.enconman.2014.10.029>.
- [180] Kalina AI, Leibowitz HM. The design of a 3MW kalina cycle experimental plant. *Proc ASME Turbo Expo* 1988;3. <https://doi.org/10.1115/88-GT-140>.
- [181] Nag PK, Gupta AVSSKS. Exergy analysis of the kalina cycle. *Appl Therm Eng* 1998;18:427–39. [https://doi.org/10.1016/S1359-4311\(97\)00047-1](https://doi.org/10.1016/S1359-4311(97)00047-1).
- [182] Kalina AI, Leibowitz HM, Markus DW, Pelletier RI. Further technical aspects and economics of a utility-size Kalina bottoming cycle. *Proc ASME Turbo Expo* 1991;4. <https://doi.org/10.1115/91-gt-365>.
- [183] Marston CH. Parametric analysis of the Kalina cycle. *Proc ASME Turbo Expo* 1989;4. <https://doi.org/10.1115/89GT-218>.
- [184] Kalina AI. Combined-Cycle System With Novel Bottoming Cycle. *J Eng Gas Turbines Power* 1984;107:1047–9.
- [185] Campos Rodríguez CE, Escobar Palacio JC, Venturini OJ, Silva Lora EE, Cobas VM, Marques Dos Santos D, et al. Exergetic and economic comparison of ORC and Kalina cycle for low temperature enhanced geothermal system in Brazil. *Appl Therm Eng* 2013;52:109–19. <https://doi.org/10.1016/j.applthermaleng.2012.11.012>.
- [186] Mirolli MD. The Kalina cycle for cement kiln waste heat recovery power plants. 2005 IEEE Cem Ind Tech Conf Rec 2005;2005:330–6. <https://doi.org/10.1109/CITCON.2005.1516374>.

